

Unveiling the Mechanisms of Acclimation to Fluctuating Light Conditions: Insights from Suppressor Mutants of *pgr5*

Dissertation

zum Erwerb des Doktorgrades der Naturwissenschaften
(Dr. rer. Nat)



Dissertation der Fakultät für Biologie
der Ludwig-Maximilians-Universität München

vorgelegt von
Jan-Ferdinand Penzler

München, 09.08.2023

Die Dissertation wurde unter der Leitung von Prof. Dr. Dario Leister
an der Fakultät für Biologie
der Ludwig-Maximilians-Universität München (LMU)
angefertigt

Erstgutachter:	Prof. Dr. Dario Leister
Zweitgutachter:	Prof Dr. Thomas Nägele
Tag der Abgabe:	09.08.2023
Tag der mündlichen Prüfung:	25.10.2023

Eidesstattliche Erklärung:

Ich versichere hiermit an Eides statt, dass die vorgelegte Dissertation von mir selbstständig und ohne unerlaubte Hilfe angefertigt wurde. Des Weiteren erkläre ich, dass ich nicht anderweitig ohne Erfolg versucht habe, eine Dissertation einzureichen oder mich der Doktorprüfung zu unterziehen. Die folgende Dissertation liegt weder ganz noch in wesentlichen Teilen einer anderen Prüfungskommission vor.

Jan-Ferdinand Penzler
München, 09.08.2023

Statutory Declaration:

I declare that I have authored this thesis independently, that I have not used other than the declared sources/resources. Furthermore, I declare that I have not submitted a dissertation without success or failed to pass the oral examination. The present dissertation (neither the entire dissertation nor parts) has not been presented to another examination board.

Jan-Ferdinand Penzler
Munich, 09.08.2023

Content

Content	III
Abstract	VI
Zusammenfassung	VII
Figures	IX
Tables	XI
Abbreviations	XII
1. Introduction	17
1.1 Plants	17
1.2 Chloroplast.....	17
1.3 Thylakoid membrane	18
1.3.1 PSII	19
1.3.2 PSI	20
1.3.3 Cyt b_6/f	20
1.3.4 ATP synthase.....	21
1.3.5 CBB-cycle	21
1.4 LEF and CEF	22
1.4.1 LEF.....	22
1.4.2 CEF	23
1.5 Short-term protection mechanism of photosynthesis depending on PGR5-mediated CEF	26
1.5.1 NPQ	26
1.5.2 PGR5-mediated CEF and its role in fluctuating light acclimation	28
1.5.3 State transition	29
2. Aims of the Work	31
3. Materials and Methods	32
3.1 Chemicals	32
3.2 Plant Material	32
3.3 Plant Growth Conditions	32
3.4 <i>pgr5</i> suppressor screen	33
3.4.1 EMS-Mutagenesis.....	33
3.4.2 Selection of <i>pgr5</i> suppressor under fluctuating light.....	33
3.4.3 Whole genome extraction and sequencing.....	34
3.5 Photosynthetic measurements.....	34
3.5.1 Induction recovery curve (IRC)	35
3.5.2 IRC under different CO ₂ concentrations	35
3.5.3 Fast oxidation of P700	35
3.5.4 Light curve.....	36
3.6 Blue Native (BN)	36
3.6.1 Thylakoid Extraction.....	36

3.6.2	Sample preparation for BN-PAGE	36
3.7	Protein Extraction and Immunoblot Analysis	37
3.8	DNA-extraction	39
3.9	PCR	39
3.10	RNA-extraction	39
3.11	DNase treatment of RNA	40
3.12	cDNA-Synthesis	40
3.13	Gateway cloning	40
3.14	CRISPR-Cas	41
3.15	<i>E. coli</i> transformation by heat shock	42
3.16	Transformation of <i>A. tumefaciens</i>	42
3.17	BIFC-interaction assay /GFP-localization of proteins	42
3.18	GFP-localization of proteins	42
3.19	<i>Nicotiana benthamiana</i> leaf infiltration	43
3.20	Protoplast extraction	43
3.21	Pigment Measurements	43
3.22	Data analysis and visualization	44
3.23	Bioinformatic tools	44
3.24	Accession number of genes and proteins	45
4.	Results	50
4.1	<i>pgr5-1</i> phenotype under control and fluctuating light conditions	50
4.2	<i>pgr5-1</i> suppressor screen	52
4.2.1	Identification of causative mutations in the selected <i>pgr5-1</i> suppressors	54
4.3	Defect assembly of PSII suppresses the lethal phenotype of <i>pgr5-1</i> under FL, a proof of concept	57
4.3.1	<i>lpa66</i> suppresses the photosynthetic phenotype of <i>pgr5-1</i> under FL	61
4.3.2	From representative mutant lines of thylakoid complexes, only PSII mutants can suppress <i>pgr5-1</i> lethal phenotype under FL	65
4.3.3	Protein accumulation in the photosynthetic electron transport-single and double mutants	68
4.3.4	Photosynthetic performance of PET-lines under different light conditions	70
4.4	Activity and regulation of the CBB-cycle as a potential point to suppress <i>pgr5-1</i> lethality under FL	74
4.4.1	Photosynthetic phenotype of suppressor lines <i>pgr5-1 hcef1</i> and <i>pgr5-S336</i>	76
4.5	New proteins identified by the <i>pgr5</i> suppressor screen	85
4.6	An unknown protein suppresses <i>pgr5-1</i> lethality under FL	85
4.6.1	Cyt b ₆ f accumulates less in S261 mutant lines	91
4.6.2	S261 is predicted to form a complex with PGR5, Fd and FNR	93
4.6.3	Photosynthetic activity of <i>pgr5-1 S261-Cas</i> lines	95
4.7	Generation of <i>pgr5-Cas</i> as a true PGR5 knock-out line	101
4.7.1	Complete knock-out lines of PGR5 via CRISPR/Cas resemble in growth phenotype <i>pgr5-1</i> under control and fluctuating light conditions	101
4.7.2	The novel <i>pgr5-Cas</i> mutants are more similar in photosynthetic performance to <i>pgr1ab</i> than to <i>pgr5-1</i>	104

4.7.3	The <i>prg5-1</i> mutant is strongly affected in the accumulation and stability of chloroplast proteins	109
4.7.4	Additional SNPs in the second chromosome can be found in <i>pgr5-1</i>	111
4.7.5	PGRL1 without PGR5 is harmful under high light conditions	112
5.	Discussion	115
5.1	PSII functionality has a major impact on FL acclimation	115
5.2	Altered PSI accumulation does not improve FL acclimation	116
5.3	Cyt b ₆ f mutants are unlocking FL survival in <i>pgr5-1</i> background	117
5.4	S261 is involved in the accumulation of the Cyt b ₆ f complex, together with PGR5	118
5.5	NDH-mediated CEF compensates the lack of PGR5 under certain conditions.....	119
5.6	The FBPase functions as a security valve for PSI.....	120
5.7	Regulation of LEF by the qE component of NPQ is not sufficient to ensure survival under FL.....	122
5.8	The <i>pgr5-Cas</i> mutant a PGR5 knock-out	124
5.8.1	The PGR5 _{G130S} protein affects photosynthesis	125
5.8.2	PGR5 and PGRL1 have different functions under HL acclimation	126
6.	Conclusions.....	127
7.	Bibliography	128
8.	Danksagung.....	139
	Publikationsliste.....	141

Abstract

Plants, algae and cyanobacteria can produce chemical energy in the form of organic compounds by using light in a process called photosynthesis. In a natural environment, light intensity changes from low to high in a matter of seconds (s) during the day. These rapid changes create a challenging environment that requires specific acclimation and protection mechanisms for the plant to survive. One of these mechanisms is cyclic electron flow (CEF), mediated by PGR5, in which electrons are transferred from PSI back to the plastoquinone (PQ) pool. Indeed, plants without active PGR5-mediated CEF have a lethal phenotype under fluctuating light (FL) conditions. This alternative photosynthetic electron pathway to the linear electron flow (LEF) allows an additional transfer of protons from the stroma to the lumen and a release of electrons from PSI, maintaining a proper ATP/NADPH ratio and protecting PSI from over-reduction. In plants, the key protein for this electron pathway is PGR5, but its molecular mechanism of action and how the electrons are transferred from PSI to the PQ pool is still unclear. To elucidate this mechanism and to identify additional components of light acclimation, a suppressor screen was performed in *pgr5* under FL, using random mutagenesis. Several suppressor mutants were obtained of the lethal phenotype of *pgr5* under FL. In this thesis, four of these suppressors are described in more detail, including the mechanisms by which they allow acclimation to FL in the absence of PGR5. The most efficient way to suppress the lethal FL phenotype of *pgr5* was to downregulate LEF, in particular by reducing PSII activity. In addition, the abundance and activity of FBPase was identified as a possible key regulatory point to allow *pgr5* survival under FL. Causative mutations were identified in two genes encoding proteins of completely unknown function. One of them, in the suppressor *pgr5 S261*, is the affected protein S261, which is involved in the assembly of the Cyt b₆f complex, as recently described.

In the second part of this work, the phenotype of mutants with different levels of PGR5 was studied in detail, including new *pgr5* mutants generated by CRISPR/Cas9, *pgr5-Cas#1* and *pgr5-Cas#2*. By analysing photosynthetic performance, proteomic composition and growth under high light (HL) conditions, differences between the lines were observed. Interestingly, the original *pgr5-1* mutant showed significant differences from the new *pgr5-Cas* lines, most likely caused by an SNP in the CGL20a gene, which is present in *pgr5-1* but not in *pgr5-Cas*. Furthermore, it was found that mutants lacking both PGRL1 and PGR5 behaved differently under HL than mutants lacking only PGR5, suggesting an additional function of PGRL1 in the absence of PGR5.

Zusammenfassung

Pflanzen, Algen und Cyanobakterien können mit Hilfe von Licht chemische Energie in Form von organischen Verbindungen erzeugen. In einer natürlichen Umgebung ändert sich die Lichtintensität im Laufe des Tages innerhalb von Sekunden von schwach zu stark. Diese schnellen Veränderungen erfordern spezielle Anpassungs- und Schutzmechanismen, damit die Pflanze überleben kann. Einer dieser Mechanismen ist der PGR5-abhängige zyklische Elektronenfluss (ZEF), bei dem Elektronen aus dem PSI in den Plastochinon-Pool (PQ) geleitet werden. Pflanzen ohne aktiven PGR5-vermittelten CEF zeigen einen letalen Phänotyp unter FL-Bedingungen. Dieser alternative photosynthetische Elektronenfluss zum linearen Elektronenfluss (LEF) ermöglicht einen zusätzlichen Protonentransfer vom Stroma zum Lumen und einen Elektronentransport vom PSI, wodurch das ATP/NADPH-Verhältnis aufrechterhalten und das PSI vor übermäßiger Reduktion geschützt wird. In Pflanzen ist das Schlüsselprotein für diesen Elektronenweg PGR5, wobei der molekulare Wirkmechanismus und die Übertragung von Elektronen vom PSI zum PQ-Pool noch unklar sind. Um diesen Mechanismus zu untersuchen und weitere Komponenten der Lichtanpassung zu identifizieren, wurde ein *pgr5*-Suppressor-Screen durchgeführt. Durch zufällige Mutagenese wurden Suppressor-Mutanten, die den letalen Phänotyp von *pgr5* unter FL unterdrücken, generiert. In dieser Arbeit werden vier dieser Suppressoren genauer beschrieben, einschließlich der Mechanismen, die die Akklimatisierung an FL in Abwesenheit von PGR5 ermöglichen. Der effizienteste Weg zur Unterdrückung des letalen FL-Phänotyps von *pgr5* war die Herunterregulierung von LEF, insbesondere durch die Reduktion der PSII-Aktivität. Darüber hinaus wurde festgestellt, dass die Anreicherung und Aktivität der FBPase ein möglicher Schlüsselregulator ist, um das Überleben von *pgr5* unter FL zu ermöglichen. Mutationen in zwei Genen wurden identifiziert, die für Proteine mit völlig unbekannter Funktion kodieren. Eine davon ist im Suppressor *pgr5 S261* zu finden, wobei das betroffene Protein S261, wie kürzlich beschrieben, an der Bildung des Cyt b_6f -Komplexes beteiligt ist.

Im zweiten Teil dieser Arbeit wurde der Phänotyp von Mutanten mit unterschiedlichen Mengen an PGR5, einschließlich neuer *pgr5*-Mutanten, die mit CRISPR/Cas9 erzeugt wurden, *pgr5-Cas#1* und *pgr5-Cas#2* untersucht. Bei der Analyse der photosynthetischen Leistung, der Proteinzusammensetzung und des Wachstums unter Hochlicht (HL) wurden Unterschiede zwischen den Linien festgestellt. Interessanterweise zeigte die ursprüngliche *pgr5-1* Mutante signifikante Unterschiede zu den neuen *pgr5-Cas* Linien, die höchstwahrscheinlich auf einen SNP im *CGL20a* Gen zurückzuführen sind, der in *pgr5-*

I aber nicht in *pgr5-Cas* vorhanden ist. Darüber hinaus wurde festgestellt, dass sich Mutanten, denen sowohl PGRL1 als auch PGR5 fehlte, unter HL anders verhielten als Mutanten, denen nur PGR5 fehlte, was auf eine zusätzliche Funktion von PGRL1 in Abwesenheit von PGR5 hindeutet.

Figures

Figure 1: From plant to the thylakoid membrane.	19
Figure 2: Schematic representation of linear and cyclic electron flow.	25
Figure 3 Schematic representation of LEF and CEF in a <i>pgr5</i> knockout line.	29
Figure 4: <i>pgr5-1</i> shows a lethal phenotype under FL and impaired CEF-related parameters.....	51
Figure 5: <i>pgr5-1</i> suppressor screen.....	53
Figure 6: Analysis of M_2 selection.....	54
Figure 7: Schematical representation of thylakoid complexes and mechanisms influenced by SNPs.....	57
Figure 8: Mutating the gene <i>LAP66</i> suppresses the lethal phenotype of <i>pgr5-1</i> under FL.	58
Figure 9: Mutating <i>LPA66</i> affects the stability and the maximum quantum yield of the PSII.....	60
Figure 10: Photosystem II parameters of <i>lpa66</i> -mutatn lines under FL.....	62
Figure 11: Photosystem I parameters of <i>lpa66</i> -mutatn lines under FL.....	64
Figure 12: Growth phenotype of PET-lines under CL and FL.	67
Figure 13: Immunodetection of selected proteins in the generated PET-lines.....	69
Figure 14: Heatmap of photosynthetic activity at distinct time points under FL of PET-lines.	71
Figure 15: Photosynthetic activity of PSII and PSI under $100 \mu\text{mol photons m}^{-2} \text{s}^{-1}$ at induction-phase of PET-lines.	73
Figure 16: Knock-out lines of <i>hcef1</i> in the background of <i>pgr5-1</i> growth phenotype.	75
Figure 17: A premature stop-codon in <i>ACHT2</i> allows <i>pgr5-1</i> survival under FL conditions.....	76
Figure 18: P700 oxidation rate and plastoquinone reduction can be complemented to wild type levels in <i>pgr5-1</i> by knocking out <i>HCEF1</i> but not <i>ACHT2</i>	78
Figure 19: Photosynthetic activity around PSII in <i>pgr5-1 hcef1</i> and <i>pgr5-1 acht2-Cas</i> under FL.	80
Figure 20: PSI activity and acceptor side limitation in <i>pgr5-1 hcef1</i> and <i>pgr5-1 acht2-Cas</i> under FL.	82
Figure 21: IRC is dependent on CO_2 concentration in <i>acht2</i> mutant lines.....	84
Figure 22: <i>S261</i> encodes a chloroplast-localized protein, the knock-out of which suppresses the <i>pgr5</i> phenotype.	88
Figure 23: Bioinformatical analysis of <i>S261</i>	90
Figure 24: Protein content of the <i>S261</i> -lines.....	92
Figure 25: Alphafold 2 interaction prediction and complex modeling of <i>S261</i>	95
Figure 26: IRC of <i>S261-Cas</i> suppressor lines in <i>pgr5-1</i> background.	97
Figure 27: Photosystem II parameters of <i>S261</i> -mutant lines under FL.	99
Figure 28: Photosystem I parameters of <i>S261</i> -mutant lines under FL.	100
Figure 29: Growth of <i>PGR5</i> knock-out lines <i>pgr5-Cas</i> under long day and fluctuating light conditions.	103
Figure 30: Photosynthetic characterization of lines with different amounts of <i>PGR5</i> in induction and dark recovery.	105
Figure 31: Growth phenotype and photosynthetic parameters of PSII in different genotypes at seedling state.	106

Figure 32: Assessment of parameters affected by CEF activity in different genotypes.	108
Figure 33: Analysis of chloroplast proteome of PGR5 deficient genotypes.....	110
Figure 34: Phenotype of plants with different PGR5 content under high-light conditions.....	114
Figure 35: Model of the activation network of CEF around FBPase and the interacting redox regulators.....	122
Figure 36: Model of possible suppression of <i>pgr5</i> lethality under FL found in this work.	124

Tables

Table 1: Antibodies used in the thesis.....	38
Table 2: Vector-list	46
Table 3: Primer-list.....	46
Table 4: Causative mutations of the re-sequenced <i>pgr5-1</i> suppressor lines.	56
Table 5: quantification in means \pmSD of protein abundance after immunodetection in <i>pgr5-1</i>, <i>pgr11ab</i>, <i>pgr5-cas</i> and the complementation lines.	111
Table 6: Additional SNPs at the chromosome 2 or plastid localized in <i>pgr5-1</i>.	112

Abbreviations

%	percentage
°C	degrees Celsius
μ	micro-
3-PGA	3-phosphoglycerate
A	Adenine
AA	Antimycin A
ACHT2	atypical cys his rich thioredoxin 2
ADP	adenosine diphosphate
APS	ammonium peroxodisulfate
ATP	adenosine 5'-triphosphate
ATPase	ATPsynthase
BIFC	bimolecular fluorescence complementation
BN	blue native
bp	base pair
C.B.B.	Coomassie brilliant blue
CBB-cycle	Calvin-Benson-Bassham-cycle
CEF	cyclic electron flow
Chl	chlorophyll
CL	control light (12 h light)
CO ₂	carbon dioxide
Col	cEcotype Columbia of <i>A. thaliana</i>
CPLD	Conserved in Plant Lineage and Diatoms
cTP	chloroplast transit peptide
Cyt b ₆	cytochrome b ₆
Cyt b ₆ f	cytochrome b ₆ f

Abbreviations

Cyt f	cytochrome f
DNA	Deoxyribonucleic acid
EMS	Ethyl methane sulfonate
ETC	electron transport chain
EtOH	ethanol
FBPase	fructose-bisphosphatase
Fd	ferredoxin
Fe	iron
Fig.	figure
FL	fluctuating light
Fm	maximum observed fluorescence
FNR	ferredoxin NADPH reductase
Fo'	minimum fluorescence
F _{OFR}	fluorescence under far red light
FQR	ferredoxin plastoquinone reductase
FR	far-red
Fv/Fm	maximum efficiency of PSII
g	gram
G3P	Glyceraldehyde-3-phosphate
GFP	green fluorescence protein
h	hour
H ⁺	proton
H ₂ O	water
H ₂ O ₂	hydrogen peroxide
<i>hcefl</i>	ko-line of FBPase
HL	high light

Abbreviations

IRC	induction recovery curve
k	kilo-
l	liter
LD	long day (16h light)
LEF	linear electron flow
LHCI	light harvesting complex I
LHCII	light harvesting complex II
LL	low light
M	molar
m	milli-
min	minutes
n	nano-
NADP ⁺	nicotinamide adenine dinucleotide phosphate
NADPH	nicotinamide adenine dinucleotide phosphate reduced form
NDH	NAD(P)H dehydrogenase-like complex
NPQ	non-photochemical quenching
NTRC	NADPH-dependent thioredoxin
OD	optical density
P	phosphate
P680	reaction center of PSII
P700	reaction center of PSI
PAM	pulse amplitude modulation
PC	plastocyanin
PET	photosynthetic electron transport
PGR5	Proton gradient regulator 5

Abbreviations

PGRL1	proton gradient regulator 5 like 1
PGRL2	proton gradient regulator 5 like 2
pH	acidity
pmf	proton motive force
PQ	Plastoquinone
PSI	photosystem I
PSII	photosystem II
PVDF	polyvinylidene fluoride
Q-cycle	Quinone-cycle
qE	energy dependent quenching
qI	Photoinhibition quenching
qP	photochemistry
qT	state transition quenching
RNA	ribonucleic acid
ROS	reactive oxygen species
RuBP	ribulose-1,5-bisphosphate
SD	standard deviation
SDS	sodium dodecyl sulfate
s	seconds
SNP	single nucleotide polymorphism
syn	Synechocystis
synPGRL1	synechocystis PGRL1
T	Thymine
$t_{1/2}P700$	half time of P700 oxidation
T-DNA	transfer DNA
TEMED	N,N,N',N'-Tetramethylethylenediamine

Abbreviations

tNPQ _{max}	maximum of NPQ in the transient phase
Trx f	thioredoxin f
Trx m	thioredoxin m
v/v	volume/volume
w/v	weight/volume
WT	wild type
Y(I)	PSI activity
Y(II)	PSII activity
Y(NA)	acceptor side limitation
Y(ND)	donor side limitation
Y(NO)	non-regulated energy dissipation quantum yield
Y(NPQ)	NPQ of PSII depending on Y(II)
YFP	yellow fluorescence protein

1. Introduction

1.1 Plants

Plants are defined as multicellular organisms with cell walls containing cellulose and the ability to photosynthesise. They are sessile organisms, influenced by their environment and changing conditions, with no form of protection other than their own. The process of photosynthesis converts light energy into chemical energy and produces organic matter from water and carbon dioxide while producing oxygen. The ability of plants to photosynthesise, together with other photosynthetic organisms such as algae and cyanobacteria, has made life on earth, as we know it, possible. Due to the high abundance of plants and algae on earth, our planet is referred to as "The Green Planet". In this thesis, one of the most widely used plant model organisms, *Arabidopsis thaliana*, was used (Figure 1A).

Plants evolved from one or more eukaryotic cells that formed a symbiotic relationship with cyanobacteria, which were ingested but not digested by the cell and formed an organelle, the plastid (Figure 1B). The plastid has its own chromosome, but parts of the ancestral genome of the formerly free-living cyanobacteria have been transferred into the nucleus of the eukaryotic cell. The newly formed organelle, called a chloroplast, is able to carry out photosynthesis for the host cell and provide it with the resources it needs. This created a codependency between these cells. From this primary endosymbiont, different lineages were derived, which are: Glaucophytes, Rhodophytes and Chloroplastida (Löffelhardt 2006). Plants belong to the Chloroplastida, which evolved in a highly divergent branch.

1.2 Chloroplast

The chloroplast is surrounded by a double-layered membrane and has its own chromosome with a size of 1545-1515 bp and 123 genes (in *Arabidopsis thaliana*) (Stadermann et al., 2016). The majority of chloroplast-localised proteins are encoded in the nuclear genome and imported into the organelle after translation. The relocalisation of the coding sequence of about 95 % of the chloroplast proteins took place during the evolution from free-living cyanobacteria to a symbiotic plant organelle (Kleine et al., 2009). For proteins encoded in the chloroplast genome, the chloroplast has its own translation machinery. The chloroplast ribosome (70S ribosome) is very similar to the ones in prokaryotes. Chloroplast proteins encoded by nuclear genes are imported from the cytosol. Localisation is

determined by the chloroplast transit peptide (cTP), an amino acid sequence at the N-terminus of the protein that is cleaved post-translationally before import into the chloroplast (Richter & Lamppa, 2002). These proteins are then introduced into their specific localisation in the chloroplast, which can be in the stroma or the thylakoid lumen. The chloroplast can be divided into two parts: the stroma and the thylakoids, where the thylakoid itself consists of a thylakoid membrane and the lumen (Figure 1C).

1.3 Thylakoid membrane

Thylakoids consist of a membrane that encloses an inner space called the lumen. They are found in plants, algae and organisms that do not have plastids, such as cyanobacteria. It is a trait inherited from the assimilation of the ancestral cyanobacteria. The protein complexes essential for photosynthesis are integral membrane protein complexes. The thylakoid membrane is organised into grana, which are stacks of membranes connected by lamellae, individual sections of the thylakoid membrane. The thylakoid membrane divides the chloroplast into two compartments: the lumen and the stroma. In the light-driven photosynthetic reactions, electrons, driven by light as an energy source, move through the electron transport chain (ETC), which takes place across the thylakoid membrane, and all the complexes associated with it have their own essential role. The complexes of the thylakoid membrane involved in the ETC are photosystem II (PSII), the cytochrome b_6f complex (Cyt b_6f) and photosystem I (PSI). The light-driven reaction starts at PSII and is fuelled by charge separation after excitation, which excites an electron to a higher energy state and transports it via plastoquinone (PQ) to Cyt b_6f . At Cyt b_6f and PQ, protons are pumped from the stroma into the lumen to create a proton gradient. This proton gradient is used by ATP synthase, also located in the thylakoid membrane, to generate ATP from ADP and P_i . From Cyt b_6f , the electron moves on to PSI, which it reaches with the help of plastocyanin (PC). At PSI, the chlorophyll is excited by light energy and the electron is transferred to ferredoxin (Fd). The reduced Fd is used to reduce $NADP^+$ to NADPH in a reaction mediated by ferredoxin NADPH reductase (FNR). This electron transport pathway is also known as the linear electron flow (LEF). The ATP and NADPH are then used in the Calvin-Benson-Bassham (CBB)-cycle to fix CO_2 and produce triosephosphate (Figure 1D). In an alternative pathway, an electron is transferred from PSI via the proton gradient regulator 5 (PGR5) or the NAD(P)H dehydrogenase-like complex (NDH) back to Cyt b_6f . From there, the electron is transferred to

PSI, which completes the cycle. This pathway is called cyclic electron flow (CEF). In the CEF, there is only a proton gradient and no net production of NADPH.

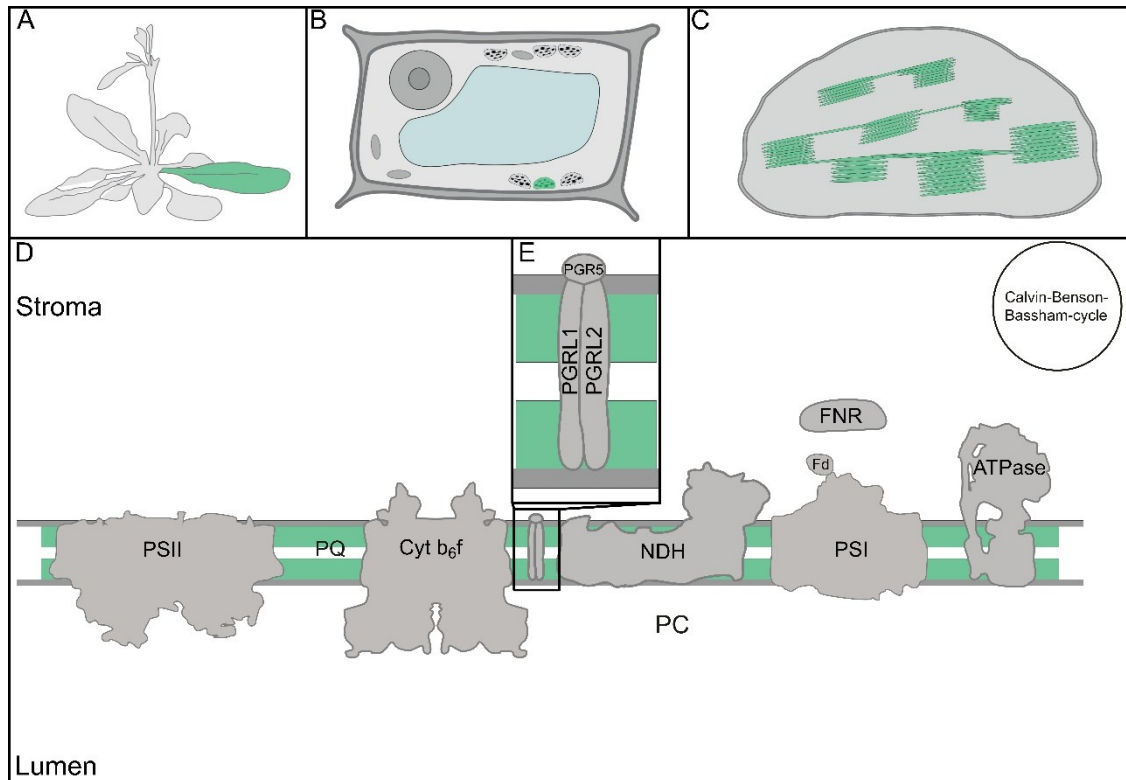


Figure 1: **From plant to the thylakoid membrane.** **A.** An adult plant in the early stages of flowering. **B.** Plant cell with nucleus, vacuole, mitochondria and chloroplast (green). **C.** Representation of a chloroplast with double-layered outer membrane and thylakoid membrane organised into grana and lamella. **D.** Thylakoid membrane with indication of stroma and lumen side and visualisation of thylakoid membrane complexes and proteins (PSII, Cyt b₆f, NDH complex, PSI, PC, FNR, Fd and ATPase) as a schematic representation of the Calvin-Benson-Bassham cycle and PQ. **E.** protein complex of PGR5, PGRL1 and PGRL2.

1.3.1 PSII

PSII is the starting point for photosynthetic reactions. It is a complex consisting of several subunits that are assembled by several assembly factors (Nickelsen & Rengstl, 2013). The electrons transported across the thylakoid membrane come from the water-splitting complex at PSII, where water is oxidised, releasing O₂, H⁺ and electrons. These electrons are then taken into the oxidised PSII reaction centre. The reaction centre is composed of the D1 and D2 subunits, which bind a dimer of chlorophyll *a* (Chl *a*), which has a maximum absorption at 680 nm. The PSII reaction centre is therefore called P680. This dimer collects the excitation absorbed by the Chl localised in the light-harvesting complexes II (LHCII) and other light-harvesting complex of PSII (LHCbs). The LHCII associated with Chl *a* and Chl *b* form the antenna of PSII, which harvests light energy. The proteins

of these complexes are Lhcbs and can be divided into two groups according to their abundance: minor for low abundance proteins (Lhcb4, Lhcb5 and Lhcb6) and major for high abundance proteins (Lhcb1, Lhcb2 and Lhcb3). The major LHCIIs occur as hetero- or homotrimers linked to the PSII core via the minor Lhcbs. In addition, the heterotrimers or homotrimers of Lhcb1, Lhcb2 and Lhcb3 can be transferred to PSI through phosphorylation by STN7 in a process known as state transition (see below). The D1 subunit has an additional role in protecting PSII by acting as a predetermined breaking point in the event of overexcitation. Due to this protective mechanism, the D1 subunit has a high turnover rate and needs to be resynthesised regularly (Jarvi et al., 2015).

1.3.2 PSI

PSI is a transmembrane protein complex that binds LHCI and is one of the essential components for linear and cyclic electron transfer. Electrons are donated to PSI by PC. PC is located on the lumen side of the thylakoid membrane and is a copper-binding protein. Fd is the electron acceptor of PSI. Fd itself is an iron-sulphur protein in the stroma of the chloroplast that links PSI to the FNR. The LHCI consists of four subunits, Lhca1, Lhca2, Lhca3 and Lhca4. The Chl incorporated into the LHCI are Chl *a* and Chl *b*, together with carotenoids. The LHCI themselves are bound to PSI in dimers, one dimer is formed by Lhca1 and Lhca4, the other by Lhca2 and Lhca3. The light energy at PSI is collected by the Chl itself in the Lhcas from where it is transferred to the reaction centre, which consists of a Chl *a* dimer (P700) bound via PsaA and PsaB. Similarly, Fe₄S₄ clusters (F_X, F_A and F_B) and phyloquinones are located in the core of PSI (Qin et al., 2015). PSI is much more exposed to photosynthetic inhibition and damage by reactive oxygen species (ROS) generation than PSII. If damage occurs to PSI, repair is slower compared to PSII due to the less efficient repair mechanism.

1.3.3 Cyt b₆f

The Cyt b₆f complex is a multiprotein transmembrane complex that links PSII and PSI in electron transfer via PQ and PC, respectively. During electron transfer through the complex, one proton is transferred from the stroma to the lumen for each electron. Electrons reaching the Cyt b₆f complex come from the PQ pool and are transferred to the PC or returned to the PQ pool to transfer an additional proton to the lumen. This process is known as the Q cycle. The Cyt b₆f complex consists of Cyt b₆, Cyt f, the Rieske protein, which has a Fe₂S₂ cluster, and smaller proteins. The assembly and disassembly of this

complex is still not fully understood (Page et al., 2004; Sandoval-Ibanez et al., 2022; Schwenkert et al., 2007). The Cyt b_6f complex is an important regulator of electron flow. Electron flow can be down-regulated when the lumen is highly acidified and photosynthetic control is induced (Malone et al., 2021).

1.3.4 ATP synthase

The ATPase is a multi-subunit complex located in the thylakoid lamella that produces ATP from ADP using the proton motive force (pmf) generated by the ETC. This is achieved by a rotational motion of the γ -subunit. The protons that fuel the motions enter the ATPase from the luminal side and are released after a complete rotation of the head (Cingolani & Duncan, 2011). The head has three binding sites for ADP, which pass through three different conformations: open, tight and loose. At the same time, three ADPs can bind to the synthase subunit, allowing the production of three ATPs from ADP and phosphate for one complete rotation.

1.3.5 CBB-cycle

The CBB-cycle is a reaction in the chloroplast stroma that fixes CO_2 into organic compounds/sugars. Several proteins are involved, with Rubisco, the most abundant protein on earth, being a key player in the cycle. The CBB-cycle uses ATP and NADPH produced during the ETC. The ATP/NADPH ratio is important for the proper functioning of the cycle and is tightly regulated. The CBB-cycle can be divided into three main steps. The first is carboxylation. In this step, CO_2 is fixed via Rubisco and two molecules of 3-phosphoglycerate (3-PGA) are formed from ribulose-1,5-bisphosphate (RuBP). In the next step, reduction, 3-PGA is used to synthesise glyceraldehyde-3-phosphate (G3P) using ATP and NADPH. G3P is then used to produce glucose, as well as sugars and other organic molecules that are essential in the plant's metabolic pathways. G3P is also used in the final three steps of the CBB-cycle: regeneration. In the final step, regeneration, RuBP is made again using GAP and ATP. Throughout this reaction, ATP and NADPH are used in a ratio of 1:5, which results in a higher demand for ATP than for NADPH.

Activation of the CBB-cycle is light dependent and occurs mainly through redox activation. Redox regulation consists of the post-translational modification of a protein by the formation of sulphur bridges between cysteines and is modulated by thioredoxin enzymes. These modifications cause a change in the conformation of the protein, activating or inactivating it. Most of the enzymes of the CBB-cycle are redox sensitive (Michelet et

al., 2013). In particular, fructose-1,6-bisphosphatase (FBPase) is redox-regulated and is redox-activated by thioredoxin f (Trx f) and thioredoxin m (Trx m) at the onset of light (Cejudo et al., 2019). Inactivation occurs by oxidation by the protein ACHT2 in the dark (Yokochi et al., 2021). FBPase catalyses the reaction of fructose 6-phosphate to fructose 1,6-bisphosphate in the regeneration step. Surprisingly, the protein itself is not essential for plant survival, as shown by Livingston et al. (2010). In their experiments, a knockout line of the FBPase (*hcefl*) was found to be growth retarded and to have highly induced CEF (Livingston et al., 2010).

1.4 LEF and CEF

Linear and cyclic electron flow are strongly intertwined. Both move electrons through a light-driven reaction. In the linear electron flow a proton gradient is built up and NADP^+ is reduced to NADPH, whereas in the cyclic electron flow only a proton gradient is built up. The cyclic electron flow is highly dependent on the LEF because the electrons transferred in the CEF initially come from the LEF.

1.4.1 LEF

The LEF is a light-driven electron transfer from water to the target, NADP^+ . It starts at PSII where light is collected by the LHCIIs and the PSII itself. The excitation is transferred to the PSII reaction core (P680). There, the Chl *a* dimer is excited (P680*) and an electron is then transferred to the pheophytin (PHE). The PHE in turn reduces the first plastoquinone in the electron chain, Q_a . From Q_a , Q_b plastoquinone is reduced, which finally binds two electrons and two protons from the stroma side. When these two electrons and protons are bound, the Q_b plastoquinone is replaced by an unreduced PQ and released into the intermembrane space. Meanwhile, the displaced electron from Chl *a* is replaced by an electron that is released by oxidising water. As a result of this reaction, elemental oxygen and protons are released.

The PQH_2 transfers its electrons to the Cyt b_6f complex and the two protons to the lumen. The electrons in the Cyt b_6f complex have a higher tendency to be transferred via the Rieske iron-sulphur cluster and Cyt *f* to plastocyanin. In a lower potential pathway, the electrons are transferred back to the PQ pool, allowing the transfer of additional protons from the stroma to the lumen via the PQ. This cycle is called the Q cycle. This cycle generates a pmf. The electron that was transferred to the PC via the higher potential pathway is transferred through the lumen to the PSI.

The PC binds to the PSI and transfers the electron, which reduces the PSI. In order for the electrons to be transferred further, the reactive centre of the PSI must be excited. This is achieved by the LHCI and PSI itself, which photoexcites the P700. The excitation oxidises the PSI and transfers the electron through the F_x to the F_A and F_B , which in turn reduce the Fd. In the final steps of the LEF, the Fd binds to the FNR, which in turn generates NADPH from $NADP^+$ and H^+ by reducing the former (Figure 2).

1.4.2 CEF

There are two alternative pathways for cyclic electron flow in higher plants. Both pathways are light-driven and recycle electrons from PSI. One pathway is mediated by the PGR5 protein and is known as the antimycin A-sensitive CEF (Munekage et al., 2002; Rühle et al., 2021), the other is antimycin A-insensitive and is mediated by the NDH complex. In both pathways, electrons are transported from PSI to Fd. From Fd, the electrons are accepted by the NDH complex and then supplied into the PQ pool (Schuller et al., 2019). In PGR5-mediated CEF, the electrons are transferred via PGR5 to the PQ pool, but the exact mechanism is still unclear. At the PQ pool, the two pathways intertwine again and the electrons then take the same route as in the LEF back to PSI, which closes the cycle and gives the pathway its name. The idea of a CEF was first proposed by Arnon et al. in 1954. He proposed, that CEF generates ATP and maintains the ATP/NADPH ratio (Arnon et al., 1954). ATP is generated by ATP synthase using a pmf generated during photosynthetic electron transport. The pmf is generated in both the LEF and CEF pathways by pumping protons from the stroma into the lumen in the Q-cycle (Figure 2).

1.4.2.1 NDH-mediated CEF

The NDH complex is the key element for NDH-mediated CEF. The NDH complex is L-shaped and consists of at least 28 subunits that are nuclear or plastid encoded (Shikanai, 2016). It is a homologue of complex I of the respiratory chain found in bacteria and mitochondria. The NDH complex is found in cyanobacteria, algae and plants. In cyanobacteria, it is the predominant CEF pathway compared to the PGR5-dependent CEF. During evolution, this pathway has lost its importance and only plays a minor role in higher plants. The electrons transferred through the NDH complex to plastoquinone are received from Fd (Schuller et al., 2019). The complexity of the NDH complex requires an assembly involving proteins such as CRR2 (Hashimoto et al., 2003). When these proteins are knocked out, a strong reduction of the complex can be detected (Hashimoto et al., 2003).

1.4.2.2 PGR5-mediated CEF

PGR5-mediated CEF requires the protein PGR5 (Munekage et al., 2002) and its binding/regulatory partners PGRL1 (DalCorso et al., 2008) and PGRL2 (Rühle et al., 2021) (Figure 1E) to transfer electrons from Fd to the PQ pool. PGR5 is a rather small protein with 133 amino acids and 70 amino acids in its mature form and is localised in the chloroplast (Munekage et al., 2002). PGR5 is thought to be bound to the thylakoid membrane by the thylakoid membrane protein PGRL1 (DalCorso et al., 2008). In a recently published paper on the evolution of PGR5, bacterial ferritin was proposed to be an ancestor of PGR5 (Leister et al., 2022). Interestingly, the PGR5 protein can be found in algae such as *Chlamydomonas reinhardtii* and in cyanobacteria. The PGR5-mediated CEF pathway exists in all these organisms, but plays different roles of importance. In addition, there are two isoforms of the PGRL1 protein in plants, PGRL1a and PGRL1b. PGRL1b is less abundant than PGRL1a (DalCorso et al., 2008). PGRL1 is localised in the thylakoid membrane and has two membrane domains. The exposed N- and C-termini contain cysteines that allow binding of other proteins and potential regulation of CEF by PGRL1 (Hertle et al., 2013). Its role in CEF is to stabilise and protect PGR5 from degradation (Rühle et al., 2021) and also to regulate the activity of the protein (Okegawa & Motohashi, 2020). PGRL1 is also found in algae such as *Chlamydomonas reinhardtii*, but only one homologue. In this organism, PGR5 and PGRL1 form a super-complex with PSI, Cyt b₆f and LHCI that promotes CEF (Iwai et al., 2010; Steinbeck et al., 2018). In cyanobacteria, a protein with weak homology, synPGRL1, can interact with Arabidopsis PGR5 expressed in *Synechocystis* (Dann & Leister, 2019). In Dann and Leister's work, an effect on CEF was demonstrated by knocking out synPGRL1 (Dann & Leister, 2019). The last and recently identified part of the PGR5-mediated CEF is PGRL2, a protein found on the basis of its homology to PGRL1 (Rühle et al., 2021). PGRL2 is found in higher plants and some algae. Like PGRL1, it has two transmembrane domains and an exposed N- and C-terminus. The work of Rühle and colleagues showed that PGRL2 is involved in the degradation of PGR5 in the absence of PGRL1 or when the activity of PGR5 is impaired (Rühle et al., 2021). One of the main differences between the NDH complex and PGR5-mediated CEF is the activation time. The NDH complex seems to work at a steady level, which is low in plants, but in the presence of high levels of H₂O₂, an overaccumulation of the complex is observed (Strand et al., 2015), as can be seen in the *hcef1* mutant line, which

is a knock-out line of the plastid FBPase with high NDH-dependent CEF (Livingston et al., 2010).

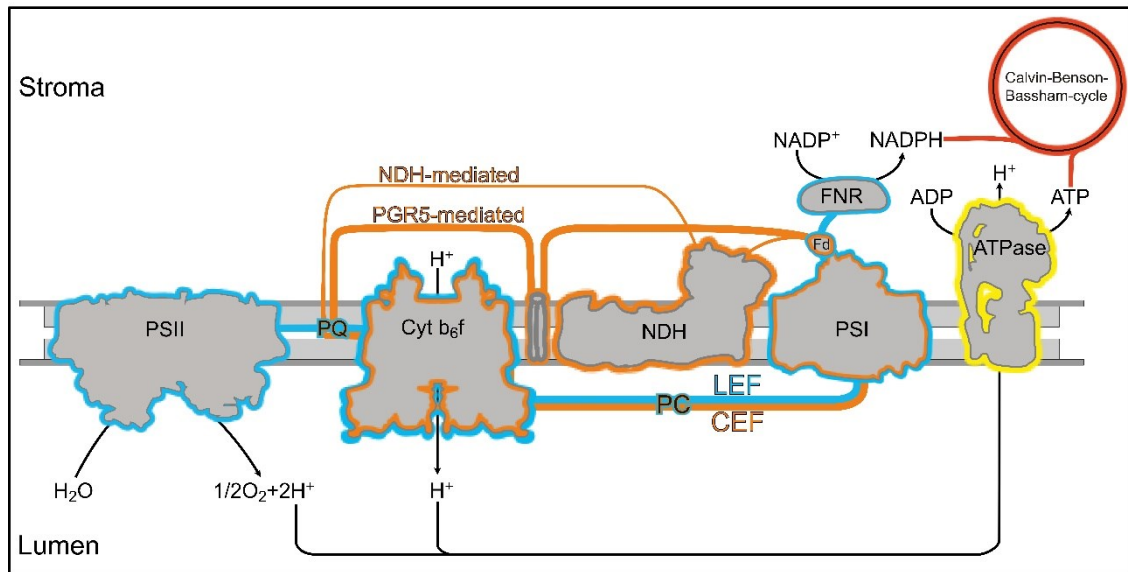


Figure 2: **Schematic representation of linear and cyclic electron flow.** The LEF and its associated complexes are shown in blue. The CEF and its associated proteins and complexes are shown in orange. The ATPase that uses the pmf is highlighted in yellow. The sink for the products of photosynthesis is visualised in red (Calvin-Benson-Basham cycle).

Antimycin A (AA) can inhibit the PGR5-mediated CEF. AA binds to the Q_i side of the mitochondrial cytochrome bc_1 complex (Yu et al., 1996). This binding suppresses the respiratory chain (Yu et al., 1996). In contrast, no similar binding is observed at the Cyt b_6f complex in the chloroplast. However, a specific effect of antimycin A can be observed in chloroplasts, namely the suppression of PGR5-mediated CEF (Munekage et al., 2002). In the search for the binding site of AA, PGRL1 was one of the potential candidates based on *in vitro* interaction (Hertle et al., 2013). Although the protein that connects PSI and the PQ pool through electron transfer is still unknown, it should have the function of a ferredoxin plastoquinone reductase (FQR), an essential component of the PGR5-CEF. The FQR is thought to be a single protein or complex capable of reducing the PQ pool by oxidising Fd and closing the gap between PSI and the Cyt b_6f complex (Hertle et al., 2013). In initial *in vitro* assays, PGRL1 showed the ability to reduce DMBQ, an analogue of PQ, by oxidising Fd (Hertle et al., 2013), making it a strong candidate to be the FQR. This would imply that PGRL1 is an essential protein required for PGR5-mediated CEF. The subsequent discovery of PGRL2 as an additional protein involved in PGR5 CEF showed that under certain conditions PGR5 can be sufficient to mediate electron flow from Fd to the PQ pool. Further experiments showed that the target of AA is PGR5 or a closely associated complex or protein (Rühle et al., 2021). Furthermore, in a paper by

Sugimoto and colleagues, PGR5 from *Pinus taeda* was expressed in Arabidopsis, resulting in increased insensitivity to AA (Sugimoto et al., 2013). In this work, the amino acid responsible for the AA sensitivity was found to be a valine in the third position of the mature Arabidopsis PGR5 (Sugimoto et al., 2013).

Redox regulation of a protein can be mediated by an exposed cysteine pair and PGR5 has only one cysteine. PGRL1, on the other hand, has 4 exposed cysteines, making it a candidate for redox regulation of PGR5-mediated CEF. The work of Hertle and colleagues suggested a link between the regulation of CEF and the exposed cysteines in the PGRL1 protein. It was suggested that PGRL1 undergoes a conformational change by forming sulphur bonds between the cysteines. This either activates or inactivates PGRL1 through regulation of the sulphur bridges (Hertle et al., 2013). Possible candidates for regulation of PGR5-mediated CEF were NTRC and Trx m4, both located in the stroma of the chloroplast. The interaction between PGR5 and NTRC (Nikkanen et al., 2018) and the dependence of a strongly induced NPQ in the NTRC knockout line (*ntrc*) on the PGR5-mediated CEF (Naranjo et al., 2021) strengthened the idea of a PGR5-mediated CEF redox regulation. Furthermore, regulation of PGR5-mediated CEF was demonstrated by the discovery of a complex consisting of PGRL1 and Trxm4 that inactivates the activity of PGR5-CEF by forming (Okegawa & Motohashi, 2020). The PGR5-mediated activation of CEF is not fully understood, and one of the mechanisms involved would be the dissociation of the Trx m4-PGRL1 interaction.

1.5 Short-term protection mechanism of photosynthesis depending on PGR5-mediated CEF

The photosynthetic apparatus requires additional protection or adjustments of the thylakoid complexes to survive under HL or changing light conditions. These protective mechanisms are to some extent dependent on PGR5-mediated CEF, through induction by acidification of the lumen (NPQ) or faster reduction of the PQ pool (state transition).

1.5.1 NPQ

NPQ is a protective mechanism of PSII that dissipates the excess energy at PSII as heat, thereby reducing LEF. It can be divided into three components: qE (ΔpH dependent), which describes energy-dependent quenching and represents the main part of NPQ in plants, qT (state transition), which is the relocation of LHCII between PSII and PSI, and

qI, which represents photoinhibition. The energy of an excited Chl in PSII can be dissipated in three different ways. The excitation energy can be emitted as fluorescence from the Chl (a component used to measure PSII activity via PAM measurements), can also be used to drive photochemistry (qP) or can be dissipated as heat via NPQ. If the excitation energy of Chl is not utilised, a triplet Chl can be formed, which generates a singlet oxygen molecule leading to photooxidic damage of PSII. An essential part of the qE component of NPQ is the xanthophyll cycle. Activation of the cycle is dependent on the pH gradient in the lumen and reaches peak activity at a ΔpH of 5.8 (Pfundel & Dilley, 1993). Violaxanthin-deepoxidase catalyses the conversion of violaxanthin-thin to zeaxanthin via the intermediate product anteraxanthin. Zeaxanthin is a carotenoid involved in quenching overexcitation energy (Strand & Kramer, 2014) and is bound to LHCII in the presence of PsbS. The PsbS protein belongs to the family of LHCs and binds to PSII in a pH-dependent manner, and acidification of the lumen activates the proteins involved in the xanthophyll cycle (Niyogi et al., 2005). Neutral pH promotes the binding of violaxanthin and PsbS, whereas at low pH PsbS binds to zeaxanthin, making PsbS a critical component for the induction of NPQ (Niyogi et al., 2005). The activation of NPQ can be observed particularly in saturating light and in the first s of illumination after dark adaptation of the plant. The dark-to-light induction of the NPQ is highly dependent on the PGR5-mediated CEF and the acidification of the lumen by this pathway. Indeed, this effect can be used to estimate PGR5-mediated CEF activity (Munekage et al., 2002). For example, in lines with a defect in PGR5-mediated CEF, no induction of NPQ can be observed after dark-to-light transitions. Other lines may show an over-induced NPQ, which may originate from different mechanisms, such as a more active NDH complex (*hcef1* mutant line (Livingston et al., 2010), lower accumulation of ATP synthase *cgl160* (Rühle et al., 2014) or a more active PGR5 CEF *ntrc* (Naranjo et al., 2021). The induction and relaxation of NPQ was used in an approach to produce plants that are better able to cope with changing light conditions and have a higher yield production compared to the conventional plants. Faster induction and relaxation of NPQ was achieved by the generation of genetically modified tobacco, called VPZ lines. In these lines, the protein PsbS, the violaxanthin de-epoxidase and the zeaxanthin epoxidase were overexpressed, resulting in tobacco lines that required a shorter time frame for NPQ up- and down-regulation (Kromdijk et al., 2016). Under field conditions, a significant increase in yield was observed in the VPZ lines (Kromdijk et al., 2016). In the approach to reproduce this effect in Arabidopsis or potato, no beneficial growth could be observed by VPZ expression (Garcia-Molina &

Leister, 2020; Lehretz et al., 2022), while in soybean, a higher yield of fresh and dry weight could be achieved (De Souza et al., 2022), showing that a deeper understanding of the complexity of photosynthesis is needed. This is one of the aims of this work.

1.5.2 PGR5-mediated CEF and its role in fluctuating light acclimation

Light intensity can change from low (e.g. when the sun is obscured by a cloud) to high (direct sunlight) several times a day. These changes can occur in a matter of s, and the plant needs to adapt quickly to the new conditions to avoid damage to the photosynthetic apparatus. Therefore, fluctuating light (FL) is frequent under natural conditions.

The knock-out lines of PGR5 (*pgr5-1*) and PGRL1 (*pgrllab*) are not affected in growth under constant light conditions such as long day (LD) or short day (DalCorso et al., 2008; Munekage et al., 2002), but under FL the phenotype of these lines changes drastically and lethality can be observed after a short growth period, in contrast to WT plants (Penzler et al., 2022; Rühle et al., 2021; Suorsa et al., 2012). In plants without functional PGR5, stromal over-reduction occurs due to a decreased ATP:NADPH ratio, which is triggered by a lower ATP production by ATP synthase. The imbalance in the ATP:NADPH ratio affects the efficiency of the CBB-cycle, leading to an overaccumulation of NADPH and a reduced need for its production. This, in turn, affects the electron flow from PSI to FNR and increases the acceptor-side limitation of PSI. In the absence of CEF and the over-reduction of the stroma (lower consumption of NADPH), PSI is over-reduced and ROS are generated in the active centre as in the FeS clusters, which photoinhibits PSI (Yamori & Shikanai, 2016 and Figure 3). This observation revealed the previously unknown role of PGR5-mediated CEF under FL. The PGR5-mediated CEF is not only responsible for balancing the ATP:NADPH ratio, but also for protecting PSI from light damage (Suorsa et al., 2012). CEF provides PSI with an additional electron acceptor that prevents over-reduction of PSI, which would lead to the generation of ROS in P700 and the accumulation of photooxidative damage (Suorsa et al., 2012). Furthermore, photosynthetic control is induced by the establishment of a proton gradient on the lumen side, which downregulates the LEF to PSI (Yamamoto & Shikanai, 2019). In addition, acidification of the lumen induces a protective mechanism called non-photochemical quenching (NPQ), which downregulates the activity of the LEF on the PSII side. PSI does not have an effective repair mechanism like PSII, which makes it more sensitive to light damage (Kudoh & Sonoike, 2002), and all these regulatory mechanisms ultimately allow the plant to survive under FL conditions. In the CEF mutant background (*pgr5-1* and *pgrllab*), the

artificial suppression of lethality under FL can be achieved by reducing PSII activity (Suorsa et al., 2016) or, as in the *pgr11ab pgr12* line, by restoring the accumulation and activity of PGR5 (Rühle et al., 2021).

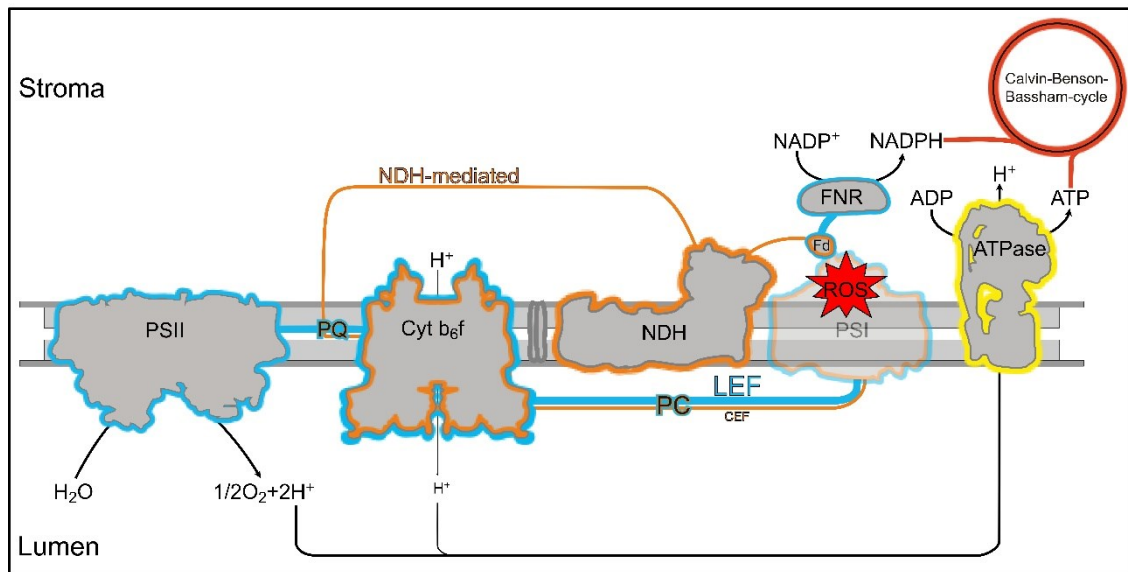


Figure 3 **Schematic representation of LEF and CEF in a *pgr5* knockout line.** The LEF and its associated complexes are shown in blue. The CEF and its associated proteins and complexes are shown in orange. The ATPase that uses the pmf is highlighted in yellow. The sink for the products of photosynthesis is visualised in red (Calvin-Benson-Bassham cycle). The strength of the electron flow and the pmf is indicated by the thickness of the line. The formation of ROS is visualised in the PSI as a red star.

1.5.3 State transition

State transition is a mechanism that helps the plant adapt to a light source that would alter the balance between the activity of PSII and PSI. Depending on the light source, there is a transfer of LHCIIs from PSII to PSI or back. The movement of the antenna is triggered by reversible phosphorylation. In particular, the transferred LHCIIs are the main antennae of PSII (Lhcb1, Lhcb2 and Lhcb3) (Allen, 1992). STN7 is the kinase that catalyses the switch from state I to state II (Bonardi et al., 2005). This reaction is reversed by the protein phosphatase PPH1/TAP38 (Pribil et al., 2010). The signal that induces the shift is the reduction state of the PQ pool. If the light received by the plant excites mainly PSII, the PQ pool will be more reduced, inducing state II. In the case of a light source that mainly excites PSI, the antenna is dephosphorylated and switches to state I (Vener et al., 1997). In the process of state transition, the heterodimer consisting of the main antenna is transferred, of which only Lhcb1 and Lhcb2 can be phosphorylated, Lhcb3 affects the time

frame required for the switch (Damkjaer et al., 2009). Interestingly, lines lacking the proteins involved in PGR5-mediated CEF show altered LHCII phosphorylation compared to WT or mutants lacking other components (Rühle et al., 2021).

2. Aims of the Work

The aim of this work was to investigate PGR5-mediated CEF and its role in plant light acclimation, and to identify novel components involved in this process. To achieve this, the following steps were taken:

1. Identification and investigation of alternative acclimation mechanisms by performing a *pgr5* suppressor screen under fluctuating light.
2. In-depth characterization of selected *pgr5* suppressor mutants and study of their role in light acclimation.
3. Detailed study of different lines with different PGR5 levels and functionality.

The overall aim was to improve our understanding of how plants respond to fluctuating light conditions depending on the PGR5-mediated CEF and to uncover new aspects involved in this process.

3. Materials and Methods

3.1 Chemicals

Chemicals that were used in the experiments were purchased from Applichem (Darmstadt, Germany), Invitrogen (Waltham, USA), Roth (Kalsruhe, Germany) and Sigma-Aldrich (St. Louis, USA).

3.2 Plant Material

The two *Arabidopsis thaliana* accessions Columbia-0 (Col-0) and Columbia-5 (Col-5), also known as glabia, were used as wild-type controls in this work. The knockout line *pgr5-1* was used for the *pgr5* suppressor screen (Munekage et al., 2002). The suppressor lines were generated by *pgr5-1* EMS mutagenesis. Seeds of the lines *pgr5-1* (Munekage et al., 2002), *pgr1* (Munekage et al., 2001) and *pgr5-1 pgr1* (Yamamoto & Shikanai, 2019) were provided by Prof. Dr. Shikanai. The T-DNA lines *pam68* (Armbruster et al., 2010), *psad1* (Ihnatowicz et al., 2004), *pgr1lab* (DalCorso et al., 2008) and *cgl160* (Rühle et al., 2014) were first described in the group of Prof. Dr. Leister. The knock-out line of NTRC (*ntrc*) (Perez-Ruiz et al., 2006) was provided by Prof. Dr. Cejudo. The knock-out line of FBPase was previously described in the work of Rojas-González and colleagues (Rojas-González et al., 2015) and was obtained from the NASC Institute collection (GK-472G06). The *pgr5-Cas* lines were generated by introducing a CRISPR/Cas9 construct specific for PGR5 into the Col-0 background. All double mutant lines further characterised in this work were generated by crossing the single mutant lines or by introducing a CRISPR/Cas9 construct specific for the target gene into the selected background (Col-0 or *pgr5-1*). Overexpression lines of PGR5 in the T₁ generation were provided by Prof. Dr. Shikanai.

3.3 Plant Growth Conditions

Seeds of the different lines were stratified (in the dark and at 4 °C for 48 h) and sown on potting soil (A210, Stender). After stratification, the pots were transferred to growth chambers at 22 °C and 60 % humidity, but with different light conditions: Long Day (LD, 16 h of light at 100 $\mu\text{mol photons m}^{-2} \text{ s}^{-1}$ and 8 h of darkness), short day, 8 h of light at 100 $\mu\text{mol photons m}^{-2} \text{ s}^{-1}$ and 16 h of darkness), High Light (HL, 16 h of light at 500 $\mu\text{mol photons m}^{-2} \text{ s}^{-1}$ and 8 h of darkness), fluctuating light (FL, 12 h light (with cycles

of 5 min at 50 $\mu\text{mol photons m}^{-2} \text{ s}^{-1}$ and 1 min at 500 $\mu\text{mol photons m}^{-2} \text{ s}^{-1}$) and 12 h dark), control light (12 h light at 100 $\mu\text{mol photons m}^{-2} \text{ s}^{-1}$ and 12 h dark)). Plants were grown for a period of time depending on the specific experiment, during which the parameters of humidity and illumination were controlled. For seedling experiments, sterilised seeds were sown on 0.5 % (w/v) MS medium (PhytoTechnology Laboratories, LLCTM, USA) and 0.7 % (w/v) agar plates with or without 1 % (w/v) sugar. For sterilisation, seeds were shaken in a solution containing 70 % (v/v) EtOH and 0.01 % (v/v) Tween-20 for 20 min, followed by shaking in 90 % (v/v) EtOH for 10 min. The seeds were then dried on sterile Whatman filter paper under a clean hood and transferred to the MS medium in Petri dishes. The Petri dishes were then wrapped in aluminium foil and stored in a refrigerator at 4 °C for 48 h to stratify the seeds. After stratification, the plates were transferred to different growth conditions as described above.

3.4 *pgr5* suppressor screen

To carry out the *pgr5* suppressor screen, *pgr5-1* seeds were mutagenised using ethylmethanesulphonate (EMS). The mutant plants were then propagated and selected for survival under FL. A subsequent selection was made by Fv/Fm. The final candidates were backcrossed with *pgr5-1* and the causative mutations were analysed by whole genome resequencing.

3.4.1 EMS-Mutagenesis

Approximately 500-600 mg of freshly harvested seeds (~ 20,000 M_0 seeds) from *pgr5-1* were placed in a 50 ml tube containing 35 ml H_2O and 30 mM EMS (Sigma-Aldrich, St. Louis, USA). The EMS was first solubilised by shaking the tube for 5 min. The seeds were incubated in the EMS solution for 15 h with shaking. After 15 h, the seeds were washed 30 times with 50 ml H_2O . The EMS solution was inactivated with 0.1 M NaOH. Finally, the mutagenised seeds (M_1) were dried on Whatman filter paper overnight (O/N) and sown in 40 batches of approximately 500 M_1 seeds each. Harvested seeds from each batch (M_2) were later used for selection under the specific conditions.

3.4.2 Selection of *pgr5* suppressor under fluctuating light

For selection of the *pgr5* suppressor under FL, trays containing approximately 3,000 seeds of the M_2 generation were stratified. After stratification, the M_2 plants were grown for 4 weeks under FL conditions (12 h light with cycles of 5 min at 50 $\mu\text{mol photons m}^{-2}$

s⁻¹ and 1 min at 500 $\mu\text{mol photons m}^{-2} \text{ s}^{-1}$). Most of the mutants died within this time frame. The surviving plants were selected and transferred to individual pots which were transferred to LD (16 h light at 100 $\mu\text{mol photons m}^{-2} \text{ s}^{-1}$ and 8 h dark) growth conditions. After two weeks of recovery under LD conditions, a second selection was made by measuring Fv/Fm (see below). Plants with a high Fv/Fm value were selected for backcrossing with the M₀ *pgr5-1* line. The backcrossed lines (F₁) were propagated in batches of 8,000 seeds under FL conditions and selected again in the next generation (F₂).

3.4.3 Whole genome extraction and sequencing

For each candidate suppressor of interest, plant material from a pool of 60-100 F₂ plants selected under FL was ground to a fine powder using liquid nitrogen. The ground sample was transferred to a beaker, kept cold on ice and mixed with 100 mL of cold extraction buffer (0.4 M sucrose, 10 mM Tris-HCl (pH 7), 1 % (v/v) beta-mercaptoethanol and 0.1 % (v/v) Triton X). The mixture was incubated for 10 min with stirring. After incubation, the material was filtered through two layers of Mira-cloth (Calbiochem) into a Falcon tube and centrifuged at 4 °C for 15 min at 2.500 g. The supernatant was discarded after the centrifugation step and the pellet resuspended in 1 mL of extraction buffer. The dissolved sample was then transferred to a 1.5 mL Eppendorf tube and pelleted by a further centrifugation step for 15 min at 2.500 g and 4 °C. Genomic DNA was extracted from the enriched nuclear sample using a Qiagen DNA extraction kit (Qiagen DNeasy Plant Mini Kit, Qiagen, Hilden, Germany) according to the manufacturer's instructions.

3.5 Photosynthetic measurements

To study the photosynthetic activity of the different genotypes, in vivo measurements of Chl fluorescence (using an Imaging-Pam, DUAL-PAM and DUAL-KLAS-NIR, (Walz, Effeltrich, Germany) and P700 absorption (using a DUAL-PAM and DUAL-KLAS-NIR) were performed. A number of different protocols were used to monitor specific photosynthetic mechanisms: induction-recovery curves (IRC), light curves (LC), fluctuating light (FL) measurement and fast oxidation of P700 (P700ox) (see below). Photosynthetic parameters were calculated by the Spec-Trophotometer software (Klughammer & Schreiber, 2008; Schreiber & Klughammer, 2008) and displayed as a graph or used for further analysis. Different PAMs were used depending on whether only the whole plant and PSII (Imaging-PAM spectrophotometer Walz, Effeltrich, Germany) or individual leaves and additionally PSI, PSII, Fd and PC (Dual/KLAS-NIR spectrophotometer (Walz,

Effeltrich, Germany)) were examined. The absorption maxima of plastocyanin, ferredoxin and P700 were determined before the specific protocol was carried out with the Dual/KLAS-NIR PAM.

3.5.1 Induction recovery curve (IRC)

To determine the photosynthetic activation/inactivation kinetics of PSI, PSII, Fd and PC, IRC was performed. Plants were incubated in the dark for 30 min prior to measurement. F_m and F_0 were determined by a saturation pulse (SP, 8,000 $\mu\text{mol photons m}^{-2} \text{s}^{-1}$ of 0.3 s) in the dark. Forty s later, actinic light was turned on for 360 s (induction period), followed by 180 s of darkness (recovery). Yield measurements were made by applying saturation pulses every 20 s for the duration of the curve. The intensity of the actinic light was adjusted to mimic growth conditions or different irradiance intensities: control light (110 $\mu\text{mol photons m}^{-2} \text{s}^{-1}$), mild HL (280 $\mu\text{mol photons m}^{-2} \text{s}^{-1}$), HL (580 $\mu\text{mol photons m}^{-2} \text{s}^{-1}$), strong HL (900 $\mu\text{mol photons m}^{-2} \text{s}^{-1}$) or LL (50 $\mu\text{mol photons m}^{-2} \text{s}^{-1}$).

3.5.2 IRC under different CO₂ concentrations

To measure the photosynthetic activity of PSII and PSI under different CO₂ concentrations, measurements were performed with the Dual/KLAS-NIR PAM and the GFS-3000 gas exchange system (Walz, Effeltrich, Germany). The IRC measurements were performed as described above with an additional incubation of the leaf for 15 min under 0 ppm, 400 ppm and 800 ppm CO₂.

3.5.3 Fast oxidation of P700

The rapid oxidation of P700 was measured to provide information on CEF activity. For the measurement, plants were incubated in the dark for 30 min. After the dark incubation, the leaves were exposed to actinic light (600 $\mu\text{mol photons m}^{-2} \text{s}^{-1}$) for 5 s. The light was then switched off for 2 s to allow complete reduction of P700, followed by 23 s of exposure to far-red (FR) light and recording of the oxidation state of P700. For analysis, the data were normalised by setting the minimum to 0 and the maximum to 1. The normalised data were used to determine the half-life of P700 oxidation, expressed as $t_{1/2}\text{P700ox}$.

3.5.4 Light curve

In order to measure photosynthetic parameters at steady state with different illumination intensities, a light curve was performed with the Dual/KLAS-NIR. The dark-adapted leaf was illuminated with actinic light. After 3 min a saturation pulse was applied and the light intensity was increased stepwise from 0 $\mu\text{mol photons m}^{-2} \text{s}^{-1}$ to 830 $\mu\text{mol photons m}^{-2} \text{s}^{-1}$ every 3 min.

3.6 Blue Native (BN)

A 4 %-12 % native gradient gel was made as described in Schagger et al. (Schagger et al., 1994). The gradient gel was loaded with the prepared samples and stained cathode buffer (50 mM Tricine, 15 mM Bis-Tris and 0.02 % (w/v) Coomassie-G; pH 7.0) and anode buffer (50 mM Bis-Tris; pH 7.0) were added. BN-PAGE was run over night at 30 mA per gel at 4 °C. When the running front of the sample reached the halfway point of the gel, the stained cathodic buffer was replaced by unstained cathodic buffer (50 mM Tricine and 15 mM Bis-TrisM; pH 7.0). Band separation was documented by scanning after an additional 2 hours of running.

3.6.1 Thylakoid Extraction

The rosette of five-week-old plants grown under 12 h of light (100 $\mu\text{mol photons m}^{-2} \text{s}^{-1}$) was harvested separately for each genotype. The samples were ground three times for 3 s in a cold blender with thylakoid extraction buffer 1 (0.4 M sorbitol and 0.1 M Tricine pH 7.8). After the mixing step, the samples were filtered through two layers of Miracloth and centrifuged at 4,000 g and 4 °C for 10 min. The supernatant was discarded and the pellet was dissolved by gentle pipetting in extraction buffer 2 (20 mM HEPES pH 7.5 and 10 mM EDTA). The dissolved pellet was lysed on ice for 10 min and centrifuged at 10,000 g for 10 min at 4 °C. Centrifugation enriched the thylakoid membrane in the pellet. The supernatant was discarded and the pellet was resuspended in extraction buffer 2, followed by Chl quantification.

3.6.2 Sample preparation for BN-PAGE

For samples to be loaded on the BN-Page, a volume containing 250 μg Chl was washed twice with wash buffer (25 mM Bis-Tris/HCl (pH 7.0) and 20 % glycerol). The pellet was then resuspended in solubilisation buffer (25 mM Bis-Tris/HCl pH 7.0, 20 % glycerol and

1 % n-dodecyl-beta-D-maltosid). The sample was then incubated on ice for 10 min, followed by centrifugation at 12,000 g for 10 min at 4 °C. Finally, the supernatant was transferred to a new reaction tube with 1/10 of the volume added as BN sample buffer (100 mM BisTris/HCl pH 7.0, 750 mM 6-ACA and 5 % (w/v) Comassie-G).

3.7 Protein Extraction and Immunoblot Analysis

For immunoblotting analysis, proteins were extracted from whole leaves. Leaf material from wellgrown Arabidopsis plants was weighed and disrupted using the TissueLyser II (Qiagen, Hilden, Germany). Sample buffer was added to the material in a 1:10 ratio and incubated at 70 °C for 5 min, followed by centrifugation at 16,000 g for 10 min. The supernatant was loaded onto 10 % Tricine-SDS PAGEs (Schagger, 2006). Cathode buffer (100 mM Tris, 100 mM Tricine, 0.1 % (v/v) SDS and 1 mM EDTA; pH 8.9) and anode buffer (200 mM Tris; pH 8.9) were used for the run. The gel was run until the running front of the samples exited the gel. Separated proteins were transferred from the gel to a polyvinylidene fluoride (PVDF) membrane by semi-dry blotting with a three-buffer system (anode buffer I: 300 mM Tris; pH 10.4; anode buffer II: Tris 25 mM; pH 10.4; Cathodic buffer: Tris 25 mM, amino-caproic acid 40 mM; pH 9.4). A PVDF membrane with a pore size of 0.2 µm was used for Western blotting of proteins smaller than 20 kDa, while a pore size of 0.45 µm was used for larger proteins. Transfer was performed using a Trans-Blot Turbo system (Bio-Rad, Hercules, USA). After blotting, the membranes were dried and reactivated with methanol to ensure protein binding to the membrane and stained with Commassie Brilliant Blue. The staining of the membranes was used to visualise proteins (Lhcs, Rubisco large subunit and Rubisco small subunit) by washing with destaining solution I (10 % acetic acid and 40 % methanol) for 15 min followed by destaining solution II (10 % acetic acid and 90 % methanol) for 5 min. Commassie Brilliant Blue staining of the larger Rubisco subunit was used as a loaded control. After scanning, the blue staining was completely removed by washing with methanol. Subsequently, non-specific signals on the membrane were minimised by blocking with 5 % milk in TBS-T (20 mM Tris, 150 mM NaCl pH 7.5 and 0.25 % (v/v) Tween° 20) for 1 h at room temperature, followed by O/N incubation with primary antibodies. The primary antibodies were used at a dilution in TBS-T (Table 1). The antibody was decanted and the membrane was washed three times for 15 min with TBS-T and shaking. At room temperature, the membrane was incubated with the secondary antibody for one hour with shaking and then washed three times with TBS-T. To visualise the signal on the membrane, ECL solution

(Agrisera ECL kit Bright/SuperBright, Agrisera, Vännäs, Sweden) was added and the signal was detected using an ECL reader (Fusion FX, Vilber Lourmat, Eberhard-zell, Germany).

Table 1: Antibodies used in the thesis.

antibody	dilution	Dissolved in	Supplier
α -CGL160	1:5.000	TBS-T	Thilo Rühle
α -CP47	1:2.000	TBS-T	Agrisera
α -Cyt b6	1:5.000	TBS-T	Agrisera
α -Cyt f	1:5.000	TBS-T	Agrisera
α -FBPas	1:20.000	TBS-T	Agrisera
α -Lhca1	1:2.000	TBS-T	Agrisera
α -LhcB2	1:5.000	TBS-T	Agrisera
α -NDHB	1:1.000	TBS-T	Agrisera
α -NTRC	1:2.000	TBS-T	Francisco Javier Cejudo
α -PC	1:2.000	TBS-T	Agrisera
α -PetC	1:5.000	TBS-T	Agrisera
α -PGR5	1:2.500	TBS-T	Toshiharu Shikanai
α -PGRL1	1:10.000	TBS-T	Dario Leister
α -PsaA	1:5.000	TBS-T	Agrisera
α -PsaD	1:5.000	TBS-T	Agrisera
α -PSBE/F	1:5.000	TBS-T	Agrisera
α -PsbO	1:5.000	TBS-T	Agrisera

3.8 DNA-extraction

A leaf from a wellgrown *Arabidopsis thaliana* plant was incubated over night (for 12 h) in 500 µl CTAB buffer (1 % CTAB, 0.7 M NaCl, 500 mM Tris (pH 8.0) and 10 mM EDTA; pH 8.0) at 65 °C. After incubation, the sample was incubated on ice for 10 min, then 500 µl of chloroform was added and mixed by vigorous vortexing. The organic and inorganic phases were separated by centrifugation for 10 min at 16,000 g and 4 °C. The upper phase was transferred to a new Eppendorf tube, 500 µl of isopropanol was added and the mixture was centrifuged for 30 min at 16,000 g. The supernatant was removed and the pellet was washed with 1 ml of 70 % EtOH and dried. DNA was dissolved in 20-50 µl ddH₂O and the concentration was measured using a NanoDrop 2000 (Thermo Fisher Scientific, Waltham, USA).

3.9 PCR

To amplify specific DNA sequences by PCR, 20 nucleotide long oligonucleotides were designed to target the sequence of interest. The primer pairs were tested for specificity using the Primer BLAST function of the website: <https://www.ncbi.nlm.nih.gov/tools/primer-blast/> (27.01.2023), and *Arabidopsis thaliana* was selected as the target organism. Primers with high specificity for the sequence of interest were selected and ordered from Metabion (Planegg, Germany). PCR was performed using Verify Polymerase (PCR Biosystems Inc., Pennsylvania, USA) or Q5 Polymerase (New England BioLabs, Ipswich, USA) according to the manufacturer's instructions.

3.10 RNA-extraction

For RNA extraction, 60 mg of leaf material was harvested and frozen with liquid nitrogen. The sample material was ground under freezing conditions at 30 Hz for 1 min using the TissueLyzer (Qiagen Venlo, The Netherlands). After grinding, 1 ml of TRIzol (Thermo Fisher Scientific, Waltham, USA) was added and mixed by inversion. After mixing, the samples were centrifuged for 10 min at 4 °C and 12,000 g and the supernatants were transferred to new Eppendorf tubes. The samples were then incubated at room temperature (RT) for 5 min, followed by the addition of 200 µl of chloroform and vigorous mixing. The samples were incubated for a further 2 min at room temperature (RT) and centrifuged for 15 min at 4 °C and 12,000 g. After centrifugation, the upper phase was transferred to a new tube containing 500 µl of isopropanol and mixed by inversion. A further

incubation step was performed at RT, followed by centrifugation for 10 min at 12,000 g and 4 °C. The pellet was washed with 1 ml of 75 % EtOH and centrifuged at 7,500 g for 5 min at 4 °C. The washing step was repeated a second time and the pellet was dried. The RNA pellet was resuspended in ddH₂O by incubation at 55 °C for 10 min. The concentration of the isolated RNA was measured in a volume of 1 µl using a nanodrop.

3.11 DNase treatment of RNA

From the total amount of extracted RNA, 10 µg of RNA was pelleted and dissolved in DNase I reaction buffer mixed with 1 µl of DNase and incubated at 37 °C for 10 min. After incubation, EDTA (5 mM final concentration) was added and the sample was heated to 75 °C for 10 min to stop the reaction. After inactivation, 3 M NaAcet was added in a volume of 1/10 and twice the volume of the sample in EtOH. The RNA was then precipitated O/N at -20 °C. The next day, the RNA was pelleted by centrifugation at 12,000 g for 15 min at 4 °C, followed by washing with 75 % EtOH. After washing, the RNA was dissolved in ddH₂O and the concentration determined.

3.12 cDNA-Synthesis

To clone the genes of interest, cDNA was synthesised from extracted RNA. The iScript™ cDNA Synthesis Kit (Bio-Rad, Hercules, USA) was used according to the instructions. 500 ng of RNA was used as template. The cDNA was diluted to a concentration of 2 ng/µl.

3.13 Gateway cloning

For Gateway Invitrogen cloning, cDNA extracted from Col-0 was used to generate a PCR fragment of the gene of interest by PCR. Primers specific for the sequence of the gene of interest and including the attb sequences were designed. A PCR was performed and the fragment with the estimated size of the gene was purified from an agarose gel. The purified fragment was cloned into the donor vector (pDONR-207) by a BP reaction to generate an entry clone. The reaction was performed according to the manual (Gateway, Invitrogen, Waltham, USA) O/N and used to transform competent *E. coli* cells. The *E. coli* cells were selected on an appropriate antibiotic and the surviving colonies were used to inoculate a liquid LB culture. The culture was grown O/N followed by plasmid extraction via minprep (EasyPure Plasmid MiniPrep Kit; TransGen Bio-tech, Beijing, China). In the

next step, the entry clone was combined with the destination vector (pGWB5, pGWB14 and pBifc-2in1-CC) in an LR reaction performed according to the instructions in the manual (Gateway, Invitrogen, Waltham, USA). An expression vector was generated from this reaction and transformed into *E. coli*, followed by selection for positive transformed colonies. A miniprep of a liquid culture was performed from a positively selected colony. The DNA obtained was transformed into agrobacteria strain GV3101, which was later used for plant transformation by flower dipping.

3.14 CRISPR-Cas

The different CAS lines of the genes of interest were generated by CRISPR/Cas in the background of Col-0 or *pgr5-1*. A vector with an oocyte-specific promoter, the pHEE401-E (Wang et al., 2015), was ligated via a GoldenGate reaction with the guide RNAs (gRNAs) designed using the web tools CRISPOR (<http://crispor.tefor.net/> 18.02.2023). In the next step, *E. coli* cells (strain Dh5 α) were transformed with the construct. Positive cells were selected and used for miniprep. After checking for inaccuracies in the construct by sequencing the gRNA DB3.1, agrobacteria (strain GV3101) were transformed with the construct.

GoldenGate reaction		program		
pHEE401-E	1 μ l (100 ng/ μ l)	37 °C	2 min	30x
gRNA	2 μ l (0.2 μ M)	16 °C	2 min	
Cutsmart buffer	1.5 μ l	50 °C	50 min	
ATP	1.5 μ l (10 mM)	80 °C	80 min	
Ligase	1 μ l	16 °C	∞	
BsaI	1 μ l			
H ₂ O	7 μ l			

3.15 *E. coli* transformation by heat shock

For transformation of DH5 α *E. coli* cultures, competent cells were thawed on ice from a -80 °C frozen stock. After 5 min of incubation on ice, the plasmids were added to the cells and the mixtures were incubated for 30 min on ice. The cells were then heated to 42 °C for 90 s, followed by a further incubation on ice for 5 min. After the cold shock on ice, 1 ml of LB medium (0.5 % (w/v) yeast extract, 0.5 % (w/v) NaCl and 1 % (w/v) peptone; pH 7.5) was added to the cells and transferred to 37 °C with shaking for 1 hour. In the final step of *E. coli* transformation, the cells were plated on LB medium containing the appropriate antibiotic for O/N cell selection at 37 °C.

3.16 Transformation of *A. tumefaciens*

Competent cells of *Agrobacterium tumefaciens* strain GV3101 were thawed on ice for 5 min, followed by the addition of 500 ng of the plasmid to be transformed into the cells and further incubation on ice for 5 min. After incubation, the cells were shock frozen in liquid nitrogen for 2 min and heat shocked by heating the cells to 37 °C for 1 min. After heat shock, the cells were incubated in LB medium for 4 hours at 28 °C. Finally, the cells were plated on LB plates containing the appropriate antibiotic for cell selection and selected at 28 °C for 3 days.

3.17 BIFC-interaction assay /GFP-localization of proteins

To analyse an interaction between two proteins, their coding sequences were cloned into the pBIFC-2in1-CC vector (Grefen & Blatt, 2012). The resulting vectors were transformed into agrobacteria strain GV3101. After transformation, one colony was picked and used for infiltration of *Nicotiana benthamiana* leaves.

3.18 GFP-localization of proteins

To localise proteins in the plant cell, a construct of the protein of interest fused to GFP was expressed in *Nicotiana benthamiana* leaves. This construct was made by cloning the CDS of the gene of interest into the Gateway vector pGWB5. This vector was then transferred into GV3101 cells. The positively selected transformed cells were then used to infiltrate *Nicotiana benthamiana* leaves.

3.19 *Nicotiana benthamiana* leaf infiltration

Two-week-old *Nicotiana benthamiana* plants grown under greenhouse conditions (22 °C, 60 % humidity, 16 h light at 100 $\mu\text{mol photons m}^{-2} \text{s}^{-1}$ and 8 h dark) were selected for leaf infiltration with transformed *Agrobacterium tumefaciens* GV3101. The *Agrobacterium* strains were grown O/N in LB medium plus the appropriate antibiotic for the selection at 28 °C with shaking. After 24 h of growth, OD₆₀₀ was measured and cells were harvested by spinning the cultures at 2,000 g for 20 min. The cells were resuspended in 5 ml infiltration medium (85 mM NaH₂PO₄, 15 mM Na₂HPO₄ and 25 mM MgCl) at an OD₆₀₀ density of 0.3 and incubated for 2 h at 28 °C with shaking. After incubation, the cells were filled into a 1 ml syringe and carefully introduced into the abaxis of the leaves by applying constant light pressure on the syringe. After infiltration, the leaves were carefully dried with a paper towel and transferred to the dark for 12 hours. After the dark phase, *Nicotiana benthamiana* plants were grown for three days, followed by protoplast extraction or detection of fluorescence signal in leaf discs.

3.20 Protoplast extraction

For protoplast extraction, infiltrated *Nicotiana benthamiana* leaves were cut into small strips (~1 mm) and incubated in an enzyme solution (0.01 % Macerozyme R10, 0.1 % Driselase and 0.2 % Cellulase "Onzuka" dissolved in 10 mM MES pH 5.6 and 10 mM MgCl₂) and protoplast medium (4.3 g/L MS, 0.5 g/L MES pH 5.6, 20 g/L sucrose and 80 g/L mannitol). Leaves are incubated in the enzyme solution for 2 hours in the dark with constant shaking. After incubation in the dark, the protoplast solution was used for detection and localisation of the protein of interest fused to GFP by microscopy.

3.21 Pigment Measurements

Approximately 100 mg of fresh leaf material was frozen in liquid nitrogen and ground. The measurement of Chl content was normalised to fresh weight (FW). The ground material was then incubated in 2 ml 80 % [v/v] acetone at 4 °C O/N in the dark with shaking, and the sample was centrifuged to separate the extracted Chl in the supernatant from the plant debris. The extract was measured according to the method described by Lichtenthaler and Wellburn (Lichtenthaler & Wellburn, 1983). For the measurement of anthocyanins, 300 μl of 1 % [v/v] HCl in methanol was added to the ground material and the anthocyanins of the leaves were extracted overnight by shaking at 4 °C without light.

Approximately 500 µl of chloroform and 200 µl of distilled water were added to the sample and mixed vigorously. Phase separation was achieved by centrifugation at maximum speed for 5 min. Then 400 µl of the upper phase was transferred to a new tube and made up to a final volume of 800 µl by adding 400 µl of acidified methanol (60 % methanol, 1 % HCl, 40 % water) to each tube. To calculate the anthocyanin content, the absorptions at 530 nm and 657 nm were measured using a spectrophotometer (Ultra-spec 2100 pro; Biochrom, Holliston, MA, USA). The measured values were entered into the formula: $(A_{530} - 0.25 * A_{657}) * \frac{TV}{FW}$

Neff and Chory 1998, *TV*=total volume of extract (800µl), *FW*= fresh weight.

3.22 Data analysis and visualization

Data analysis of PAM measurements, pigment levels or other measurements were analysed using the Microsoft Office Excel program. The significance of the values was calculated using the web tool (https://astatsa.com/OneWay_Anova_with_TukeyHSD/ (12-02-2023)) using post hoc Tukey HSD. Charts and graphs were created using ex-cel. Final figures were created using CorelDraw and later exported as JPG or PNG.

3.23 Bioinformatic tools

The sequences of genes and proteins were acquired from online resources: the Arabidopsis Information Resource (TAIR), which is a database dedicated to Arabidopsis research (<http://www.arabidopsis.org>), the Universal Protein Resource (Uniprot; <http://www.uniprot.org/>), and the plant membrane protein database (Aramemnon; <http://aramemnon.uni-koeln.de/>).

For the sequence alignment and the generation of phylogenetic trees, the program QIAGEN CLC Main Workbench was used.

To find the localization of the T-DNA insertions and primers for genotyping, the webpage T-DNA Express from the SALK institute was used (<http://signal.salk.edu/cgi-bin/tdnaexpress>).

The tool that was used to predict the structure of a protein and the interaction between proteins is the web tool Alphafold2 (<https://colab.research.google.com/github/sokrypton/ColabFold/blob/main/AlphaFold2.ipynb>).

Calculation of significance was performed with the web tool One-way ANOVA with post-hoc Tukey HSD (https://astatsa.com/OneWay_Anova_with_TukeyHSD/).

For the generation of the expression map in the different tissues of Arabidopsis, the website BAR ePlant was used (<https://bar.utoronto.ca/eplant/>).

3.24 Accession number of genes and proteins

Gene	ATG-number	Accession
<i>ACHT2</i>	AT4G29670	Q8LCT3
<i>CGL160</i>	AT2G31040	O82279
<i>CFBP1</i>	AT3G54050	P25851
<i>LAP66</i>	AT5G48910	Q9FI80
<i>NTRC</i>	AT2G41680	O22229
<i>PAM68</i>	AT4G19100	O49668
<i>PGR1</i>	AT4G03280	Q9ZR03
<i>PGR5</i>	AT2G05620	Q9SL05
<i>PGRL1A</i>	AT4G22890	Q8H112
<i>PGRL1B</i>	AT4G11960	Q8GYC7
<i>PGRL2</i>	AT5G59400	F4KJ54
<i>PSAD1</i>	AT4G02770	Q9S7H1
<i>S261</i>	AT2G27290	A0A654EY72

Materials and Methods

Table 2: **Vector-list**

Name	Resistance in bacteria	resistance in plants	tag	usage
pDONR207	Gentamycin	non	non	used for entry vector in Gateway cloning
pDONR221	Gentamycin	non	non	used for entry vector in Gateway cloning (specific pBIFC-2in1-CC)
pGWB5	Kanamycin	Hygromycin	GFP	used for overexpression of protein of interest tagged with GFP (localization)
pGWB14	Kanamycin	Hygromycin	HA	used for overexpression of protein of interest tagged with HA-tag
pGW7GH2	Spectomycin	Hygromycin	non	used for overexpression without tag
pAlligator3	Spectomycin	GFP-seedcoat	non	used for overexpression without tag and selection through fast selection cassette
pBIFC-2in1-CC	Spectomycin	non	split YFP	used to investigate interaction of two proteins at their C-terminus

Table 3: **Primer-list**

Primer name	Sequence 5'-3'	Usage	Gene target
Genotyping			
PAM68 LP	TGATTCCAACCTTAATGGCGTC	Genotyping	<i>PAM68</i>
PAM68 RP	CTCAAGCATGCCTCTTCTGAG		
PGRL1A LB	CCAAAGAAGGAGGTGTTTTCC	Genotyping	<i>PGRL1A</i>
PGRL1A RB	CAAGAGTTTCTCCAAGCGTTG		
PGRL1B LB	GTTTGGGAACACAGTGGCTT	Genotyping	<i>PGRL1B</i>

PGRL1B RB	ATCAAGGAGGTCCACAAGTCT		
PsaD1-LB	ATGGCAACTCAAGCCGCCGG	Genotyping	<i>PsaD1</i>
PsaD1-RB	TATGGTTTTGGATCGGAGACT		
NTRC Fw	TCACCAACATGTGGCCC	Genotyping	<i>NTRC</i>
NTRC Rv	TTCTTCATCTTCACACCCGA		
PGR5 Fw	AGGTGATCACTGAGTTTTGC	Genotyping	<i>PGR5</i> (<i>pgr5-1</i>)
PGR5 Rv	TTCTTTTTAAGACCTAAGCA		
LPA66 RP	GATGA- TATCGGGTTATTCGCTGAACGG	Genotyping	<i>LPA66</i>
LPA66 LP	GTGAAAACGTTTCCGGTCTCG- TACC		
mTERF5_59_LP	TCCATTGAACTCCAAGAGTGG	Genotyping	<i>mTERF5</i>
mTERF5_59_RP	AACCGATAACCTGAAACCGAC		
CGL160-LB	AAGTTAAGATTCCATTTTCG CATC	Genotyping	<i>CGL160</i>
CGL160-RB	TCCCTAAACATCACATCCTG C		
PGR5-CAS_fw	TGCCTACTAGGTTGCGTGTG	Genotyping	<i>PGR5</i> (<i>pgr5-cas</i>)
PGR5-CAS_rev	CTGCTTCGATTTCTGCAATAG		
S261-Cas-g-fwd	ATTACTCTGGAACCTCTA	Genotyping	<i>S261-Cas</i>
S261-Cas-g-rv	ACATCAACACCGGAAGTCACA		
ACHT2-Cas-g-fwd	ATCTGCGTTCCGTGTTAAAA	Genotyping	<i>ACHT2-Cas</i>
ACHT2-Cas-g-rv	TCAATAGCATCACCGTCTCT		
Hcef1_LP	GATATCTCAGCTCTTGGGTC	Genotyping	<i>CFBP</i>
Hcef1_RP	GATGTATCTCAGTCGGTTGG		
GBKT	ATATTGACCATCATACTCATTGC	Genotyping	GK-lines
LBb1.3	ATTTTGCCGATTTTCGGAAC	Genotyping	SALK-lines

Materials and Methods

SAIL-LB	GCATCTGAATTTTCATAAC- CAATCTCGATACAC	Genotyping	SAIL-lines
CRISPR/Cas			
S261_Cas_fwd	ATTGTCCTCCGCCTTCTCACGGA	gRNA	S261-Cas
S261_Cas_rev	AAACTCCGTGAGAAGGCG- GAGGA		
CAS_ACT2_gR NA_s	ATTGACACGAACCACTTGGCTCT	gRNA	ACHT2- Cas
CAS_ACHT2_g RNA_as	AAACAGAGCCAAGTGGTTCGTGT C		
Cloning			
attB1-S261- ATG-for	AAAAA- GCAGGCTTCATGGCGATGATGCT TCTG	Localiza- tion-GFP	S261
attB2-S261-non- stop-rev	AGAAAGCTGGGTCCTT- GTCATCATCCTTCTC		
BIFC-S261-Fw	GGGACAAGTTTGTACAAAAAA- GCAGGCTTAATGGCGATGATGCT TCTGCAAA	BIFC	S261
BIFC-S261-Rv	GGGACAAC TTTGTATA- GAAAAGTTGGGTGCTT- GTCATCATCCTTCTCCTTGTC		
BIFC-prps1-Fw	GGGACAAGTTTGTACAAAAAA- GCAGGCTTAATGGCGTCTTT- GGCTCAGCA	BIFC	PRPS1
BIFC-prps1-Rv	GGGACAAC TTTGTATA- GAAAAGTTGGGTGAA- TATCAACTGCAGAAGGAA		

Materials and Methods

PGR5-attB3-fw	GGGGACAACCTTTGTATAA- TAAAGTT- GGAATGATGGCTGCTGCTTCGAT TTCT	BIFC	PGR5
PGR5-attB2-rev	GGGGACCACTTTGTACAAGAAA- GCTGGGTGAGCAAGGAAACCAA- GCCTCTCT		

4. Results

4.1 *pgr5-1* phenotype under control and fluctuating light conditions

The PGR5-deficient line *pgr5-1* (Munekage et al., 2002) was used to achieve the aims of this work. The *pgr5-1* mutant was generated in an EMS screen (Shikanai et al., 1999). The mutation in the *PGR5* gene (AT2G05620) resulted in an amino acid exchange at position 130 (G130S) and destabilisation of the PGR5 protein (Munekage et al., 2002).

It has been shown that in the absence of PGR5, the antimycin A-sensitive pathway of CEF is severely compromised (Munekage et al., 2002; Rühle et al., 2021), resulting in retarded growth or even plant death under FL and HL conditions (Barbato et al., 2020; Munekage et al., 2002; Suorsa et al., 2012; Tikkanen et al., 2010). Under LD growth conditions ($100 \mu\text{mol photons m}^{-2} \text{s}^{-1}$), the *pgr5-1* mutant showed no differences in growth compared to the WT control (Col-5). The duration of illumination, such as short day or 12 h light / 12 h dark conditions, also had little effect on *pgr5-1* (Figure 4A). However, when plants were grown under fluctuating light (FL), the *pgr5-1* mutant showed a lethal phenotype at the seedling developmental stage (Figure 4A) (Suorsa et al., 2012). Under these conditions, plants are exposed to cycles of low light interrupted by high light peaks repeated during the day; in our case, cycles of 5 min at $50 \mu\text{mol photons m}^{-2} \text{s}^{-1}$ and 1 min at $500 \mu\text{mol photons m}^{-2} \text{s}^{-1}$ for 12 h, followed by 12 h of darkness (Tikkanen et al., 2010). Further examination of the amount of PGR5 protein detectable in the *pgr5-1* line showed that the accumulation of PGR5 was severely impaired, and in some cases only a minimal amount of the mutant PGR5_{G130S} could be detected (Figure 4B).

In addition, the CEF-related parameters, maximum transient NPQ (tNPQ_{max}), measured as the NPQ maximum in dark-adapted leaves upon illumination (Munekage et al., 2002), and the parameter assessing the time required to oxidise half of the total P700 (t_{1/2}P700_{ox}), were determined in the *pgr5-1* mutant. Efficient tNPQ_{max} requires an active PGR5-mediated CEF, which leads to a rapid acidification of the lumen after a dark to light transition (Munekage et al., 2002). Plants lacking PGR5 cannot induce non-photochemical quenching at the level of the WT after a dark/light transition (Figure 4C) (Munekage et al., 2002). This defect in NPQ induction is explained by a reduced formation of the proton gradient across the thylakoid membrane, which is one of the major functions attributed to PGR5 (Munekage et al., 2002). Furthermore, the measurement of t_{1/2}P700_{ox} indicates the half-life oxidation rate for fully reduced P700 using far-red light

(FR), which preferentially oxidises PSI. The half-life is prolonged by a more active CEF because electrons are preferentially transferred to the PQ pool instead of the FNR, where they would leave the reduction cycle of P700 (Okegawa et al., 2008). Thus, P700 is oxidised faster in the *pgr5-1* mutant than in the WT, indicating a lower active CEF (Figure 4C) (Nandha et al., 2007).

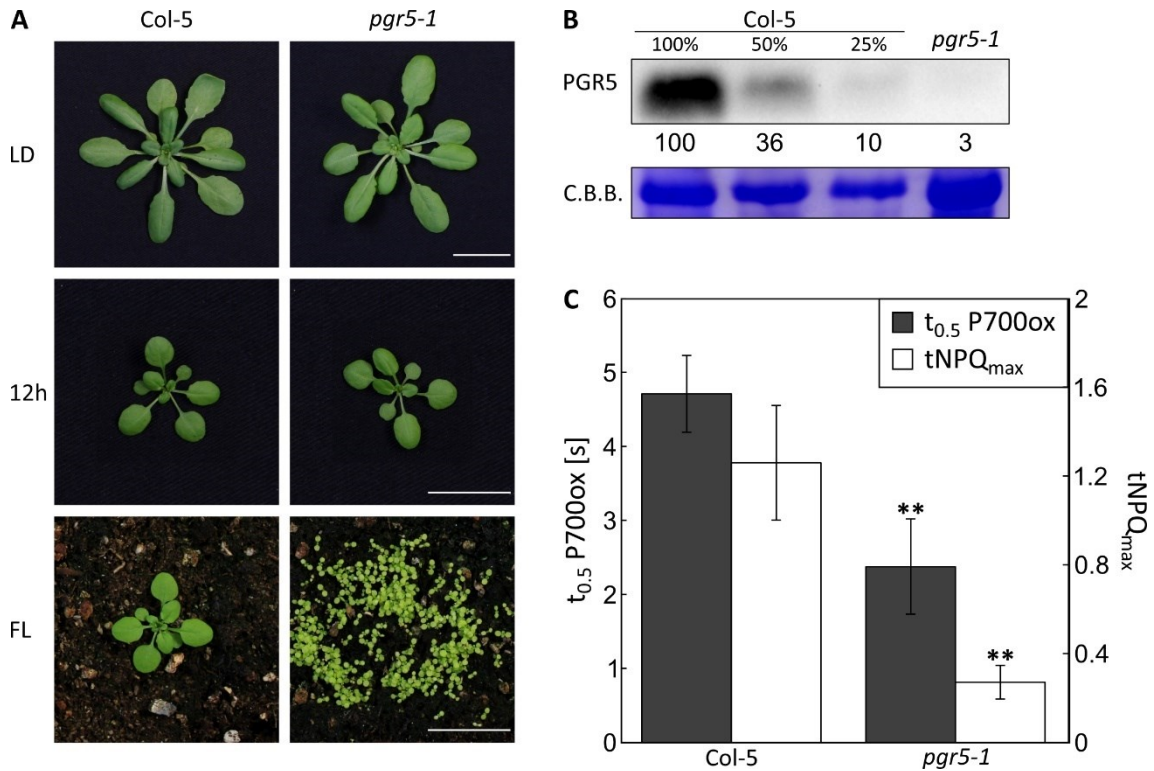


Figure 4: *pgr5-1* shows a lethal phenotype under FL and impaired CEF-related parameters. **A**, Growth phenotype of 3-week-old Col-5 and *pgr5-1* plants grown under long-day conditions ($100 \mu\text{mol photons m}^{-2} \text{ s}^{-1}$) for 16 h light (LD) or 12 h light / 12 h dark and the same genotypes grown for 3 weeks under fluctuating light (12 h light, cycles of low light ($50 \mu\text{mol photons m}^{-2} \text{ s}^{-1}$) for 5 min and high light ($500 \mu\text{mol photons m}^{-2} \text{ s}^{-1}$)). The scale bar corresponds to 2 cm. **B**, Immunodetection of PGR5 protein extraction from whole leaves of Col-5 and *pgr5-1* plants grown under LD conditions for 3 weeks. A 10 % Tris/Tricine gel was loaded with 3 ng of sample. The numbers below indicate the intensity of the detected band relative to the Col-5 100 % band. Coomassie Brilliant Blue (C.B.B.) represents protein loading. One representative blot out of three is shown. **C**, Mean time required to oxidise 50 % of P700 ($t_{1/2}\text{P700ox}$) (grey). Plants grown under the LD conditions shown in (A) were dark adapted for 30 min followed by illumination with actinic light ($660 \mu\text{mol photons m}^{-2} \text{ s}^{-1}$) for 5 s, then the light was switched off for 2 s. After the dark period, the plants were exposed to far-red light (FR) and the P700 oxidation state was observed by measuring the absorbance at 875 nm minus the absorbance at 830 nm. Mean of maximum transient non-photochemical quenching ($t\text{NPQ}_{\text{max}}$) after a dark to light transition (white). Plants were dark adapted followed by 6 min of actinic light ($100 \mu\text{mol photons m}^{-2} \text{ s}^{-1}$) to induce photosynthesis. After illumination, plants were allowed to recover in the dark for 3 min. During the induction and recovery periods, non-photochemical quenching values were obtained by applying saturation pulses every 20 s. Eight replicates were measured for each genotype. Error bars indicate \pm SD. Statistical differences were determined by Tukey's test (**= $p < 0.01$).

4.2 *pgr5-1* suppressor screen

The lethal phenotype of plants deficient in PGR5-mediated CEF under fluctuating light was the starting point to identify additional factors such as proteins or pathways involved in light acclimation under these conditions, which resemble natural light flux.

A suppressor screen for the lethal phenotype of *pgr5-1* under FL was performed by mutagenizing the *pgr5-1* line (M_0) with EMS and selecting survivors in subsequent generations (Figure 5). EMS generates random mutations leading to three possible outcomes: a silent mutation, a nonsense mutation or a missense mutation. For the screen, approximately 20,000 M_0 seeds were mutated according to the protocol described (Maple & Møller, 2007). The *pgr5-1* mutant seeds, now called M_1 seeds, were propagated under standard LD growing conditions in batches of 500 plants, resulting in 40 M_1 batches. The next generation of plants (M_2) was selected under fluctuating light (low light 50 $\mu\text{mol photons m}^{-2} \text{s}^{-1}$ for 5 min followed by high light 500 $\mu\text{mol photons m}^{-2} \text{s}^{-1}$ for 1 minute) in a sample size of 3,000 plants per tray. After screening 273.00 M_2 plants, the screening process reached saturation as only genes were rediscovered, that were already known to be responsible for suppression. These M_2 seeds were screened from the different M_1 batches (about 16 M_2 per 1 M_1). The surviving plants (*pgr5-1* suppressor candidates) were selected and further grown under standard light (100 $\mu\text{mol photons m}^{-2} \text{s}^{-1}$). The suppressor candidates were genotyped for the *pgr5-1* mutation and, after confirmation, a small number of contaminants (WT allele for PGR5) were detected and removed. However, not all suppressors produce seeds, which reduced the number of selected M_2 candidates from 496 to 332 M_3 lines (Figure 6A). Since a PSII mutant in the *pgr5-1* background has already been described to be able to suppress the lethality of *pgr5-1* under FL (Suorsa et al., 2016), a Fv/Fm screening was set up. In an additional step, the Fv/Fm of the surviving candidates was measured to distinguish between suppressors with PSII mutation (low Fv/Fm) and others (Figure 6B). This was necessary because the activity of PSII can be affected in many ways, for example by assembly factors, stability proteins, or more directly by the abundance or activity of the subunits themselves. A quarter of the selected suppressors showed a WT-like Fv/Fm higher than 0.78, while $\text{Fv/Fm} < 0.4$, indicating severe PSII impairment, was observed in 14 selected suppressors (Figure 5B). Suppressors with higher Fv/Fm (from 0.7) were selected and backcrossed to the *pgr5-1* line and the resulting crosses were propagated (F_2) (Figure 5).

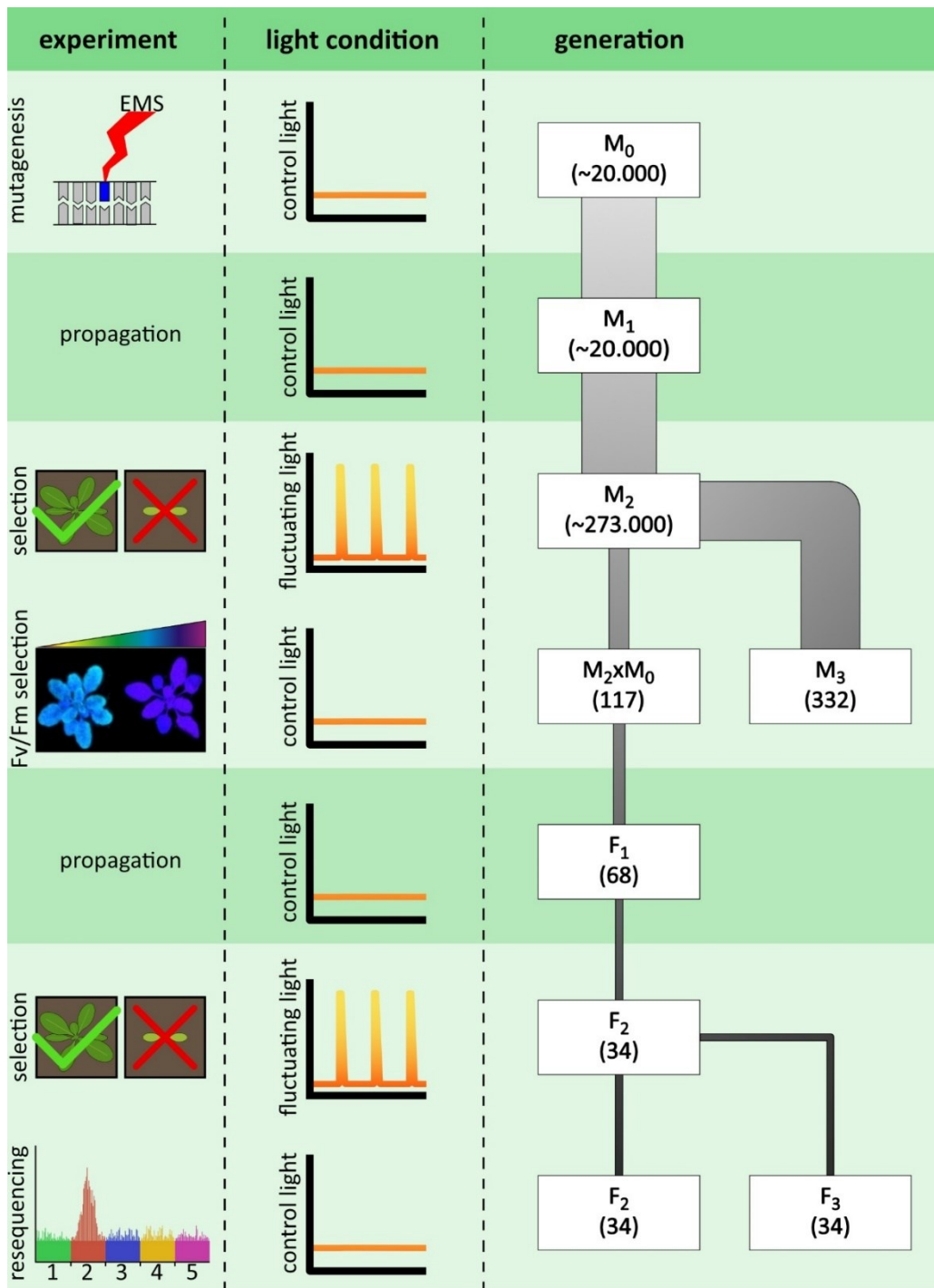


Figure 5: *pgr5-1* suppressor screen. *pgr5-1* (M_0) seeds were mutated by EMS (M_1) and propagated under standard conditions of 16 h light ($100 \mu\text{mol photons m}^{-2} \text{s}^{-1}$) in batches of 500 plants to produce M_2 generation seeds. M_2 lines were selected in samples of 3,000 plants under 12 h fluctuating light (low light of $50 \mu\text{mol photons m}^{-2} \text{s}^{-1}$ for 5 min followed by high light of $500 \mu\text{mol photons m}^{-2} \text{s}^{-1}$ for 1 minute). Lines that survived this condition were transferred to individual pots and grown under LD conditions. M_3 seeds were produced from each line and stored. An additional selection step was performed by measuring the Fv/Fm of the suppressor lines. Lines with high Fv/Fm were backcrossed with the M_0 mother line (*pgr5-1*). The generation resulting from this cross was designated F_1 and propagated under standard conditions to obtain the F_2 generation. The F_2 generation was selected under FL conditions to obtain plants of a line carrying the causative mutation suppressing the lethal phenotype. The plants were then grown under standard conditions for 3 weeks and used for DNA extraction and whole genome sequencing. Plants selected in the F_2 generation were propagated to produce F_3 seed.

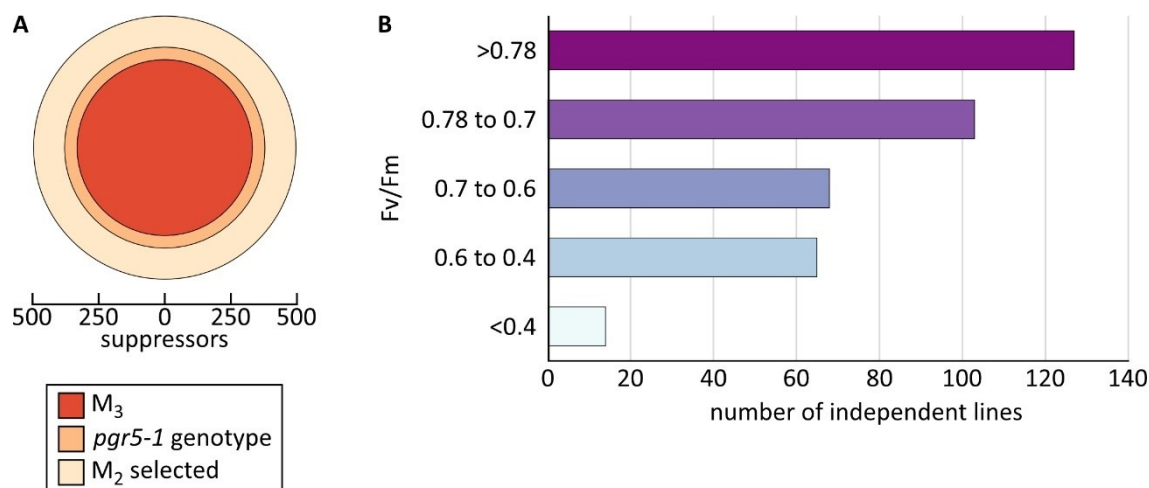


Figure 6: **Analysis of M₂ selection.** **A**, In the M₂ generation, 496 *pgr5-1* suppressors were selected under FL. These suppressors were genotyped to exclude possible wild-type contamination. Suppressors with the *pgr5-1* genotype were used to generate M₃ generation lines. **B**, Suppressors of the lethal phenotype of *pgr5-1* under FL were further characterised by measuring Chl fluorescence and determining the maximum quantum efficiency of PSII (Fv/Fm) after 30 min of dark incubation. Plants were grouped according to their Fv/Fm values.

4.2.1 Identification of causative mutations in the selected *pgr5-1* suppressors

From approximately 273,000 individual M₂ plants at the start of the screen, 34 lines in the F₂ generation were selected under FL and by their WT-like Fv/Fm for resequencing and further investigation of the causative mutation. Only one line per batch was selected to avoid repeated resequencing of identical alleles. F₂ plants were grown under FL and surviving candidates were used for genomic DNA extraction in pools of 100 plants. The resequencing of these samples was performed by Novogene (Cambridge, UK) and the data set analysed by Dr Tatjana Kleine. The single nucleotide polymorphisms (SNPs) with annotated mutations and genes were provided for further analysis.

Based on the enrichment of SNPs with an allele frequency of 1, putative causative mutations were selected for each *pgr5-1* suppressor. In addition, the localisation of the protein was considered, with plastid-localised proteins being favoured in the analysis. Chloroplast-localised proteins are more likely to affect photosynthesis and related proteins. A strong indicator of the causative mutation was the effect a point mutation would have on the protein, ideally those mutations that produced a premature stop codon. Splicing defects were also considered as a criterion for possible mutations that would suppress the lethal phenotype of *pgr5-1* under FL. In a final step, the described function of the possible candidates of the causative mutation was compared with already established methods to suppress the *pgr5-1* phenotype, such as down-regulation of LEF (Suorsa et al., 2016), introduction of a more sensitive photosynthetic control (Yamamoto & Shikanai, 2019), or providing PSI with an additional electron acceptor as MV (Munekage et al., 2002).

As with the first suppressor found (*pgr5-S1*), many causative mutations were assigned to genes encoding proteins involved in PSII assembly or stability. This was surprising because our previous selection was based on a high Fv/Fm, meaning that the criterion of high Fv/Fm was not sufficient to discriminate PSII-related suppressors from the resequencing; moreover, the sheer number of possibilities for suppressing the *pgr5* phenotype by PSII defects seemed too large to be completely excluded out from the pool of resequencing lines. In addition, the suppressor screen yielded many interesting mutations not previously described to suppress the lethal phenotype of *pgr5-1*: for example, a protein involved in ion transport (PAA1)(Shikanai et al., 2003), mutations leading to altered state transitions (LHCB4.1 and PsbP-like protein 1) (Che et al., 2020; de Bianchi et al., 2011), and two suppressors carrying the causative mutations in proteins of unknown function (AT2G04360 and AT2G27290) (Table 4 and Figure 7).

Results

Table 4: Causative mutations of the re-sequenced *pgr5-1* suppressor lines.

Suppressor	Gene	Name	Localized	nt	AA	Fv/Fm
Transport						
<i>pgr5-S61</i>				G/A	G/R	0.77
<i>pgr5-S232</i>	AT4G33520	PAA1	Plastid	G/A	G/R	0.79
<i>pgr5-S367</i>				G/A	C/Y	0.80
Calvin-Benson-Bassham-Cycle						
<i>pgr5-S111</i>	AT3G54050	FBPase	Plastid	C/T	S/L	0.79
<i>pgr5-S336</i>	AT4G29670	ACHT2	Plastid	G/A	R/*	0.80
PSII-related						
<i>pgr5-S1</i>				C/T	W/*	0.62
<i>pgr5-S37</i>	AT5G48910	LPA66	Plastid	G/A	A/V	0.63
<i>pgr5S30</i>				G/A	G/E	0.44
<i>pgr5S277</i>	AT4G14605	MTERF5	Plastid	G/A	splicing	0.77
<i>pgr5S44</i>				G/A	G/D	0.62
<i>pgr5-S341</i>	AT1G06680	PsbP	Plastid	G/A	C/Y	0.71
<i>pgr5-S251</i>	AT3G01480	CYP38	Plastid	G/A	splicing	0.80
<i>pgr5-S290</i>	AT1G02910	LPA1	Plastid	C/T	splicing	0.50
<i>pgr5-S355</i>	AT1G71500	PSB33	Plastid	G/A	G/E	0.79
<i>pgr5-S400</i>	AT1G73530	ORRM6	Plastid	C/T	splicing	0.66
State Transition						
<i>pgr5-S81</i>	AT5G01530	LHCB4.1	Plastid	C/T	A/V	0.74
<i>pgr5-S120</i>				G/A	Q/*	0.79
<i>pgr5-S271</i>				C/T	W/*	0.79
<i>pgr5-S327</i>	AT3G55330	PsbP-like protein 1	Plastid	G/A	Q/*	0.81
<i>pgr5-S386</i>				G/A	P/S	0.81
<i>pgr5-S393</i>				G/A	Q/*	0.80
Cyt b₆f complex						
<i>pgr5-S89</i>	AT5G54290	CcdA	Plastid	G/A	M/I	0.73

Unknown						
<i>pgr5-S42</i>				G/A	Q/*	0.69
<i>pgr5-S141</i>	AT2G04360	unknown	Plastid	C/T	W/*	0.79
<i>pgr5-S410</i>				G/A	R/*	0.83
<i>pgr5-S261</i>	AT2G27290	unknown	Plastid	C/T	G/D	0.78

Suppressors marked in bold after confirming causative mutation

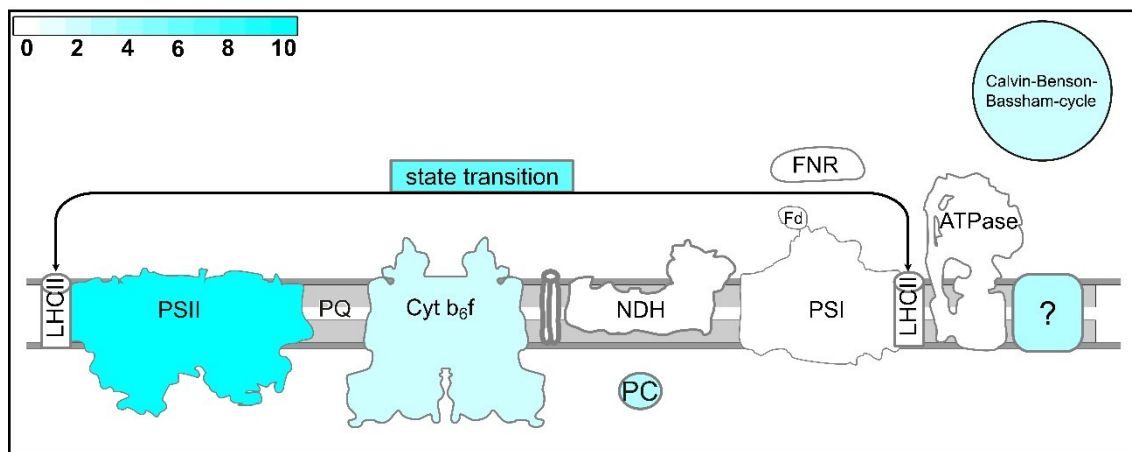


Figure 7: **Schematical representation of thylakoid complexes and mechanisms influenced by SNPs.** Complexes or mechanisms affected by a SNP were colour coded according to the number of hits for that particular target. The lowest number of hits was 0 (white) and the highest number of SNPs found to affect was 10 (cyan). Unknown proteins were indicated as question mark (?).

4.3 Defect assembly of PSII suppresses the lethal phenotype of *pgr5-1* under FL, a proof of concept

In the resequencing data of both lines, *pgr5-S1* and *pgr5-S37*, a mutation was found in the LPA66 gene, but at different positions (Table 4). In line *pgr5-S1*, a mutation was detected at position 1938 of the gene, just before the endogenous stop codon, resulting in a premature stop codon. The line *pgr5-S37* carried the mutation in LPA66 at position 1048, resulting in an amino acid exchange (Figure 8A and B).

The fact that two independent alleles were found in the screen made LPA66 a very likely candidate for the causative mutation suppressing the lethal phenotype. As additional evidence, and to generate a line with a minimum of background mutations, a T-DNA insertion line of LPA66 (Figure 8A, Cai et al., 2009) was crossed with *pgr5-1* and all resulting lines were tested for survival under FL. The suppressor lines *pgr5-S1* and *pgr5-S37* were able to suppress the lethal phenotype of *pgr5-1* under FL, but showed retarded growth compared to the wild-type line (Col-5). Furthermore, under control light conditions (CL),

pgr5-S1 and *pgr5-S37* were smaller than *pgr5-1* and WT plants (Figure 8C). The single T-DNA line (*lpa66*) showed retarded growth as *pgr5-S1* and *pgr5-S37* under control light compared to the WT background line (Col-0). Surprisingly, the double mutant of *pgr5-1* and *lpa66* showed slightly enhanced growth compared to *lpa66*. Under FL, both lines *lpa66* and *pgr5-1 lpa66* resembled the suppressor lines *pgr5-S1* and *pgr5-S37* in their growth and development (Figure 8C).

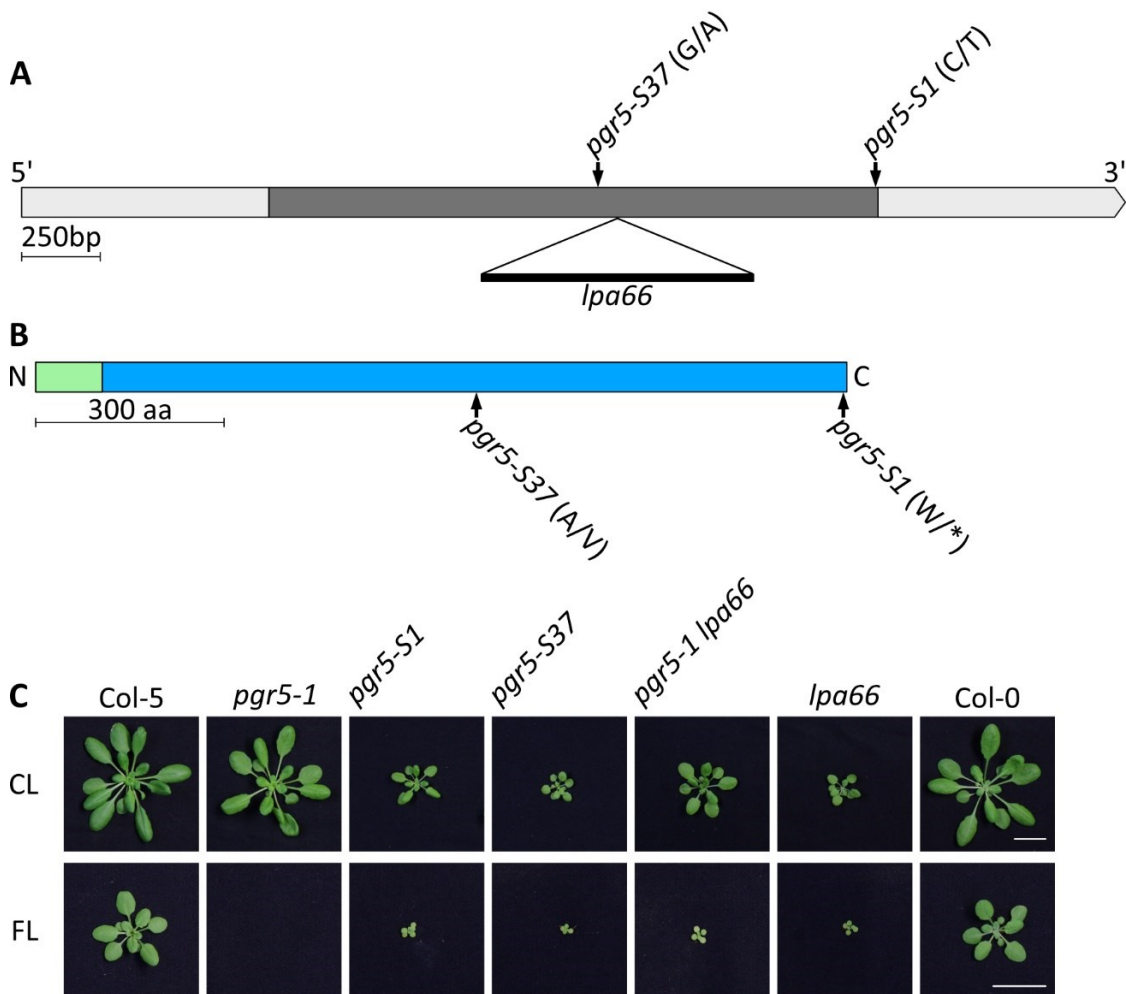


Figure 8: Mutating the gene *LAP66* suppresses the lethal phenotype of *pgr5-1* under FL. **A**, Schematic representation of the *LPA66* gene (AT5G48910). The exonic sequence is marked in dark grey and the UTR regions as light grey boxes. The orientation of the gene is indicated by the marking of the 5' and 3' ends. The size of the gene is indicated by a scale bar correlating to 250 bp. The positions of the mutations induced by EMS treatment are indicated by an arrow and the name of the line represented (*pgr5-S1* and *pgr5-S37*). The nucleotide exchange found is given in parantheses. The T-DNA insertion site is marked with a triangle and labelled *lpa66*. **B**, Schematic representation of the Lpa66 protein to scale. The N- and C-termini of the protein are labelled and the cTP is indicated by a green box. The mature protein is shown as a blue box. The scale bar represents 300 amino acids. Position of the mutated amino acids of the suppressor lines are labelled accordingly and in brackets the detected mutation (*= stop codon). **C**, Growth phenotype of Col-5, *pgr5-1*, suppressor lines *pgr5-S1*, *pgr5-S37* and double mutant *pgr5-1 lpa66*, single T-DNA insertion line *lpa66* and Col-0 plants grown for 5 weeks under control light conditions (CL, 12 h light 100 $\mu\text{mol photons m}^{-2} \text{s}^{-1}$ and 12 h dark) or fluctuating light (FL, 12 h light, cycles of low light (50 $\mu\text{mol photons m}^{-2} \text{s}^{-1}$) for 5 min and high light (500 $\mu\text{mol photons m}^{-2} \text{s}^{-1}$). Scale bar correlates to 2 cm.

Whether the defect in the accumulation of PSBE/F and the maximum efficiency of PSII (Fv/Fm), as occurs in the single line *lpa66*, was present in the newly generated double

mutant line *pgr5-1 lpa66*, were of interest (Cai et al., 2009). Therefore, Fv/Fm was measured in the *lpa66* line and the double mutant line generated from *pgr5-1* and *lpa66*. Interestingly, both lines *lpa66* and *pgr5-1 lpa66* showed a lower Fv/Fm value, 0.45 and 0.42 respectively, than the EMS line *pgr5-S1*, 0.63. In all cases, these values were lower than for Col-5 and *pgr5-1*, 0.80 and 0.79, respectively (Figure 9A). However, the accumulation of PSBE/F was lower in *pgr5-S1* than in *pgr5-1 lpa66* and the single mutant *lpa66*. Furthermore, with respect to PGR5 and PGRL1 protein levels, a lower accumulation of PGRL1 was detected in the *pgr5-1* and *pgr5-1 lpa66* lines as in the Col-5 line and *lpa66*. Interestingly, the level of PGRL1 was rescued in the EMS suppressor line *pgr5-S1* compared to the *pgr5-1* line. It was observed that in the mutant lines (*pgr5-1*, *pgr5-1 lpa66*, and *pgr5-S1*), the detectable amount of PGR5 was 5 % of the wild-type control (Col-5). A notable observation was a higher level of PGR5 detectable in the *lpa66* line compared to the wild-type control (Col-5) (Figure 9B).

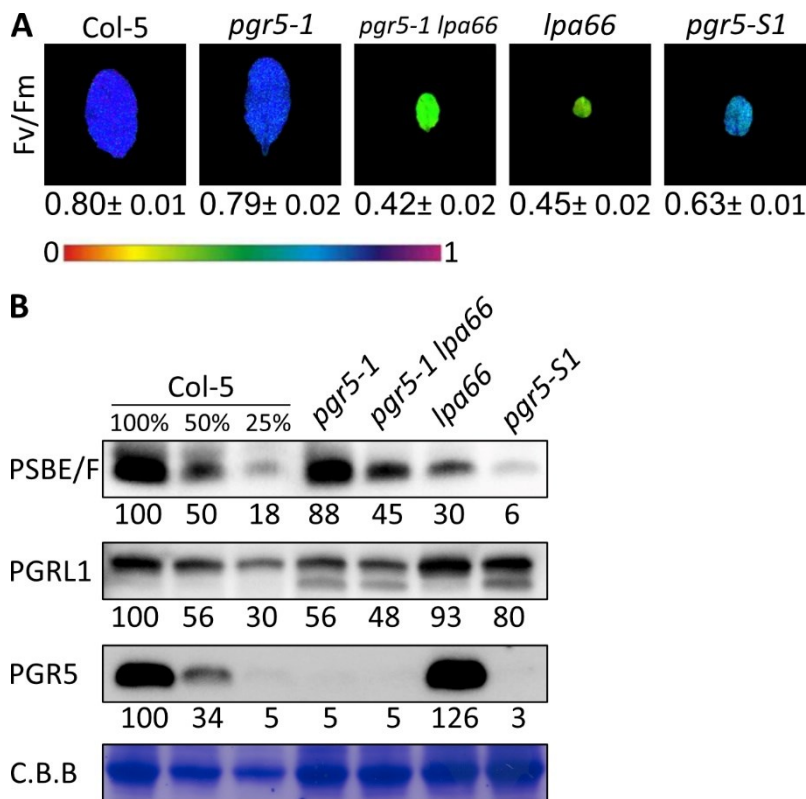


Figure 9: Mutating *LPA66* affects the stability and the maximum quantum yield of the PSII. **A**, Genotypes were grown under control conditions (12 h light, 100 $\mu\text{mol photons m}^{-2} \text{s}^{-1}$) for 5 weeks. WT (Col-5) and mutant (*pgr5-1*, *pgr5-1 lpa66*, *lpa66* and *pgr5-S1*) plants were dark adapted. After dark adaptation, a saturation pulse was applied and the maximum quantum yield (F_v/F_m) was calculated from Chl fluorescence. Five replicates were measured and the \pm standard deviation was calculated. **B**, Immunodetection of PGRL1, PSBE/F and PGR5 from whole leaves of 5-week-old plants grown under CL conditions (12 h light 100 $\mu\text{mol photons m}^{-2} \text{s}^{-1}$ and 12 h dark). Col-5, *pgr5-1*, *pgr5-1 lpa66*, *lpa66* and *pgr5-S1* were used as wild-type controls. For PGRL1 and PSBE/F detection, 1 μg of extracted proteins were loaded, while for PGR5, 3 μg of samples were loaded on 10 % Tris-Ticine gel and separated according to size. The proteins were transferred to a PVDF membrane by semi-dry blotting. The membrane was blocked with 5 % milk for one hour and decorated with the specific antibodies against the detected proteins. C.B.B. staining was performed as a loading control. Numbers below the detected band represent quantification of band intensity normalised to the 100 % wild-type control.

In summary, by generating an additional allele, it was demonstrated that the mutation in *LPA66* can suppress the lethal phenotype of *pgr5-1* under FL. Furthermore, a reduced accumulation of PSBE/F and a lower maximum PSII activity were observed in the found suppressor *pgr5-S1*, the T-DNA line *lpa66* and the generated double mutant *pgr5-1 lpa66*. Interestingly, the accumulation of PGRL1 was restored in *pgr5-S1*. Furthermore, protein levels of PSBE/F were more reduced in the EMS mutant line (*pgr5-S1*) than in the generated second allele (*pgr5-1 lpa66*) or the single mutant line *lpa66*, suggesting a different effect of the present mutation and possible affected functional regions.

4.3.1 *lpa66* suppresses the photosynthetic phenotype of *pgr5-1* under FL

Photosynthetic measurements were performed to study in more detail how a mutation in *LPA66* suppresses the lethal phenotype of *pgr5-1* under FL. Using a DualPAM fluorimeter, a program that mimics the fluctuating light conditions was applied to analyze the different photosynthetic parameters. The newly generated suppressor line *pgr5-1 lpa66* and its background lines *pgr5-1* and *lpa66* were measured together with WT plants (Col-5) as a control. The effect of the mutations on the photosynthetic activity under FL was analyzed for the different lines.

PSII activity (Y(II)) was measured as quantum yield by measuring the Chl fluorescence. Y(II) was only slightly affected in the *pgr5-1* line compared to Col-5. Interestingly, over the time frame of the measurement, Y(II) in *pgr5-1* decreased after each HL period (1 min), but recovered in the dark phase at the end of the protocol, indicating that photoinhibition had ceased at least after this number of LL/HL cycles. In contrast, both lines lacking LPA66 (*lpa66* and *pgr5-1 lpa66*) showed a strongly inhibited Y(II) parameter, especially under LL (Figure 10A).

Furthermore, it was observed that NPQ was not induced in the HL peak of the FL PAM measurements for the *pgr5-1* line, in contrast to the wild-type line (Col-5), as previously described (Suorsa et al., 2012). However, during low light, NPQ was not fully recovered in the *pgr5-1* mutant and remained higher than in WT plants. Interestingly, *lpa66* and *pgr5-1 lpa66* mutants showed a stronger induced NPQ than Col-5 during the first HL peaks after the transition from dark incubation to light. However, after this initial phase of dark-light acclimation, the NPQ of these plants dropped below the WT level in the HL phases and required a longer time frame to relax in the LL phase. In addition, the double mutant (*pgr5-1 lpa66*) maintained a more stable NPQ level over all HL peaks used in the measurement (Figure 10B).

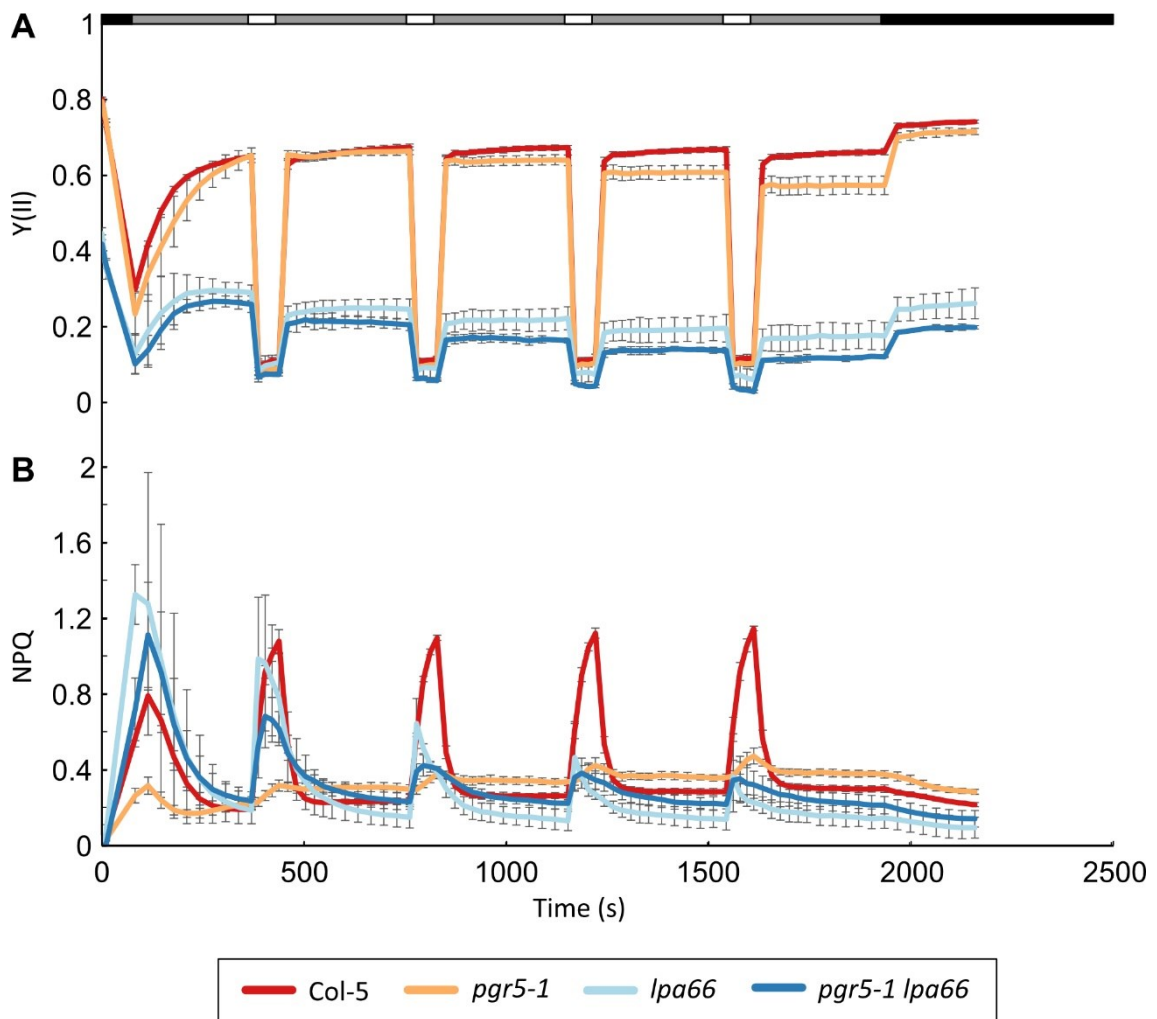


Figure 10: **Photosystem II parameters of *lpa66*-mutant lines under FL.** The different genotypes were grown for 5 weeks under control conditions (12 h light, $100 \mu\text{mol photons m}^{-2} \text{s}^{-1}$). WT (Col-5) and mutant (*pgr5-1*, *lpa66* and *pgr5-1 lpa66*) plants were dark-adapted (black bar) followed by illumination with actinic light ($50 \mu\text{mol photons m}^{-2} \text{s}^{-1}$, dark grey bar) for 5 min. After the low light illumination, the plants were exposed to high light for 1 min ($500 \mu\text{mol photons m}^{-2} \text{s}^{-1}$, white bar). The low light and high light phases were repeated four times alternately, followed by a recovery period of 5 min in darkness (black bar). During the induction and recovery periods, photosynthetic parameters were measured by applying saturation pulses every 20 s during the low light and recovery periods and every 15 s during the high light period. Three replicates were measured for each genotype. **A**, Photosystem two quantum yield (Y(II)) was measured from Chl fluorescence in the plants described. **B**, Analysis of the values of NPQ calculated from the values measured in (A). \pm SD are shown as error bars.

By measuring PSI activity, it is possible to estimate the limitation of electrons from the donor side of PSI (Klughammer & Schreiber, 2008). This allows the estimation of the values for PSI activity (Y(I)), the limitation of PSI due to a deficit of electron donors (electrons from PC) (Y(ND)) and the limitation of PSI activity due to a deficit of electron acceptors (Y(NA)). Regarding the parameter representing Y(I), *pgr5-1* showed almost no activity under HL, but recovered to the level of the WT in the LL phases, although a decrease was also observed after several peaks of HL. The decrease in Y(I) of *pgr5-1* correlated with an increase in Y(NA), while Y(ND) did not change with respect to the

WT. The high limitation of PSI electron acceptors during HL, due to an overreduction of the stroma, is characteristic for mutants lacking PGR5, as described before by Suorsa et al. (Suorsa et al., 2012; Suorsa et al., 2016). Furthermore, the *lpa66* mutant and the double mutant *pgr5-1 lpa66* did not reach the PSI activity of the WT or *pgr5-1* during the LL phase, with the Y(I) being almost half that of the WT. However, during the HL peaks, the Y(I) of plants lacking *lpa66* was almost at the WT level and higher than that of *pgr5-1*, even in the double mutant *pgr5-1 lpa66*. Interestingly, in the recovery part of the measurement (dark phase), an over-reduction of PSI was observed in both lines without LPA66, indicated by a higher Y(I) value than in the WT line without light (Figure 11A). The low Y(I) of the *lpa66* mutants correlated with the limitation of the donor side observed in the different light phases, and this could explain why the double mutant *pgr5-1 lpa66* had a lower reduced PSI compared to *pgr5-1*, protecting the plant from overreduction on the PSI side and possible ROS formation in the active centre.

A study of donor restriction was conducted. The wild type (Col-5) was slightly restricted on the donor side in the initiation phase. This limitation was almost undetectable at later times in the LL phase. Under HL, Col-5 was limited by its PSI activity on the donor side. The line *pgr5-1* showed no limitation of the PSI donor side in either HL or LL phase. A strong limitation of the donor side was observed in the LL phase in the lines *lpa66* and *pgr5-1 lpa66*. In particular, in the HL phase, the *lpa66* line showed a limitation comparable to the WT. Interestingly, the same level of limitation was measured in the *pgr5-1 lpa66* line as in *lpa66*, indicating that the photosynthetic phenotype of *lpa66* dominates that of *pgr5-1* (Figure 11B).

The WT showed a low level of limitation on the acceptor side of PSI in the LL phases, with a peak at the beginning of the HL phases of the measurement. A limitation comparable to that of the wild-type control (Col-5) was observed in the LL phases of the measurement in the *pgr5-1* line. In the HL phases, *pgr5-1* showed the strongest observable acceptor side limitation of all lines. The single line *lpa66* also had a strong limitation at the beginning of the measurement, but after acclimation to light, Y(NA) dropped below the level of Col-0, being almost zero. The same level of limitation on the acceptor side of PSI was observed in the HL as in the LL of the measurement. Interestingly, in the double mutant *pgr5-1 lpa66*, Y(NA) was always higher than in the single *lpa66* mutant, but lower than in *pgr5-1* and even in the WT (after the dark-light transition), thus suppressing the *pgr5-1* phenotype together with the recovery of Y(I) under HL (Figure 11C).

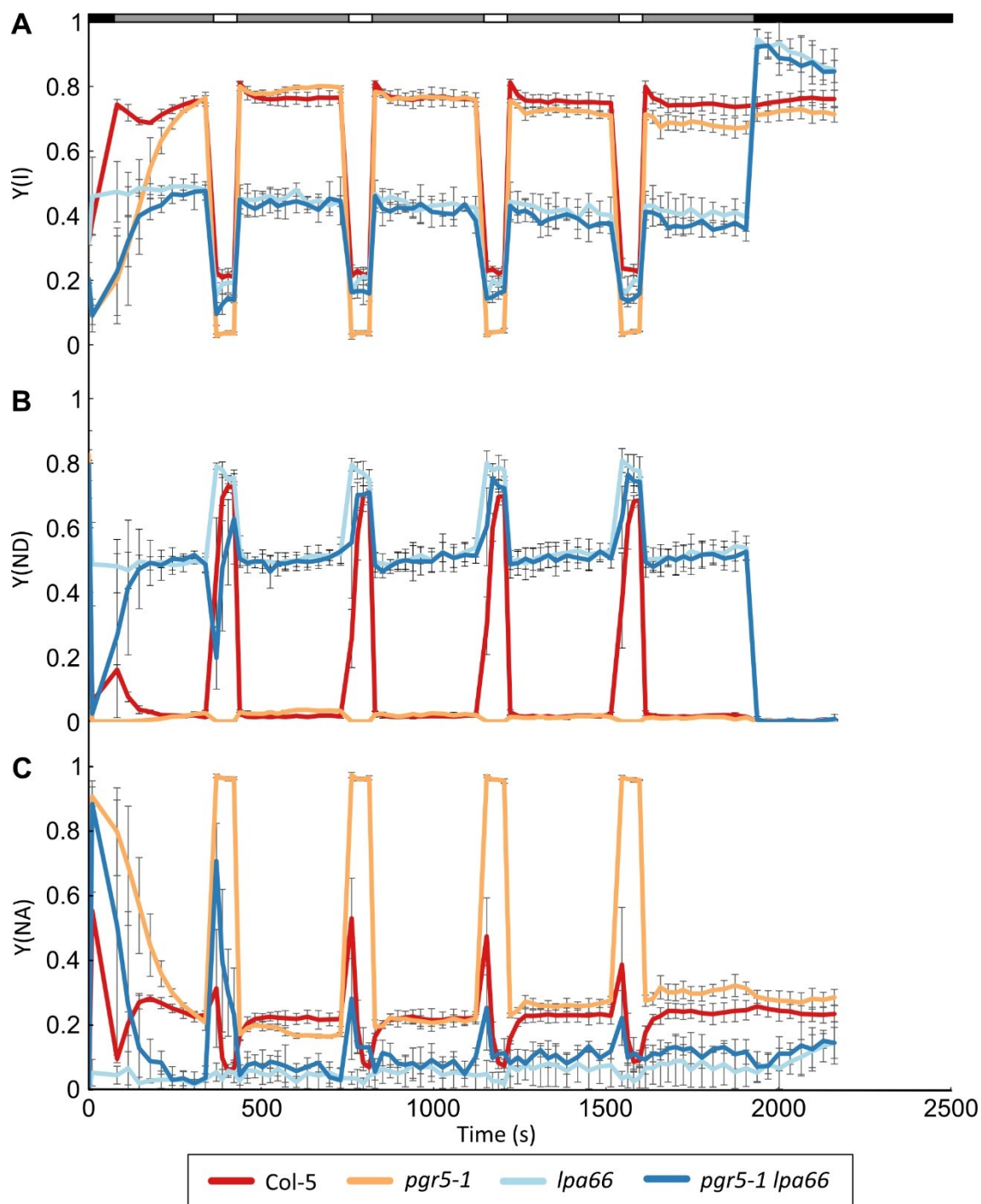


Figure 11: **Photosystem I parameters of *lpa66*-mutant lines under FL.** The different genotypes were grown for 5 weeks under control conditions (12 h light, 100 $\mu\text{mol photons m}^{-2} \text{s}^{-1}$). WT (Col-5) and mutant (*pgr5-1*, *lpa66* and *pgr5-1 lpa66*) plants were dark-adapted (black bar), followed by illumination with actinic light (50 $\mu\text{mol photons m}^{-2} \text{s}^{-1}$, dark grey bar) for 5 min. After low light, plants were exposed to high light for 1 min (500 $\mu\text{mol photons m}^{-2} \text{s}^{-1}$, white bar). The low light and high light phases were alternated four times, followed by a recovery period of 5 min in darkness (black bar). During the induction and recovery periods, photosynthetic parameters were measured by applying saturation pulses every 20 s during the low light and recovery periods and every 15 s during the high light period. Three replicates were measured for each genotype. **A**, The quantum yield of photosystem I ($Y(I)$) was revealed by measuring the absorbance at 875 nm minus 830 nm. **B**, Donor-side limitation of PSI was calculated from the measurements shown in (A). **C**, Acceptor-side limitation of Photosystem I was calculated from the measurements shown in (A). Error bars represent \pm SD.

In conclusion, the results of the photosynthetic measurements showed a lower PSII activity in both *lpa66* and *pgr5-1 lpa66* lines. Both mutants were able to induce NPQ in the HL phases, even when PGR5 was missing in the double mutant *pgr5-1 lpa66*. Furthermore, a strong donor-side limitation of PSI was detected in both mutant lines *lpa66* and *pgr5-1 lpa66*, leading to lower PSI activity compared to WT and *pgr5-1*. The mutant lines *lpa66* and *pgr5-1 lpa66* were less limited in PSI activity by acceptor-side than the WT and *pgr5-1* lines in the LL and HL phases. Overall, the introduced downregulation of *LPA66* through a T-DNA insertion in the *pgr5-1* background partially suppressed the photosynthetic phenotype of *pgr5-1*, which is comparable to the observation of Suorsa and colleagues in their $\Delta 5$ *pgr5* mutant line (Suorsa et al., 2016).

4.3.2 From representative mutant lines of thylakoid complexes, only PSII mutants can suppress *pgr5-1* lethal phenotype under FL

As demonstrated earlier, the first suppressors identified in the *pgr5* screen primarily impacted the integrity of PSII. Therefore, the question of whether mutations affecting other components of the electron transport chain would yield similar results, where downregulation of LEF at various points could suppress the lethal phenotype of *pgr5-1* under FL to the same extent as observed in the *pgr5-1 lpa66* line was raised. Therefore, different mutant lines with defects in the assembly or function of thylakoid membrane complexes involved in LEF, such as Cyt b_6f or PSI, were generated in addition to PSII. For the analysis of the PSII complex, the line *pam68*, which shows a reduced accumulation of the PSII core subunits (Armbruster et al., 2010), was selected and crossed with *pgr5-1*. As a mutant line for Cyt b_6f , *pgr1*, which shows an impaired Rieske protein (Yamamoto & Shikanai, 2019), was chosen. To show the effect of reduced PSI accumulation on the phenotype of *pgr5-1*, *psad1* (Ihnatowicz et al., 2004) were selected. Furthermore, the line *cgl160*, which exhibits a defect in ATPase assembly and displays a highly induced NPQ as a photosynthetic phenotype, was used (Reiter et al., 2023; Rühle et al., 2014). In addition, the *ntrc* mutant, which lacks the chloroplast NADPH-dependent thioredoxin NTRC (Perez-Ruiz et al., 2006) and has a strong induction of NPQ (Naranjo et al., 2016) was included, as a control to know whether high induced NPQ alone can suppress the *pgr5* phenotype under FL. All these mutants (*pam68*, *pgr1*, *psad1*, *cgl160* and *ntrc*) were grouped under the name of photosynthetic electron transport (PET) lines.

To analyse the growth phenotype of the PET lines under FL and CL, the wild-type controls Col-0 and Col-5 were used. *pgr5-1* showed the previously described lethal phenotype under FL; after five weeks of growth, the *pgr5-1* mutant was unable to produce true leaves and died at the cotyledon stage. However, under CL, *pgr5-1* showed a WT-like growth phenotype. The single mutant lines *pgr1*, *psad1*, *cgl160* and *ntrc*, which were used to generate the double mutant lines with *pgr5-1*, showed a retarded growth phenotype under FL compared to CL, similar to WT plants or even more pronounced. In contrast, the growth of the *pam68* mutant was enhanced under FL compared to CL. Interestingly, decreasing PSI or increasing NPQ in the *pgr5-1* background (*pgr5-1 psad1*, *pgr5-1 cgl160* and *pgr5-1 ntrc*) did not suppress the *pgr5* lethal phenotype under FL (Figure 12). Only a cross of *pgr5-1* with a mutant showing a decrease in PSII was able to survive and grow under FL conditions. This was observed in the *pgr5-1 pam68* line. Furthermore, *pgr1* has been described to suppress the *pgr5-1* phenotype at the photosynthetic level (Yamamoto & Shikanai, 2019). A germination under FL was observed, but no growth (Figure 12). Under CL, a similar growth to that of the single lines was exhibited by the double mutants lines *pgr5-1 pam68* and *pgr5-1 pgr1*. However, the lines *pgr5-1 psad1* and *pgr5-1 cgl160* were slightly smaller than the single lines (*psad1* and *cgl160*) (Figure 12). Interestingly, in the *pgr5-1 ntrc* line, a recovery of the *ntrc* phenotype was observed and the double mutant was larger and greener than *ntrc* (Figure 12) (Naranjo et al., 2021).

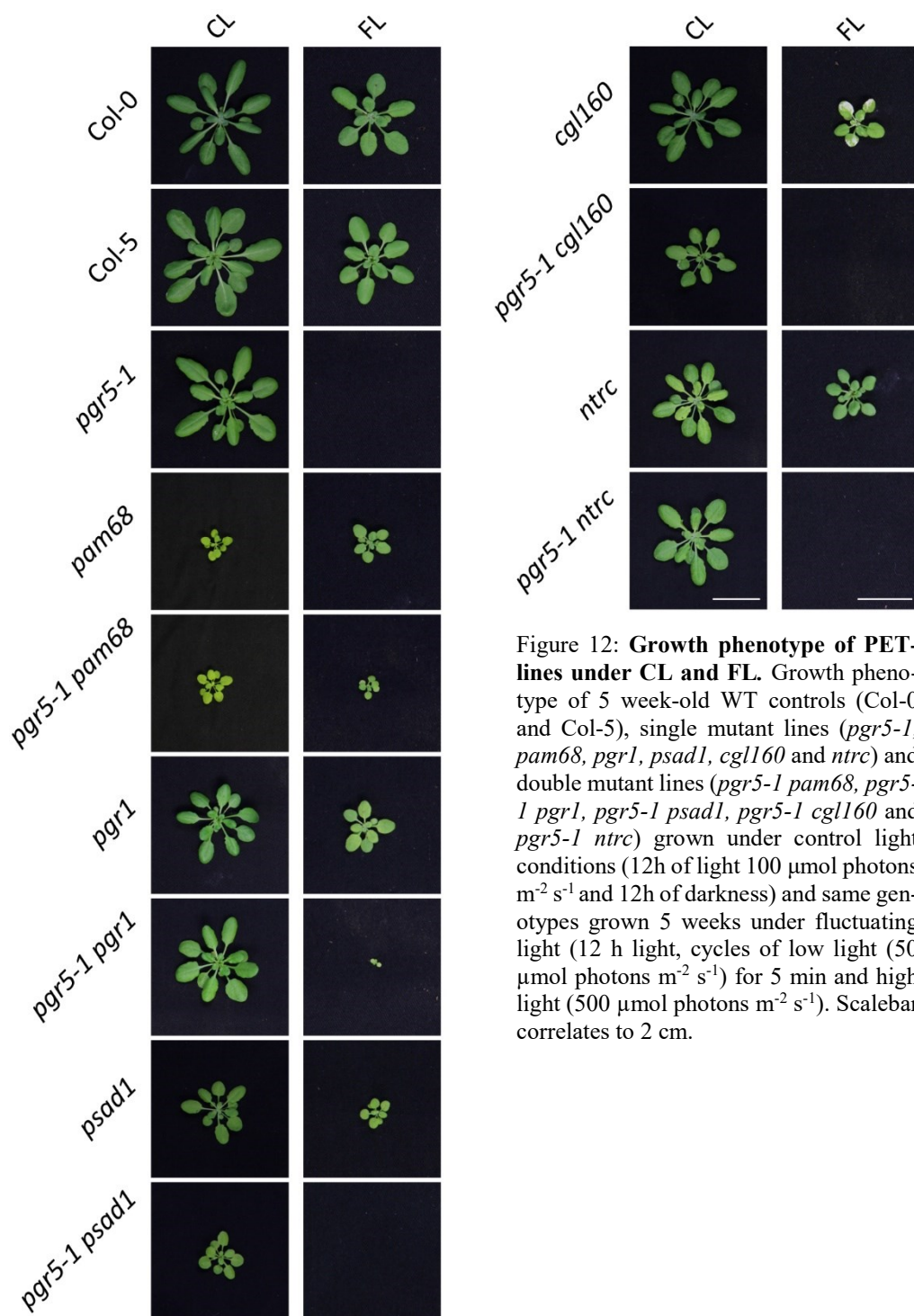


Figure 12: **Growth phenotype of PET-lines under CL and FL.** Growth phenotype of 5 week-old WT controls (Col-0 and Col-5), single mutant lines (*pgr5-1*, *pam68*, *pgr1*, *psad1*, *cgl160* and *ntrc*) and double mutant lines (*pgr5-1 pam68*, *pgr5-1 pgr1*, *pgr5-1 psad1*, *pgr5-1 cgl160* and *pgr5-1 ntrc*) grown under control light conditions (12h of light 100 $\mu\text{mol photons m}^{-2} \text{s}^{-1}$ and 12h of darkness) and same genotypes grown 5 weeks under fluctuating light (12 h light, cycles of low light (50 $\mu\text{mol photons m}^{-2} \text{s}^{-1}$) for 5 min and high light (500 $\mu\text{mol photons m}^{-2} \text{s}^{-1}$). Scalebar correlates to 2 cm.

4.3.3 Protein accumulation in the photosynthetic electron transport-single and double mutants

To investigate how the protein content of the PET lines would be affected by crossing the individual lines into the *pgr5-1* background, immunodetection assays of selected proteins were performed to represent the protein composition of PSII, Cyt b₆f, PSI and CEF, as well as CGL160 and NTRC. Detection was performed on proteins extracted from whole leaves harvested from 5-week-old plants grown under control conditions.

Specific accumulation and degradation of proteins were observed in the different PET lines. The *pgr5-1* line showed a slightly lower accumulation of CP47, Cyt f, PsaD, CGL160, NTRC and PGRL1. In the *pgr5-1* line, PGR5 itself was strongly reduced to the point of being undetectable. The other single lines (*pam68*, *pgr1*, *psad1*, *cgl160* and *ntrc*) showed a reduction in the accumulation of their specifically affected complexes and a comparable level of PGR5 to the WT. Interestingly, *ntrc* showed a more pleiotropic phenotype with an overall reduction in the proteins detected. When the individual lines were crossed into the *pgr5-1* background, a reduction of PGR5 was observed in all lines. In the double mutant lines (*pgr5-1 pam68*, *pgr5-1 pgr1*, *pgr5-1 psad1*, *pgr5-1 cgl160* and *pgr5-1 ntrc*), no changes were observed with respect to the single lines for the other proteins detected by immunodetection (Figure 13A and B).

Taken together, these results show that the introduction of the *pgr5-1* mutation in the PET lines did not alter protein levels in most cases. In addition, a recovery of the accumulation of PGR5, CGL160 and LhcB2 was observed in the *pgr5-1 pam68* line. Interestingly, the line *pgr5-1 pam68*, which survives best under FL, had the most proteins recovered to WT levels compared to *pgr5-1* and Col-5. It was also observed that PGR5 itself was nearly undetectable in all lines with the *pgr5-1* mutation. However, a slight accumulation of PGR5 was detected in *pgr5-1 pam68*, which is an interesting starting point for further investigations.

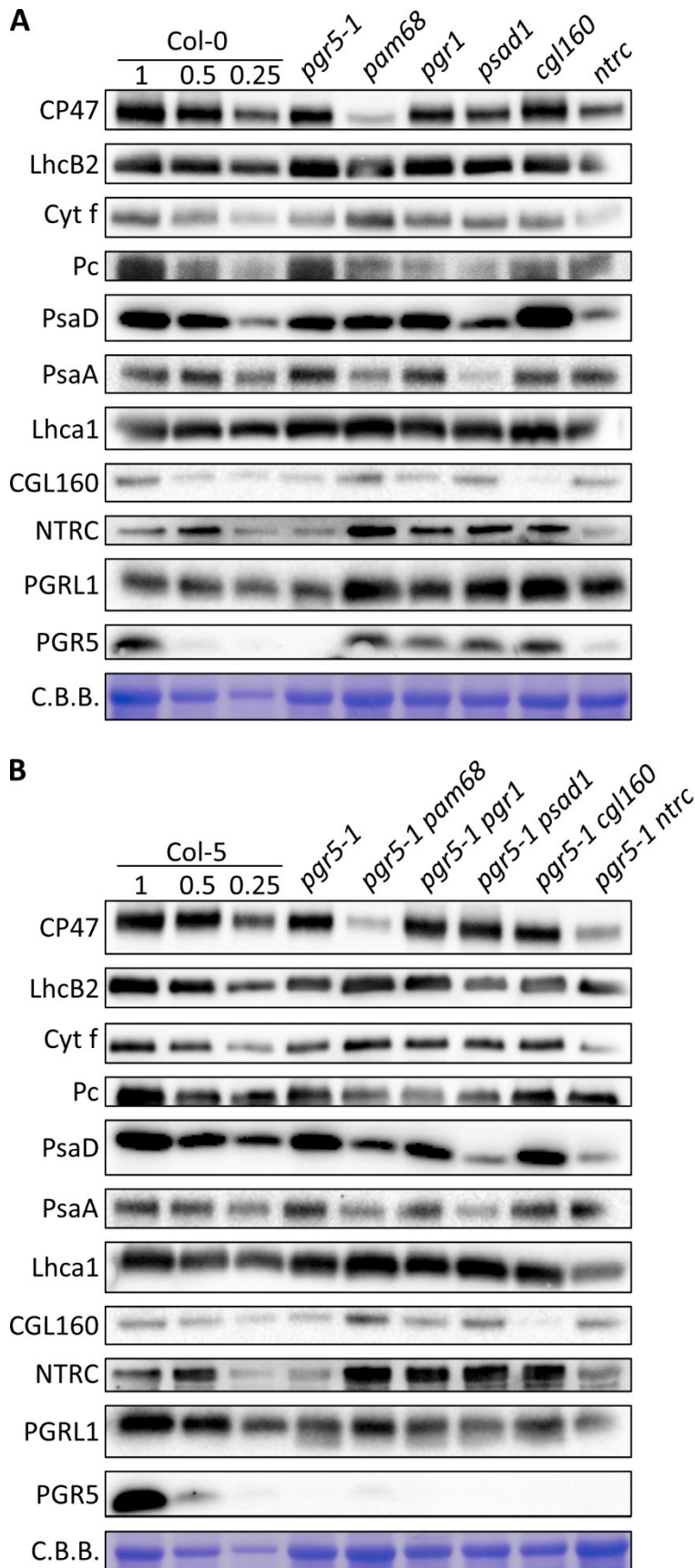


Figure 13: Immunodetection of selected proteins in the generated PET-lines. The plants were grown under 12h of light ($100 \mu\text{mol photons m}^{-2} \text{s}^{-1}$) and 12h darkness for five weeks before the samples were harvested. **A**, The single mutant lines *pgr5-1*, *pam68*, *pgr1*, *psad1*, *cgl160* and *ntrc* were used with the wild type control Col-0. **B**, The double mutants *pgr5-1 pam68*, *pgr5-1 pgr1*, *pgr5-1 psad1*, *pgr5-1 cgl160* and *pgr5-1 ntrc* together with the wild type Col-5 were harvested for samples. The detected proteins were extracted from whole leaf samples and loaded according to the fresh weight (PGR5 detection $3 \mu\text{g}$ leaf material and for other detections $1 \mu\text{g}$) onto a Tris-tricine page. From the wild type controls (Col-0 and Col-5) dilutions of 50 % (0.50) and 25 % (0.25) were loaded. After size separation, the proteins were transferred onto a PVDF-membrane and stained with Coomassie Brilliant Blue (C.B.B.) to visualize protein loading, followed by decorating with specific antibodies. Antibodies, which detect the following proteins were used: CP47, LhcB2, Cyt f, Pc, PsaD, PsaA, Lhca1, CgL160, NTRC, PGRL1 and PGR5.

4.3.4 Photosynthetic performance of PET-lines under different light conditions

The measurements described in section 4.3.1, which mimic the light conditions in the FL growth chamber, were performed with all the different PET lines (single and double mutants) as well as WT plants (Col-5) serving as a control. From these measurements, one measurement point during the LL phase (1020 s after the start of the measurement in the third LL phase) and one during the HL phase (1200 s after the start of the measurement in the third HL phase) were selected. The parameters Y(II), NPQ, Y(I), and Y(ND) were compared between these points. Furthermore, the Fv/Fm value of all lines was analyzed, which represents the maximum efficiency of PSII and can be affected by photoinhibition of PSII or a lower amount of PSII.

The maximum efficiency of PSII, represented by the Fv/Fm value, was similar to the wild type in all mutants (*pgr5-1*, *pgr1*, *pgr5-1 pgr1*, *psad1*, *pgr5-1 psad1*, *cgl160*, *pgr5-1 cgl160*, *ntrc* and *pgr5-1 ntrc*), except for *pam68* and *pgr5-1 pam68*, in which the Fv/Fm values were strongly affected. This was an expected result given the function of PAM68 in PSII assembly and the lower accumulation of the PSII core subunit (Armbruster et al., 2010).

Under LL, a similar activity of PSII was observed in Col-5, *pgr5-1*, *cgl160*, *pgr5-1 cgl160*, *ntrc* and *pgr5-1 ntrc*. However, *psad1* and *pgr5-1 psad1*, as well as *pam68* and *pgr5-1 pam68*, showed low or even no PSII activity. An increased level of Y(II) was observed in the *pgr1* and *pgr5-1 pgr1* lines. Regarding HL, as expected, Y(II) was always lower in all lines compared to LL and there were almost no differences between them.

The NPQ values in the LL phase showed that *pgr5-1*, *pam68* and *pgr1* can induce a stronger NPQ than the other PET lines, *pgr5-1* and the WT control under these conditions. The lines *pgr5-1*, *pam68*, *pgr5-1 pgr1*, *cgl160* and *pgr5-1 cgl160* had a slightly increased NPQ level compared to the WT line (Col-5), *ntrc* and *pgr5-1 ntrc*. In the third HL phase, NPQ induction was detectable at or above the WT level in the *pam68*, *pgr5-1 pam68*, *psad1*, *pgr5-1 psad1*, *cgl160*, *pgr5-1 cgl160* and *ntrc* lines. However, NPQ induction was lower in the *pgr5-1*, *pgr1*, *pgr5-1 pgr1* and *pgr5-1 ntrc* lines, at a comparable level (Figure 14).

In the LL phase, comparable Y(I) was observed in the lines *cgl160*, *ntrc*, *pgr5-1*, *pgr5-1 pgr1* and *pgr5-1 cgl160* to the WT. The lines *pam68*, *psad1*, *pgr5-1 psad1* and *pgr5-1 ntrc* showed slightly lower activity. Noteworthy was the increased Y(I) value in the *pgr1* line compared to all other lines. An almost complete loss of PSI activity was observed in

lines *pgr5-1*, *pgr5-1 psad1*, *pgr5-1 cgl160* and *pgr5-1 ntrc*. In the single mutant lines (*pam68*, *pgr1*, *cgl160* and *ntrc*), Y(I) values comparable to the WT (Col-5) were measured. Interestingly, the lines *pgr5-1*, *pam68* and *psad1* showed a higher activity of PSI, with *pgr5-1 pam68* having the highest.

The WT line (Col-5) and the mutant lines *pgr5-1*, *pgr5-1 pgr1*, *psad1*, *pgr5-1 psad1*, *cgl160*, *pgr5-1 cgl160*, *ntrc* and *pgr5-1 ntrc* showed low donor side limitation of PSI under LL. The lines *pam68*, *pgr5-1 pam68* and *pgr1* showed a stronger donor limitation of PSI activity. Under HL, the WT line (Col-5) and all single lines except *pgr5-1* (*pam68*, *pgr1*, *psad1*, *cgl160* and *ntrc*) showed high donor limitation of PSI. Of the double mutant lines, only *pgr5-1 pam68* showed donor side limitation (Figure 14).

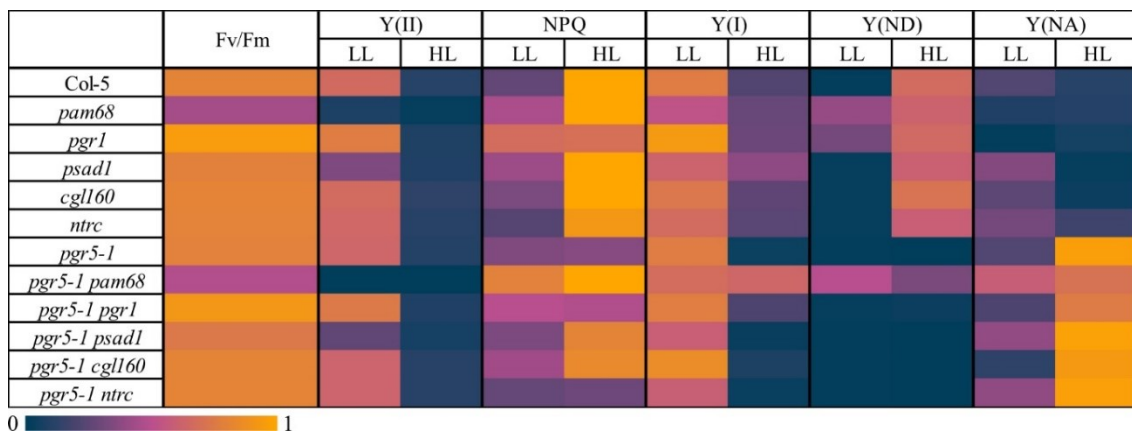


Figure 14: Heatmap of photosynthetic activity at distinct time points under FL of PET-lines. WT (Col-5) and mutant (*pgr5-1*, *pam68*, *pgr5-1 pam68*, *pgr1*, *pgr5-1 pgr1*, *psad1*, *pgr5-1 psad1*, *cgl160*, *pgr5-1 cgl160*, *ntrc* and *pgr5-1 ntrc*) plants grown for 5 weeks under control conditions (12 h light, 100 $\mu\text{mol photons m}^{-2} \text{s}^{-1}$), were dark adapted and followed by 5 min of illumination with low actinic light (50 $\mu\text{mol photons m}^{-2} \text{s}^{-1}$). After the illumination with low light, plants were subjected to high actinic light for 1 min (500 $\mu\text{mol photons m}^{-2} \text{s}^{-1}$). Low light and high light phases were repeated alternately four times followed by a recovery phase of 5 min in the dark. Over the time frame of induction and recovery, the photosynthetic parameters were measured by applying saturation pulses every 20 s in the low light phase and recovery phase and every 15 s in the high light phase. For each genotype, three replicates were measured. The parameters Fv/Fm, Y(II), NPQ, Y(I), Y(ND) and Y(NA) were represented in colour coded. For the LL, the time point 1020 s was selected and for the HL, the time point 1200 s.

In order to analyse the effects of the lack of different photosynthetic components in combination with the lack of PGR5, the photosynthetic performance of the PET lines was analyzed under different conditions: CL (100 $\mu\text{mol photons m}^{-2} \text{s}^{-1}$) and HL (500 $\mu\text{mol photons m}^{-2} \text{s}^{-1}$). For the measurements using CL and HL, the photosynthetic activity after 40 s of illumination, which represents the induction phase of photosynthesis and at the time point of 300 s after the start of illumination, which corresponds to the steady state of

photosynthesis, were examined. The thesis does not show the HL and steady state measurements.

In this experiment, the focus was on the parameters representing PSII and PSI activity under CL in the transient phase from darkness to light. With regard to PSII, it was found that *pam68* and *pgr5-1 pam68* lines exhibited the lowest PSII activity adaptation to CL, as expected for mutant lines with deficiencies in PSII assembly (Armbruster et al., 2010). In addition to *pam68*, the lines with the lowest Y(II) were *psad1* and *pgr5-1 psad1*. Similar PSII activity was observed in the wild-type control (Col-5) and the mutant lines *pgr5-1*, *pgr1*, *pgr5-1 pgr1*, *cgl160*, *pgr5-1 cgl160*, *ntrc*, and *pgr5-1 ntrc*. Interestingly, the highest transient NPQ was observed in mutants affected in PSII and PSI, i.e. *pam68* and *psad1*. Although only *pam68* could suppress the *pgr5-1* lethal phenotype under FL, suggesting that a higher transient NPQ as observed in *pgr5-1 psad1* and *pgr5-1 pam68* does not cause the suppression. In contrast, more differences in PSI activity were observed between the single PET lines and the double mutants with *pgr5-1* (Figure 15A). The high Y(NA) characteristic of *pgr5-1* was also observed in the double mutants, but in this case the rescue of the high *pgr5-1* Y(NA) corresponded to the *pgr5* suppressor phenotype: *pgr5-1 pam68* and in *pgr5-1 pgr1* to a lesser extent (Figure 15B). The measured values that were not shown in the thesis of the different lines under CL at the steady state (300 s) and HL (500 $\mu\text{mol photons m}^{-2} \text{s}^{-1}$) as in the transient phase (40 s) were similar to the measurements of CL in the transient phase (Figure 15).

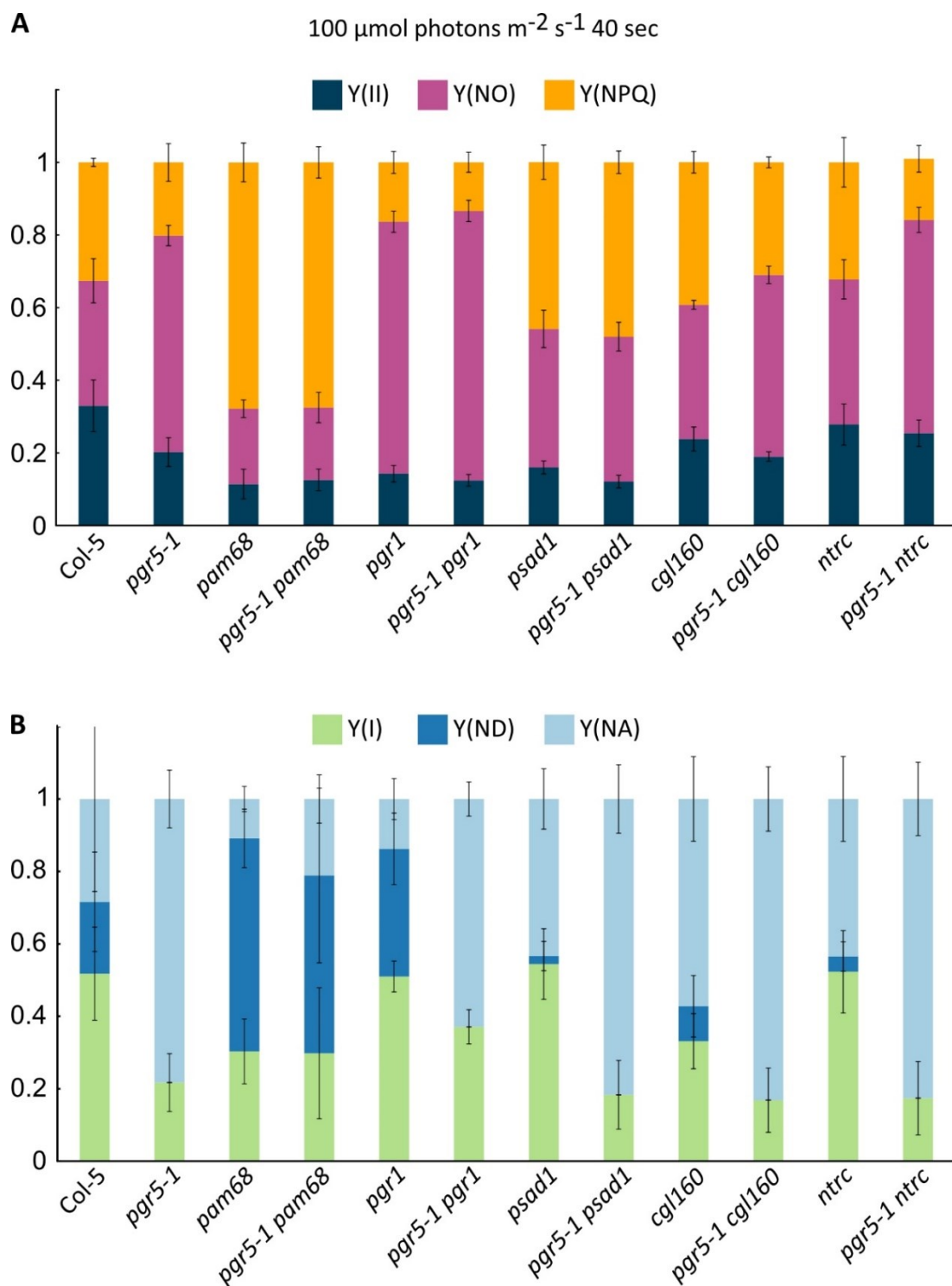


Figure 15: **Photosynthetic activity of PSII and PSI under 100 $\mu\text{mol photons m}^{-2} \text{s}^{-1}$ at induction-phase of PET-lines.** Five-week-old (12 h light, 100 $\mu\text{mol photons m}^{-2} \text{s}^{-1}$) WT (Col-5) and mutant (*pgr5-1*, *pam68*, *pgr5-1 pam68*, *pgr1*, *pgr5-1 pgr1*, *psad1*, *pgr5-1 psad1*, *cgl160*, *pgr5-1 cgl160*, *ntrc* and *pgr5-1 ntrc*) plants were dark adapted, followed by induction of photosynthesis by exposure to actinic light (100 $\mu\text{mol photons m}^{-2} \text{s}^{-1}$) for 6 min. After illumination, the plants were allowed to recover in the dark for 3 min. During the induction and recovery periods, photosynthetic parameters were measured by applying saturation pulses every 20 s. Five replicates were measured for each genotype. To analyse the acclimation of the plants during the induction phase, the data were analysed 40 s after the start of illumination. **A**, Quantum yield of photosystem II (Y(II)), quantum yield of non-regulated energy dissipation (Y(NO)) and quantum yield of non-photochemical quenching (Y(NPQ)) were measured from Chl fluorescence in the plants described. **B**, Quantum yield of photosystem I (Y(I)), donor-side limitation of photosystem I (Y(ND)) and acceptor-side limitation of photosystem I (Y(NA)) were revealed by measuring the absorbance at 875 nm minus 830 nm. Error bars represent \pm SD.

In conclusion, the results of the HL and LL measurements under FL showed that, of all the parameters analysed, only by decreasing the limitation of the acceptor side, Y(I) can be recovered in HL, as happens in *pam68*, and this seems to be the reason why *pgr5* survives under FL with this mutation. When the acceptor restriction is reduced to a certain level, the plant is able to suppress the lethal phenotype of *pgr5-1*. This was clearly observed in the double mutant line *pgr5-1 pam68* (Figure 14, Figure 15B), which showed growth under FL conditions (Figure 12). Furthermore, the ability to have at least a low level of PSI activity (Y(I): *pgr5-1* = 0.04, *pgr5-1 pam68* = 0.64 and *pgr5-1 pgr1* = 0.21) under HL ensured survival, as could be observed in the *pgr5-1 pgr1* line (Figure 14). In particular, the induction of NPQ was not sufficient for the survival of *pgr5-1*, as observed in the *pgr5-1 cgl160* line. Another interesting result was the suppression of the photosynthetic phenotype of *ntrc* by introducing the *pgr5-1* mutation, which was studied in more detail in the work of Naranjo and colleagues (Naranjo et al., 2021).

4.4 Activity and regulation of the CBB-cycle as a potential point to suppress *pgr5-1* lethality under FL

In the *pgr5* screen, mutants related to CBB-cycle activity, such as *pgr5-S111*, a mutant for the fructose 1,6-bisphosphatase (FBPase) was found. Indeed, it has already been described that an FBPase mutant, *hcefl*, can induce NDH-CEF and compensate for the absence of PGR5 (Livingston et al., 2010). In addition, the suppressor *pgr5-S336* with a mutation in the gene encoding the atypical Cys His-rich thioredoxin 2 (ACHT2) protein was also identified, which belongs to the thioredoxin family and has recently been described to redox-regulate (inactivate) the FBPase (Yokochi et al., 2021). The link between the CBB-cycle and the regulation of CEF made these mutants a very interesting subject for further investigation.

The suppressor *pgr5-S111* had a point mutation in the *HCEF1* gene (AT3G54050), which encodes the chloroplast FBPase. Therefore, a second allele of this line, designated *pgr5 hcefl*, was generated by crossing the T-DNA insertion knockout line of HCEF1 with *pgr5-1* to confirm the mutation-phenotype relationship. The newly generated double mutant and the originally found suppressor *pgr5-S111* showed a slightly lower growth than *pgr5-1* and the WT control (Col-5) under CL. In addition, the *pgr5-S111* line was slightly paler than the double mutant *pgr5-1 hcefl*. This stunted and pale phenotype was more strongly pronounced in the single mutant *hcefl*. Under FL, both *pgr5-S111* and *pgr5-1*

hcef1 survived but showed a retarded growth phenotype compared to CL. This result confirmed the results of the screen. Furthermore, the growth of the single *hcef1* mutant under FL was similar to its phenotype under CL conditions (Figure 16).

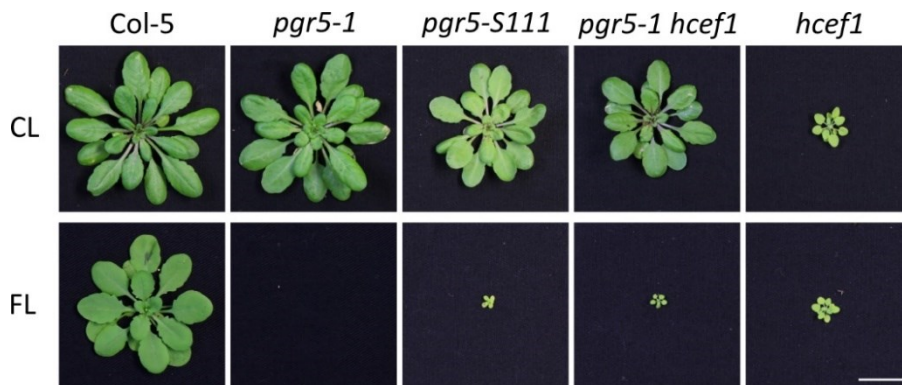


Figure 16: **Knock-out lines of *hcef1* in the background of *pgr5-1* growth phenotype.** Growth phenotype of 5-week-old Col-5, *pgr5-1*, suppressor lines *pgr5-S111*, double mutant line *pgr5-1 hcef1* and single T-DNA insertion line *hcef1* plants grown under control light conditions (CL, 12h of light 100 $\mu\text{mol photons m}^{-2} \text{s}^{-1}$ and 12h of darkness) or fluctuating light (FL, 12 h light, cycles of low light (50 $\mu\text{mol photons m}^{-2} \text{s}^{-1}$) for 5 min and high light (500 $\mu\text{mol photons m}^{-2} \text{s}^{-1}$). Scalebar correlates to 2 cm.

The causative mutation in the suppressor line *pgr5-S336* was predicted to be in the gene *ACHT2* (AT4G29670). To prove that this mutation was responsible for the survival of *pgr5-1* under FL, an additional allele using CRISPR/Cas was generated. A target sequence located near the point mutation caused by EMS treatment in the first exon of *ACHT2* was selected (Figure 17A). The mutation created by CRISPR/Cas resulted in the insertion of an extra nucleotide at position 231. Both mutations, the EMS point mutation and the additional nucleotide insertion, resulted in premature stop codons in the thioredoxin domain of *ACHT2* at positions 75 (*pgr5-S336*) and 87 (*pgr5-1 acht2-Cas* and *acht2-Cas*), respectively (Figure 17B). The growth phenotype of *pgr5-S336* under control light conditions was similar to that of Col-5 and *pgr5-1*. The single mutant line *acht2-Cas* was grown under CL and FL conditions as the WT (Col-5). *pgr5-S336* was severely impaired in growth but survived the FL treatment. The double mutant line *pgr5-1 acht2-Cas*, as the second allele, was also able to survive under FL with a growth comparable to *pgr5-S336* in FL and CL, proving that the mutation in *ACHT2* was the causative one (Figure 17C).

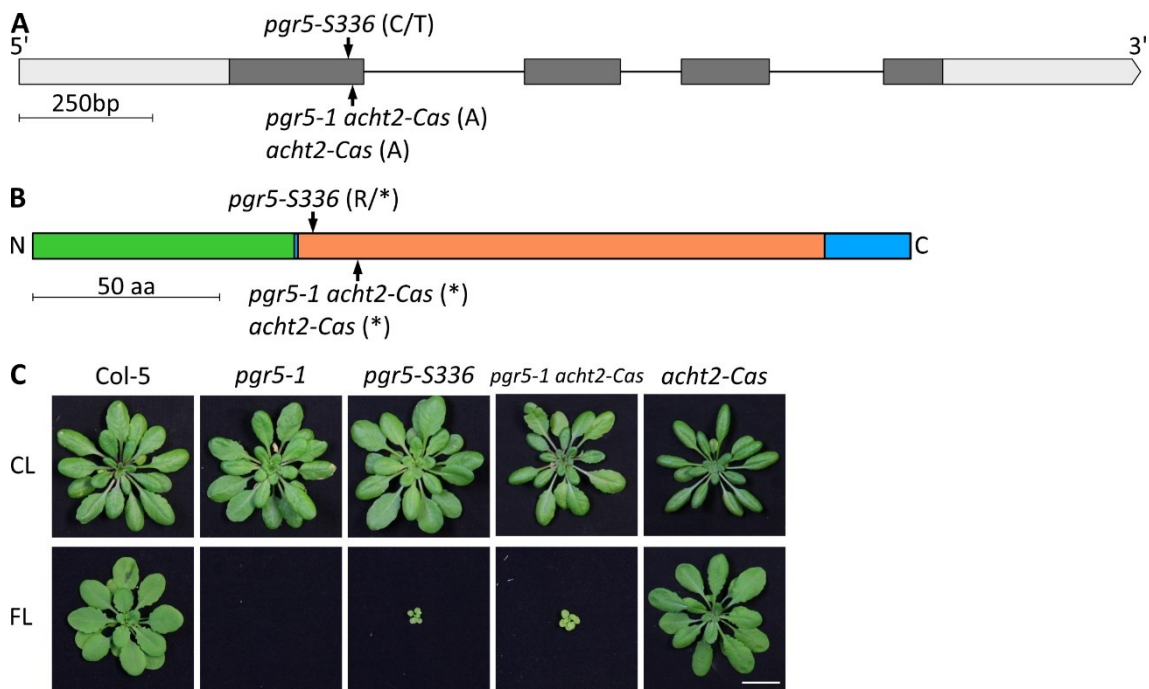


Figure 17: **A premature stop-codon in ACHT2 allows *pgr5-1* survival under FL conditions.** **A**, Schematic representation of the *ACHT2* gene. The exonic sequence is shown in dark grey, the intronic sequences are shown as black thin lines and the UTR regions are shown as light grey boxes. The orientation of the gene is indicated by the marking of the 5' and 3' ends. The size of the gene is indicated by a scale bar correlating to 250 bp. The position of the EMS mutation is indicated by an arrow and the label (*pgr5-S336*) as a nucleotide exchange (C/T). The insertion side of the additional nucleotide by homologous recombination after the cut by CRISPR/Cas is indicated by an arrow and the corresponding label (*pgr5-1 acht2-Cas* and *acht2-Cas*) and insertion (**A**). **B**, To-scale visualisation of the ACHT2 protein with marked cTP (green) and thioredoxin domain (orange). The N- and C-termini of the protein are marked with the corresponding letters (N and C). The premature stop codons resulting from the EMS mutation and the nucleotide insertion are marked with arrows and the corresponding labels (EMS (*pgr5-S336* (R/*)) and CAS (*pgr5-1 acht2-Cas* and *acht2-Cas* (*)). The scale bar represents 50 amino acids. **C**, Growth phenotype of 5-week-old Col-5, *pgr5-1* and *acht2-Cas* plants, suppressor lines *pgr5-S336* and *pgr5-1 acht2-Cas* grown under control light conditions (12 h light 100 $\mu\text{mol photons m}^{-2} \text{s}^{-1}$ and 12 h dark) and the same genotypes with additional double mutant line grown for 5 weeks under fluctuating light (12 h light, cycles of low light (50 $\mu\text{mol photons m}^{-2} \text{s}^{-1}$) for 5 min and high light (500 $\mu\text{mol photons m}^{-2} \text{s}^{-1}$). Scale bar corresponds to 2 cm.

4.4.1 Photosynthetic phenotype of suppressor lines *pgr5-1 hcefl* and *pgr5-S336*

Since the two EMS lines found, *pgr5-S111* and *pgr5-S336*, as well as the second alleles generated, *pgr5-1 hcefl* and *pgr5-1 acht2-Cas*, were able to suppress the lethal phenotype of *pgr5-1* under FL, further analysis was proceeded. The mechanism behind the survival of the suppressor lines through altered photosynthetic activity in terms of FL acclimation and CEF activity was investigated, as it has already been postulated that the *hcefl* mutant exhibits stronger CEF (Livingston et al., 2010). The double mutants *pgr5-1 hcefl* and

pgr5-1 acht2-Cas, along with Col-5, *pgr5-1* and *acht2-Cas* as controls, were used for the measurements.

To determine CEF, the fluorescence of the active center of PSII and the absorption of P700 were simultaneously measured (Figure 18A). Both photosystems are activated by applying the measurement light at a low light intensity. Due to this low light induction, the observed changes in fluorescence and P700 absorption were mainly due to CEF. The PSII fluorescence was used to calculate the plastoquinone reduction state by the minimum fluorescence (F_o) minus the measured fluorescence under far red light (F_{oFR}), normalised to the maximum fluorescence (F_m) observed in the sample (Figure 18B). The maximum P700 absorbance corresponds to oxidised P700 (P700_{ox}). The time required to oxidize 50 % of the P700 ($t_{1/2}P700_{ox}$) during the FR application was calculated (Figure 18C). Both the reduction of the plastoquinone pool and the oxidation of P700 are mainly due to the activity of the CEF under these low light conditions (Okegawa et al., 2008; Rühle et al., 2021).

In terms of plastoquinone pool reduction, the double mutant *pgr5-1 hcefl* and *acht2-Cas* behaved like the WT control (Col-5), while a lower level of reduction was measured in both *pgr5-1* and *pgr5-1 acht2-Cas* lines (Figure 18B). A faster oxidation of P700 was observed in the *pgr5-1* line compared to the WT, consistent with previous descriptions (Okegawa et al., 2008; Rühle et al., 2021), the double line *pgr5-1 hcefl* had almost the same $t_{1/2}P700_{ox}$ as the wild type with no significant differences. However, this suppression was not detectable in line *pgr5-1 acht2-Cas*, which had a shorter $t_{1/2}P700_{ox}$ than *pgr5-1* and presumably lower CEF activity, but a stronger electron flux from the PSI to the FNR (Figure 18C). The same observation of faster oxidation of the P700 was made in the *acht2-Cas* line compared to Col-5, suggesting that the knock-out of ACHT2 generates the higher electron sink at the P700. Interestingly, the photosynthetic phenotype of *pgr5-1* in P700 oxidation and PQ reduction was suppressed by knocking out HCEF1, in agreement with Livingstone et al. 2010 (Livingston et al., 2010).

Therefore, the higher CEF in *pgr5-1 hcefl* was dependent on the NDH complex, since PGR5 was missing in the double mutant of FBPase and PGR5 (*pgr5-1 hcefl*), but in the *acht2* mutant the NDH-dependent CEF is not upregulated, explaining the suppression phenotype of *pgr5-1 hcefl* but not of *pgr5-1 acht2-Cas*. In fact, an opposite trend was

observed for CEF, with $t_{1/2}$ P700ox being slightly faster in *pgr5-1 acht2-Cas* than in *pgr5-1* and significantly faster in *acht2-Cas* than in WT.

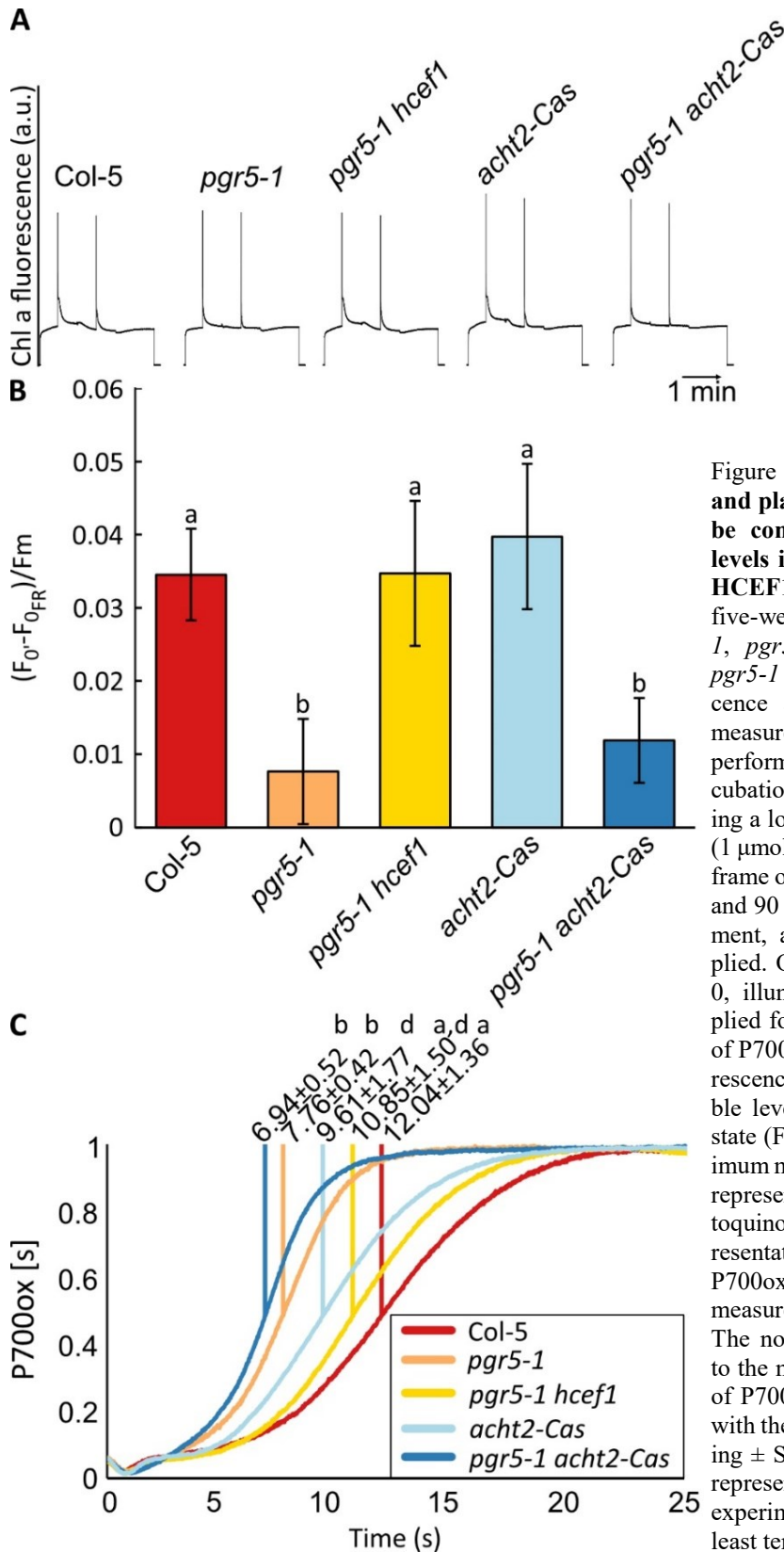


Figure 18: P700 oxidation rate and plastoquinone reduction can be complemented to wild type levels in *pgr5-1* by knocking out HCEF1 but not ACHT2. **A**, From five-week-old plants (Col-5, *pgr5-1*, *pgr5-1 hcef1*, *acht2-Cas* and *pgr5-1 acht2-Cas*), Chl *a* fluorescence and P700 absorption was measured. The measurement was performed after 1 hour of dark incubation on single leaves by applying a low intensity measuring light ($1 \mu\text{mol photons m}^{-2} \text{s}^{-1}$) over a time frame of 3 min at a time point of 30 and 90 s after start of the measurement, a saturation pulse was applied. One minute after time point 0, illumination FR light was applied for 60 s to achieve oxidation of P700. **B**, Average of Chl *a* fluorescence measured in (A) at the stable level (F_0) minus the minimal state (F_{0FR}) normalised to the maximum measured fluorescence (F_m), representing the reduction of plastoquinone under FR light. **C**, Representation of the normalized P700ox under FR light from the measurements described in (A). The normalization was performed to the maximum and the minimum of P700ox. $t_{1/2}$ P700ox is indicated with the average above, the according \pm SD and significant grouping represented as Arabic-letter. The experiment was performed with at least ten replicates per line.

To comprehend the suppression mechanism behind *pgr5-1 acht2-Cas*, the same measurements as demonstrated in Figure 10, simulating FL conditions was conducted. This was done to gather information on PSII and PSI activity under these conditions. The lines used in these measurements were a wild-type control (Col-5), *pgr5-1*, *acht2-Cas* and the double mutant lines *pgr5-1 hcefl* and *pgr5-1 acht2-Cas*. The results of the knock-out lines of ACHT2 (*acht2-Cas* and *pgr5-1 acht2-Cas*) experiment were highly anticipated due to the absence of observed cyclic electron flow (CEF) in the previous experiment. It was expected that the FL measurement could provide a possible explanation for the survival and shed light on the observed phenomenon. A lower Y(NA) was expected for the *acht2-Cas* line and the *pgr5-1 acht2-Cas* line due to the higher FBPase activity resulting from lower oxidation in the absence of ACHT2 (Yokochi et al., 2021). This would lead to a greater demand for NADPH and therefore electrons from PSI by the FNR, which would reduce the possibility of over-reduction of PSI.

An interesting observation at the beginning of the measurement was that the line *pgr5-1 acht2-Cas* showed an F_v/F_m close to 1 (0.95 ± 0.03), a higher value than the other lines (Col-5 0.84 ± 0.01 , *pgr5-1* 0.88 ± 0.05 and *pgr5-1 hcefl* 0.88 ± 0.04), and specific *acht2-Cas* (0.77 ± 0.02). In line *pgr5-1 acht2-Cas*, a higher Y(II) was observed during the LL phases, whereas WT, *pgr5-1* and *pgr5-1 hcefl* behaved more similarly (Figure 19A). The *acht2-Cas* line showed the lowest Y(II) values compared to the other lines. Interestingly, the double mutant *pgr5-1 hcefl* suppressed the impaired NPQ induction of *pgr5-1* and was able to induce NPQ during the HL peaks, reaching almost the WT level in the last HL peak of the measurement. A strong induced NPQ was observed in the *acht2-Cas* line, particularly in the HL peaks, which were more strongly induced compared to the WT at the beginning of the measurement. In the other two lines, *pgr5-1* and *pgr5-1 acht2-Cas*, no induction of NPQ was observed (Figure 19B).

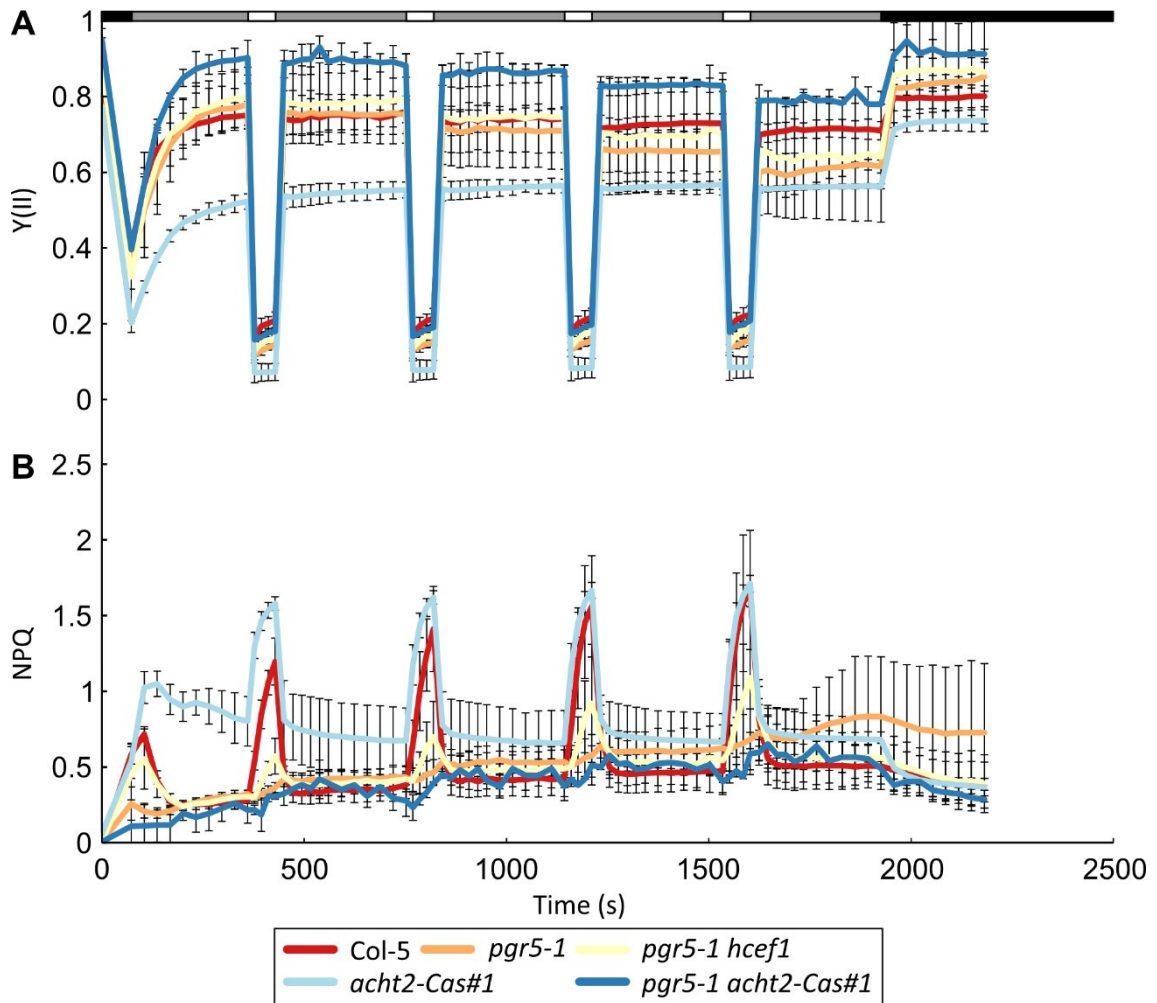


Figure 19: **Photosynthetic activity around PSII in *pgr5-1 hcef1* and *pgr5-1 acht2-Cas* under FL.** Different genotypes were grown for 5 weeks under control conditions (12 h light, 100 $\mu\text{mol photons m}^{-2} \text{s}^{-1}$). WT (Col-5) and mutant (*pgr5-1*, *pgr5-1 hcef1*, *acht2-Cas* and *pgr5-1 acht2-Cas*) plants were dark adapted (Black bar), followed by 5 min of illumination with actinic light (50 $\mu\text{mol photons m}^{-2} \text{s}^{-1}$, dark grey bar). After the illumination with low light, plants were subjected to high light for 1 min (500 $\mu\text{mol photons m}^{-2} \text{s}^{-1}$, white bar). Low light and high light phases repeated alternately four times followed by a recovery phase for 5 min in the dark (black bar). Over the time frame of induction and recovery, the photosynthetic parameters were measured by applying saturation pulses every 20 s in the low light phase and recovery phase and every 15 s in the high light phase. For each genotype three replicates were measured. **A**, Photosystem two quantum yields (Y(II)) were measured by Chl fluorescence in the described plants. **B**, Determined values of the NPQ calculated from the values measured in (A). \pm SD are represented as error bars.

The activity of PSI under FL was higher in the LL phase and decreased in the HL phase. This decrease in the HL phase was more pronounced in the mutant lines (*pgr5-1*, *pgr5-1 hcef1*, *acht2-Cas* and *pgr5-1 acht2-Cas*) than in the wild type (Col-5). In the low light phases, between the HL peaks, the double mutant *pgr5-1 hcef1* had the lowest Y(I) (Figure 20A). Donor side limitation was observed in the wild-type control (Col-5) and in the *pgr5-1 hcef1* and *acht2-Cas* mutant lines. This induction of donor-side limitation in the *pgr5-1* background by the *hcef1* mutation indicates a restoration of photosynthetic control by establishing a proton gradient through the substitution of PGR5-mediated CEF by

NDH-mediated CEF. No difference was observed between the *pgr5-1* line and the *pgr5-1 eight2-Cas* line, neither of which showed donor-side limitation (Figure 20B). Focusing on the acceptor side limitation of PSI, Col-5 showed a smaller increase in HL, while the mutant lines *pgr5-1*, *pgr5-1 hcefl* and *pgr5-1 acht2-Cas* showed a strong acceptor side limitation under this condition, almost reaching the maximum 1. During the LL phases, *pgr5-1* and *pgr5-1 hcefl* showed a steadily increasing level of acceptor side limitation, which was stronger in the *pgr5-1 hcefl* lines. Interestingly, a slightly lower Y(NA) was observed during LL in the *pgr5-1 acht2-Cas* line compared to the *pgr5-1* line. In addition, *acht2-Cas* showed a marked difference in strongly reduced Y(NA) compared to Col-5, indicating a stronger electron flux away from PSI at the PSI acceptor side (Figure 20C).

In summary, the photosynthetic measurements revealed that the *pgr5-1 hcefl* line exhibited a stronger induced CEF, allowing this line to induce NPQ and establish photosynthetic control (Y(ND)) in a manner comparable to the wild-type control. This adaptation allowed the *pgr5-1 hcefl* line to survive under FL conditions. In contrast, the *acht2-Cas* line and the *pgr5-1 acht2-Cas* line did not exhibit CEF recovery, but a lower PSI acceptor side limitation was observed. This observation aligns with a more active CBB-cycle and implies a higher electron demand from PSI resulting in a faster oxidation of the PSI. However, further experiments are needed to fully verify this result.

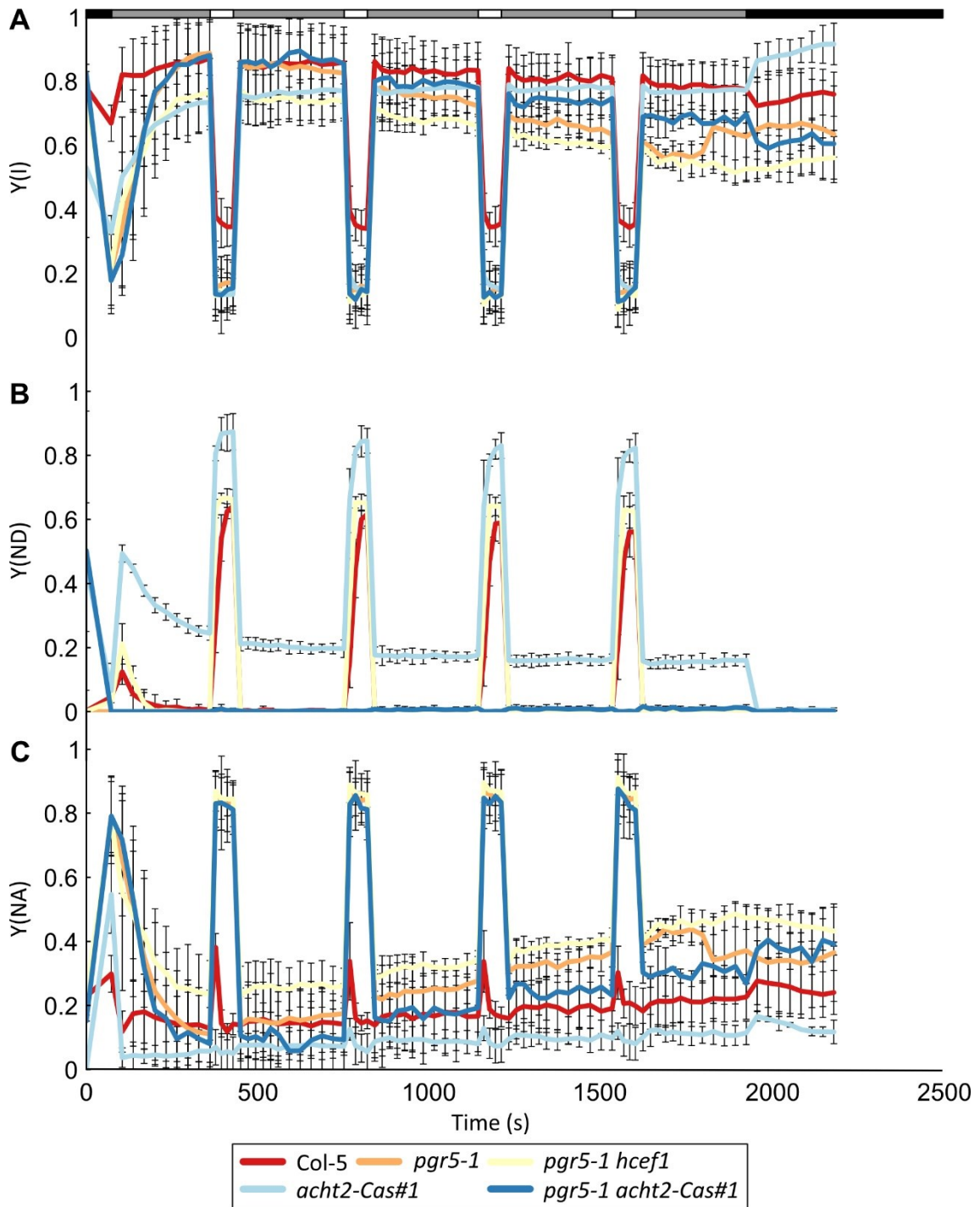


Figure 20: **PSI activity and acceptor side limitation in *pgr5-1 hcef1* and *pgr5-1 acht2-Cas* under FL.** Different genotypes were grown for 5 weeks under control conditions (12 h light, $100 \mu\text{mol photons m}^{-2} \text{s}^{-1}$). WT (Col-5) and mutant (*pgr5-1*, *pgr5-1 hcef1*, *acht2-Cas* and *pgr5-1 acht2-Cas*) plants were dark adapted (Black bar), followed by 5 min of illumination with actinic light ($50 \mu\text{mol photons m}^{-2} \text{s}^{-1}$, dark grey bar). After illumination with low light, plants were subjected to high light for 1 min ($500 \mu\text{mol photons m}^{-2} \text{s}^{-1}$, white bar). Low light and high light phases repeated alternately four times followed by a recovery phase for 5 min in the dark (black bar). Over the time frame of induction and recovery, the photosynthetic parameters were measured by applying saturation pulses every 20 s in the low light phase and recovery phase, and every 15 s in the high light phase. For each genotype, three replicates were measured. **A**, Quantum yields of Photosystem I (Y(I)) were uncovered by measuring the absorption at 875nm minus 830nm. **B**, Donor-side limitation of PSI was calculated from the measurements shown in (A). **C**, Acceptor-side limitation of Photosystem I was calculated from the measurements represented in (A). The error bars represent \pm SD.

From the plant photosynthetic activity under different CO₂ concentrations was measured to see whether higher FBPase activity could rescue it by misregulating its activity (less oxidation in the absence of ACHT2). The different CO₂ concentrations can increase or down-regulate the activity of the CBB-cycle. The plant was subjected to measurements of photosynthetic activity using 0 ppm CO₂ (down-regulation), 400 ppm CO₂ (atmospheric concentration, normal activity), and 800 ppm CO₂ (enhanced activity due to lower CO₂ limitation). It was shown that when a higher amount of CO₂ is provided, the limitation of the CBB-cycle is lifted to some extent and a higher electron flow from the PSI to the FNR takes place (Tan et al., 2021). This effect can be used to enhance the photosynthetic phenotype in the suppressor line to the point that it can be detected in the single line (*acht2-cas*) compared to the wild type control as well as in *pgr5-1* compared to the double mutant (*pgr5-1 acht2-cas*).

The photosynthetic measurement which was conducted to investigate the photosynthetic activity under different CO₂ concentrations, to monitor photosynthetic parameters in dark-adapted plants was the so-called induction recovery curve (IRC). The IRC were taken during illumination with actinic light at a growth light intensity of 100 μmol photons m⁻² s⁻¹, followed by a recovery period in the dark.

A lower Y(NA) was observed in the *acht2-Cas* line compared to the wild-type control at different CO₂ concentrations. Only at atmospheric concentration did the knock-out line behave similarly to the Col-5 line. It was found that the oxidation of PSI by the acceptor side is less limited in the *acht2-Cas* line, particularly at low CO₂ levels. Interestingly, a lower Y(NA) was observed in the double mutant line *pgr5-1 acht2-Cas* compared to the *pgr5-1* line. Under all the different CO₂ concentrations, the *pgr5-1 acht2-Cas* line showed a higher electron flow from PSI to Fd as an electron acceptor (Figure 21A, B and C).

The result of the measurement of Y(NA) under different CO₂ concentrations indicates a higher activity of the CBB-cycle, resulting in a higher demand for NADPH. NADPH is produced from NADP⁺ and H⁺ and requires reduction energy from Fd via the FNR. This results in a higher electron demand through the FNR in the mutant lines (*acht2-Cas* and *pgr5-1 acht2-Cas*) than in their specific background (Col-5 and *pgr5-1*). This, in turn, oxidises PSI faster and more efficiently, allowing a partial substitution of the PGR5-mediated CEF as an electron sink from PSI in the absence of PGR5

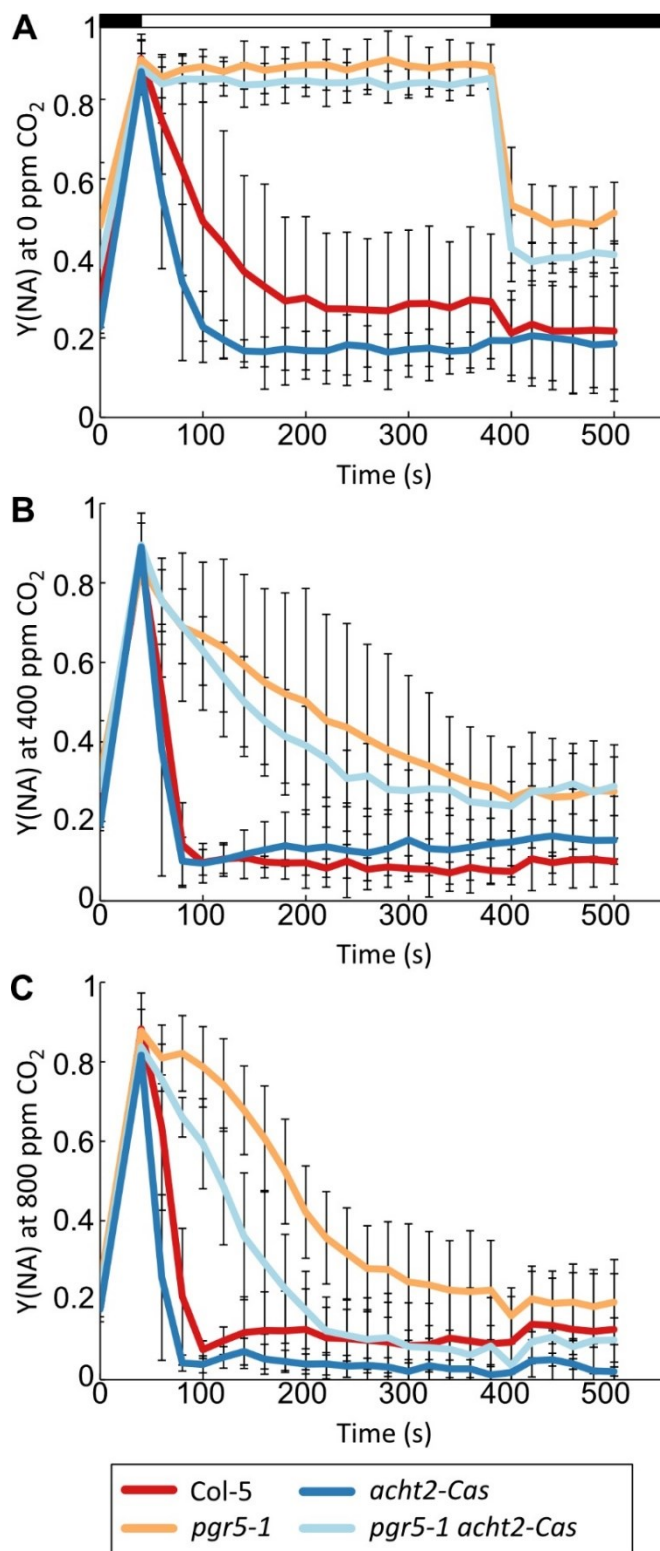


Figure 21: Y(NA) is dependent on CO₂ concentration in *acht2* mutant lines.

Five-week-old plants were grown under control conditions (12 h light, 100 $\mu\text{mol photons m}^{-2} \text{s}^{-1}$). WT (Col-5) and mutant (*pgr5-1*, *acht2-Cas* and *pgr5-1 acht2-Cas*) plants were dark adapted under different concentrations of CO₂ (0 ppm CO₂, 400 ppm CO₂ and 800 ppm CO₂), followed by 6 min of induction of the photosynthesis by subjecting to actinic light (100 $\mu\text{mol photons m}^{-2} \text{s}^{-1}$, white bar) and stable predetermined CO₂ amounts (0 ppm CO₂, 400 ppm CO₂ and 800 ppm CO₂). After the illumination, plants recovered for 3 min in the dark (black bar). Over the time period of induction and recovery, the photosynthetic parameters were measured by applying saturation pulses every 20 s. For each genotype four replicates were measured. **A**, Acceptor-side limitation of Photosystem I was calculated from the measurements of the absorption at 875 nm minus 830 nm at 0 ppm CO₂. **B**, 400 ppm CO₂ and **C**, 800 ppm CO₂. The error bars represent \pm SD.

4.5 New proteins identified by the *pgr5* suppressor screen

In the *pgr5* screen, two proteins with unknown functions were identified. The most likely causative mutations in the lines for the suppression of the lethal phenotype were located in the gene AT2G04360 (*S42*) and in the gene AT2G27290 (*S261*). The suppressor mutation in the gene *S42* was not further characterised in this work.

4.6 An unknown protein suppresses *pgr5-1* lethality under FL

The suppressor *pgr5-S261*, which has a SNP in a gene encoding an unknown protein (AT2G27290, referred to as *S261*), was discovered during the *pgr5* screen. This mutation is thought to be the most likely cause of the suppression. However, an additional line with a mutation in the *S261* gene was not found in the screen, so it was necessary to generate an additional allele using CRISPR/Cas or T-DNA to prove the suppressor function of *S261*.

To study *S261* in more detail, knock-out lines in Col-0 and *pgr5-1* backgrounds were generated using CRISPR/Cas technology. These lines were used to characterise photosynthesis, growth under FL and CL, interaction of *S261* with other proteins and protein accumulation of thylakoid complexes.

The target for the generation of the CRISPR/Cas line in *S261* was selected in the first exon. To identify the double mutant *S261 pgr5*, the seeds of the T₁ generation of transformed *pgr5-1* plants were selected under FL and the survivors were transferred to LD conditions to obtain the T₂ generation in which the experiments were performed. To generate the single mutant line, the selected *S261 pgr5* knockout lines were crossed with Col-0, and the T₂ generation was screened to identify homozygous lines through sequencing. This approach was chosen because directly knocking out *S261* using CRISPR/Cas in Col-0 resulted in seedling lethal plants.

The mutation generated by CRISPR/Cas was of particular interest to determine whether it resulted in a stop codon or a deletion/exchange of several amino acids. To accomplish this, the genomic DNA of both CAS lines was sequenced (*pgr5-1 S261-Cas#1* and *pgr5-1 S261-Cas#2*). The sequences showed a deletion of 14 nucleotides from position 113 to 127 for line 1 and a deletion of 21 nucleotides from position 102 to 123 in the first exon of *S261* for line 2 (Figure 22B). The deletion of nucleotides in line *pgr5-1 S261-Cas#1* resulted in a deletion of 4 amino acids and a frame shift with a premature stop codon at position 38, which is at the end of the predicted cTP, from position 1 to 39. In line *pgr5-*

1 S261-Cas#2, the deletion of the 21 nucleotides resulted in a deletion of 7 amino acids from 36 to 43 without altering the reading frame (Figure 22C). Interestingly, 4 of these amino acids belonged to the cTP and the newly generated sequence was interpreted as a mitochondrial transit peptide by the TargetP programme. Therefore, the deletion in *pgr5-1 S261-Cas#2* probably leads to a mislocalisation of the protein to the mitochondria instead of the chloroplast, but this remains to be shown. In the EMS line *pgr5-S261*, the suppressor mutation was located in the first exon and resulted in an amino acid exchange at position 72, where a glycine was replaced by an aspartic acid.

The EMS *pgr5-S261* line found in the *pgr5* screen showed similar growth to *pgr5-1* and Col-5 under CL (Figure 22A). The newly generated alleles of S261 by CRISPR/Cas: *pgr5-1 S261-Cas#1* and *pgr5-1 S261-Cas#2*, showed the same growth phenotype as *pgr5-S261* under CL; however, the line *pgr5-1 S261-Cas#1* was slightly smaller. Furthermore, both lines *pgr5-1 S261-Cas#1* and *pgr5-1 S261-Cas#2* survived under FL conditions mimicking *pgr5-S261*, although all these lines showed a strong growth impairment compared to Col-5 (Figure 22A).

For the generation of the single mutant line *S261* using CRISPR/Cas, a selection was performed on MS plates supplemented with hygromycin. Plants that were successfully transformed should grow on hygromycin due to the resistance introduced by the CRISPR/Cas fragment. During the selection of the T₁ generation, several plants were observed to exhibit growth on the selection media but displayed a nearly complete lack of pigmentation, appearing pale. Initial sequencing showed that these plants had an insertion that resulted in a premature stop codon. These knockout lines could not reach the adult state under CL conditions. In a further attempt to generate a single knock-out line, the *pgr5-1 S261-Cas#1* and *pgr5-1 S261-Cas#2* lines were crossed with the wild-type line Col-0. In the T₂ generation, a random selection of 16 plants was analyzed. Eight of these plants showed a pale phenotype. All selected plants were sequenced for a possible insertion or deletion. The sequencing experiment revealed that the pale lines contained either insertions or deletions, and in two of the lines, the specific deletion matched the one identified in the *pgr5-1 S261-Cas#1* line. Similar to the hygromycin selection experiment, all pale plants failed to reach the adult state (Figure 22A).

A green fluorescent protein (GFP)-tagged variant of the S261 protein was expressed in the wild-type and localised in the chloroplast. To this end, the GFP-tagged protein was transiently expressed in *Nicotiana benthamiana* leaves, followed by protoplast extraction

and visualisation by microscopy. The autofluorescence of Chl *a* was used as an indicator of the location of the chloroplast and merged with the fluorescence signal from the GFP. This result indicated that the mature wild-type protein S261 was localised in the chloroplast (Figure 22D).

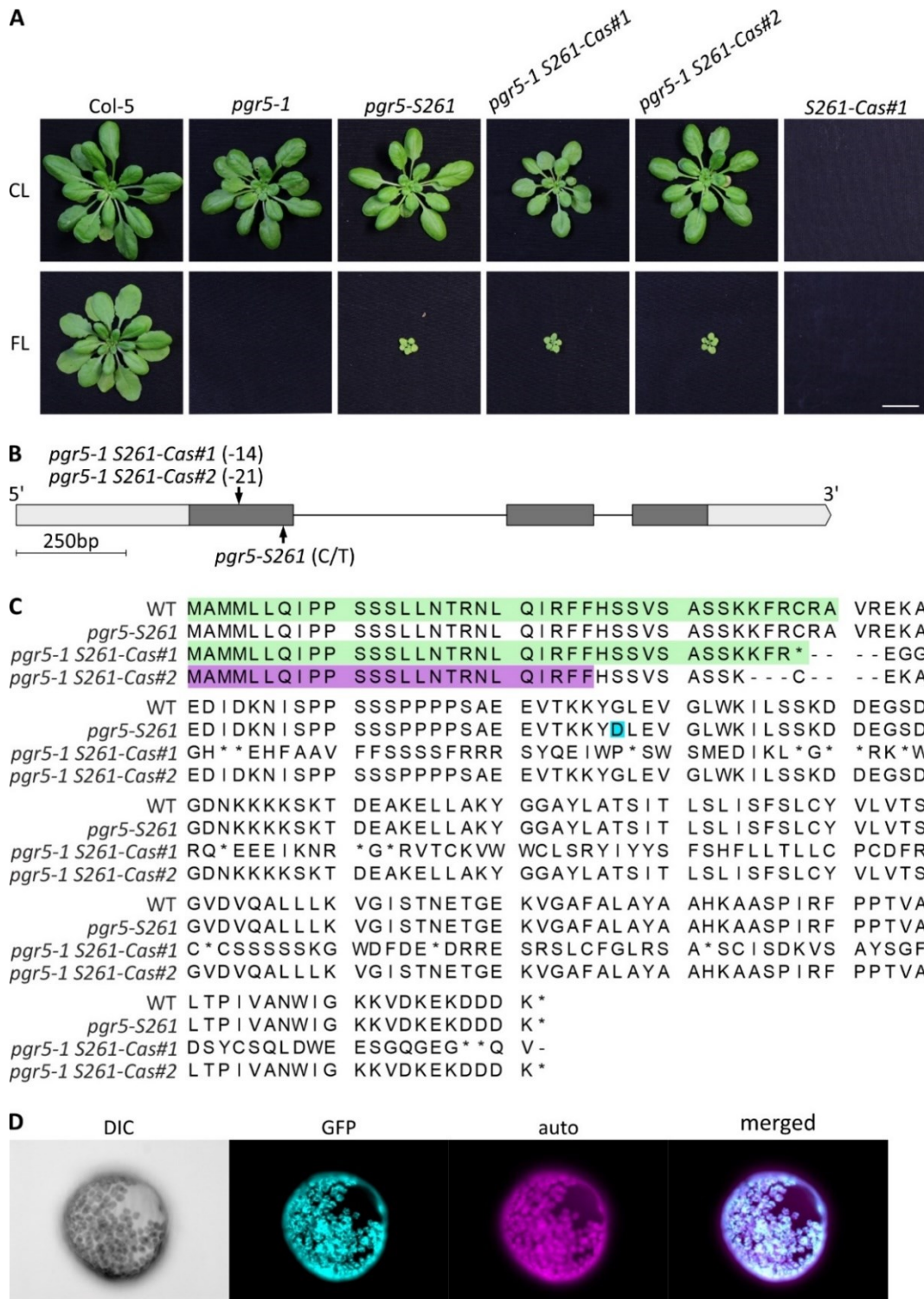


Figure 22: **S261 encodes a chloroplast-localized protein, the knock-out of which suppresses the *pgr5* phenotype.** **A**, Growth phenotype of 5-week-old Col-5, *pgr5-1*, suppressor lines *pgr5-S261 pgr5-1 S261-Cas#1* and *pgr5-1 S261-Cas#2* under control (12h of light 100 $\mu\text{mol photons m}^{-2} \text{s}^{-1}$ and 12h of darkness) and fluctuating light conditions (12 h light, cycles of low light (50 $\mu\text{mol photons m}^{-2} \text{s}^{-1}$) for 5 min and high light (500 $\mu\text{mol photons m}^{-2} \text{s}^{-1}$). Scalebar corresponds to 2 cm. **B**, Schematic representation of the gene AT2G04360. Exonic sequence is marked in dark gray, the UTR regions as bright grey boxes and intronic sequence as a black line. The orientation of the gene is indicated with the marking of the 5' and 3' end. The size of the gene is indicated by a scale bar corresponding to 250 bp. The sites of the mutations induced by the EMS treatment are labeled by an arrow and the name of the represented line (*pgr5-S261*). The found nucleotide exchanges in the *pgr5* Cas lines are stated in parentheses. **C**, Alignment of the S261 protein from Col-0 (WT), the two generated CRISPR/Cas alleles (*pgr5-1 S261-Cas#1* and *pgr5-1 S261-Cas#2*) and the mutated protein in the EMS line *pgr5-S261*. The intact transit peptide is marked with a green background.

The predicted mitochondrial transit peptide is marked in purple and the amino acid exchange of *pgr5-S261* in cyan. Premature stop-codons found in the mutant lines are marked with a star and amino acid deletion is indicated by a hyphen. **D**, Localization of the S261-protein through protein-GFP fusion. The S261-GFP protein was transiently expressed in *Nicotiana benthamiana* leaves, and protoplast were extracted from one leaf to be visualized via fluorescence microscopy. Pictures were recorded from a positive transformed protoplast. The protoplast itself was recorded through differential interference contrast image (DIC). Autofluorescence of the Chl (auto) is visualized as red to localize the chloroplast. The GFP-signal (GFP) is shown in green and indicates the location of the S261 protein GFP fusion. A merged picture of the autofluorescence and the GFP-signal (merged) was generated to show the overlapping localization.

Transmembrane domain analysis using the web tool TMHMM-2.0 showed that S261 has one such domain, and the C-terminus is exposed to the stroma and the N-terminus to the lumen (Sandoval-Ibanez et al., 2022). The structure of the protein is shown schematically in Figure 23 (Figure 23A and B). Protein S261 is conserved in green algae and plants. No homologue can be found in cyanobacteria; therefore, this protein falls into the category “Conserved in Plant Lineage and Diatoms (CPLD)” (Figure 23C).

By referring to the Klepikova atlas, which displays the expression patterns of genes in different organelles of *Arabidopsis*, it was observed that S261 is predominantly expressed in the leaves of the plant. Furthermore, its expression can be detected at all developmental stages. In addition to the predominant expression in the leaves, some level of expression of S261 was also detected in the flowers (Figure 23D).

Based on these results, S261 emerges as a transmembrane protein that exhibits conservation across plant species and diatoms. Its expression profile spans the entire duration of plant growth, indicating its involvement throughout different developmental stages.

Results

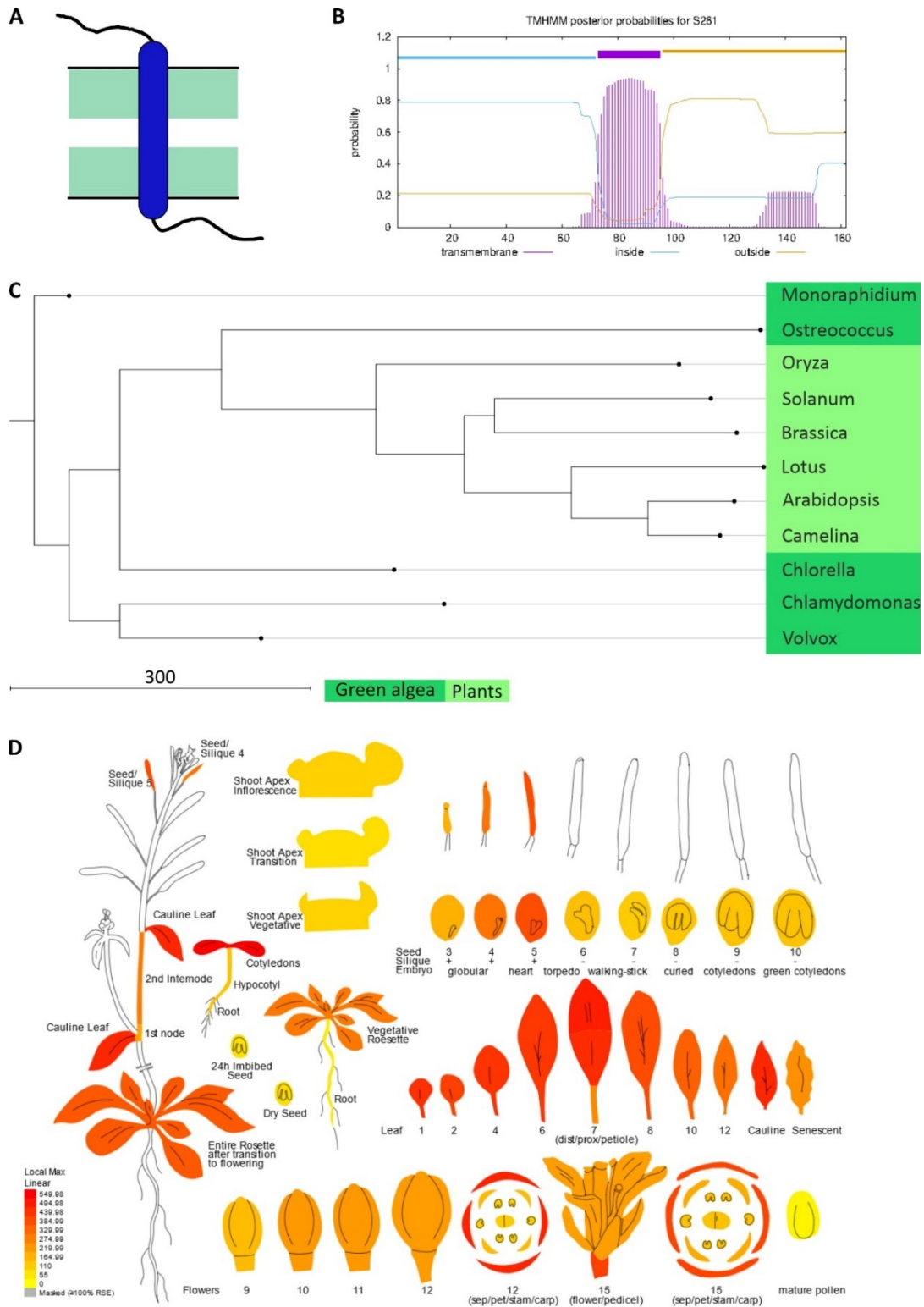


Figure 23: **Bioinformatical analysis of S261.** **A**, Schematic representation of the S261 protein localized in the thylakoid membrane. Transmembrane domains are represented in blue ellipses, non-transmembrane domains are drawn as black lines. Thylakoid membrane is visualized as a black line and green square. **B**, Transmembrane prediction of the S261 protein performed with TMHMM-2.0. **C**, Phylogenetical tree built by highest likelihood analysis with CLC main workbench, with a bootstrap of 100. Organisms representing green algae (green brown) and plants (green) were selected for the generation of the tree. **D**, Expression atlas based on the Klepikova Atlas (Klepikova et al., 2016) of the *S261* gene in Arabidopsis presented in the different development stages and organs. Expression level is color coded with the level of expression and correlating color represented in the legend.

4.6.1 Cyt b₆f accumulates less in S261 mutant lines

Recently, Sandoval-Ibáñez et al. described that the S261 protein is involved in the assembly of the cytochrome b₆f complex (Sandoval-Ibanez et al., 2022). This finding is consistent with our data on *pgr5 S261* as a suppressor of *pgr5*, as it has been shown that downregulation of the Cyt b₆f complex in the *pgr1* mutant suppresses the photosynthetic phenotype of *pgr5-1* (Figure 14, Figure 15 and Yamamoto & Shikanai, 2019).

To determine whether S261 is involved in the assembly of the Cyt b₆f complex, the accumulation of the complex was determined in the native state by separating extracted thylakoids according to their size using a blue native (BN) side. In addition immunodetection was used to determine which proteins were less abundant in the BN.

The *pgr5-1* mutant did not show any clear difference in the thylakoid protein composition on the BN compared to the wild type (Col-5). Interestingly, a lower intensity of the band representing the proteins Cyt b₆, Cyt f and PSII monomer was observed in both *pgr5-1 S261-Cas lines #1* and *#2* compared to *pgr5-1* (Figure 24A). The EMS mutant line *pgr5 S261* showed the same protein pattern as *pgr5-1* or the wild-type control (Col-5) (Figure 24A).

To validate the results obtained from BN analysis, immunodetection experiments targeting Cyt f and Cyt b₆ were conducted. All mutant lines (*pgr5-1*, *pgr5-1 S261-Cas#1*, *pgr5-1 S261-Cas#2* and *pgr5 S261*) had almost no detectable PGR5. Line *pgr5-1* showed a slightly lower accumulation of Cyt f and Cyt b₆ compared to the wild type (Col-5). In the *pgr5 S261* line, a reduction in the accumulation of Cyt b₆ was observed compared to the *pgr5-1* line. Additionally, a slight reduction in the accumulation of Cyt f was also detected in the *pgr5-1 S261-Cas#1* line compared to the *pgr5-1* line. Surprisingly, both the *pgr5-1 S261-Cas#1* and *pgr5-1 S261-Cas#2* lines displayed a similar level of Cyt b₆ accumulation compared to the *pgr5-1* line. In the mutant lines *pgr5-1 S261-Cas#1*, *pgr5-1 S261-Cas#2* and *pgr5 S261* a slight but visible increase of PGR5 compared to *pgr5-1* was detectable (Figure 24B and C).

The observations suggest that in the absence of PGR5, S261 does not play a significant role in the stability or assembly of the Cyt b₆f complex or other thylakoid complexes. This implies the existence of a previously unknown function of S261 that requires interaction with PGR5 for its proper functioning.

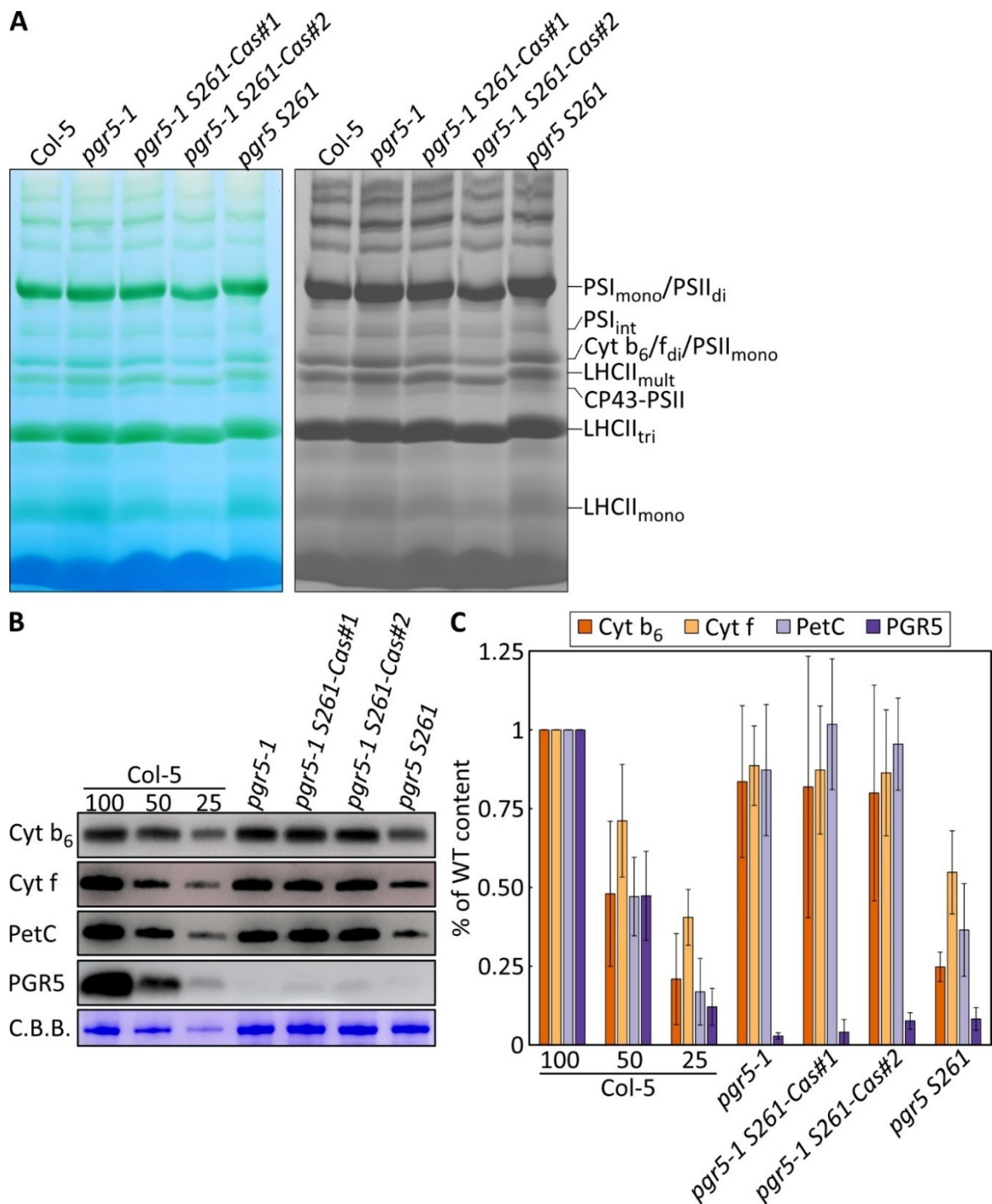


Figure 24: **Protein content of the *S261*-lines.** **A**, Scan of a BN-PAGE loaded with extracted thylakoids of plants grown for five weeks under CL conditions (12h of light $100 \mu\text{mol photons m}^{-2} \text{s}^{-1}$ and 12h of darkness). The following genotypes were used: wild type control (Col-5) and mutant lines (*pgr5-1*, *pgr5-1 S261-Cas#1*, *pgr5-1 S261-Cas#2* and *pgr5 S261*). Sample corresponding to $30 \mu\text{g}$ of Chl were loaded. The BN was documented through a color picture and a scan with a Typhoon. By employing the Typhoon scan, weaker bands can be visualized more effectively. In the color picture, the complexes can be identified based on their size, as well as the accumulation of Chl and carotenoids. The lanes were labeled with the protein complexes identified. **B**, Immunodetection of Cyt f, Cyt b₆, PetC and PGR5 from genotypes used in (A). Sample representing $30 \mu\text{g}$ whole leaf extract was loaded for PGR5 detection, and $5 \mu\text{g}$ for Cyt f, Cyt b₆ and PetC, onto a Tris-Tricin gel and separated accordingly their size. Proteins were transferred via semi-dry blotting onto a PVDF-membrane. The membrane was blocked with 5% milk for an hour and decorated with the specific antibodies against the detected proteins. As a loading control, C.B.B. staining was performed. One of four replicates was chosen for the representation **C**, Quantification of protein amount as an average of 4 replicates of the western blots presented in (B) in percentage of Col-5. Error bars indicate the standard deviation.

4.6.2 S261 is predicted to form a complex with PGR5, Fd and FNR

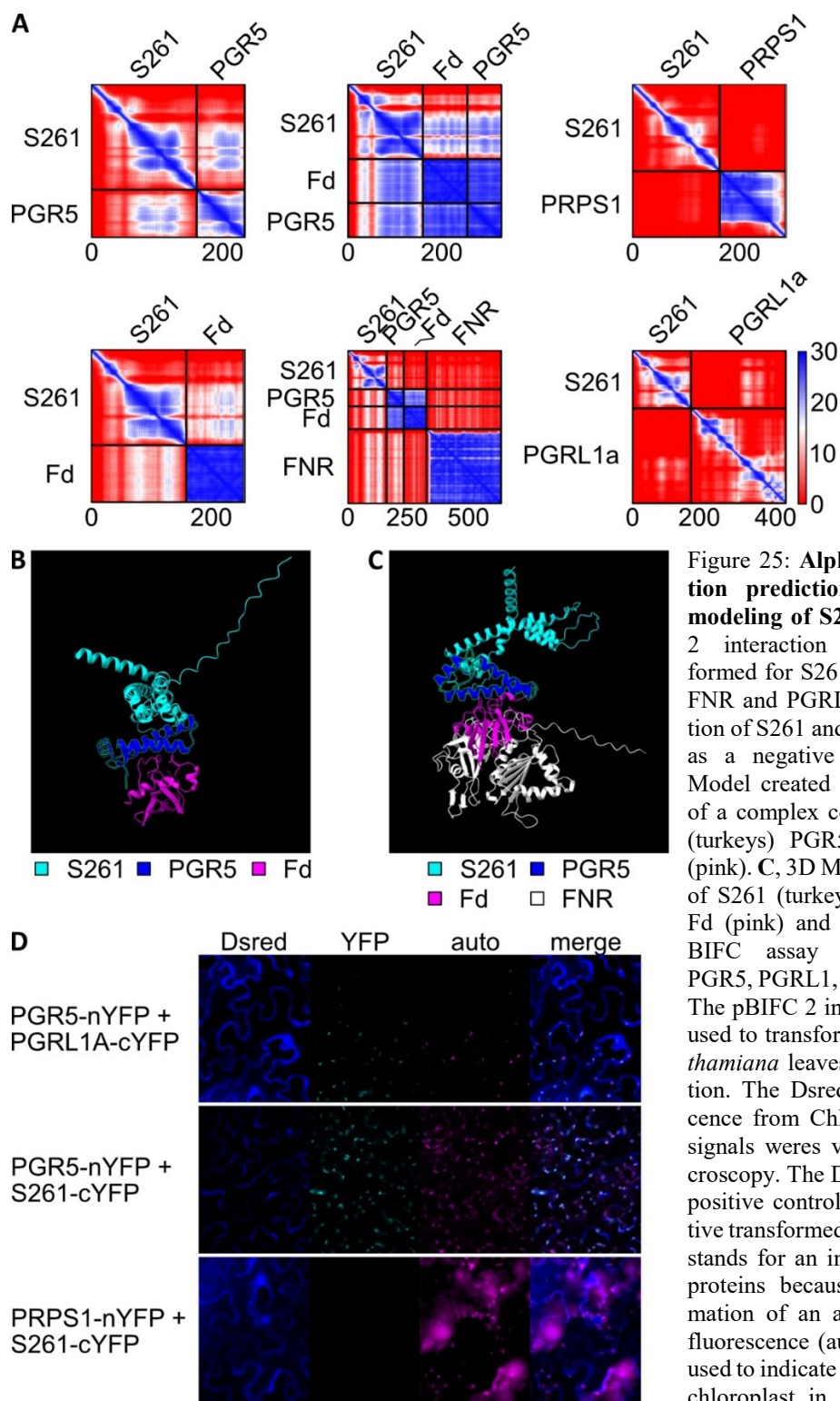
To investigate whether unknown proteins found in the *pgr5* suppressor screen could interact or form a complex with proteins involved in PGR5-mediated CEF, an interaction prediction was performed using the online tool AlphaFold 2. For the prediction the amino acid sequence of S261, PGR5, Fd, FNR and the unrelated protein PRPS1 (plastid ribosomal protein S1) without their cTP was used. The predicted interaction between PRPS1 and S261 was utilized as a negative control. The proteins PGR5, Fd and FNR were examined in single interaction and in possible complex formation.

The interactions examined showed a high probability of interaction between S261 and PGR5, as shown in the histogram generated by AlphaFold 2. Furthermore, Fd and S261 could also interact, although with a lower probability than PGR5-S261. A noteworthy finding was that when AlphaFold 2 was tasked with predicting the interaction between S261, PGR5 and Fd, within a complex, the predicted interaction was more probable compared to the interactions with the individual proteins considered separately. Interestingly, the addition of FNR to the putative S261-PGR5-Fd complex decreased the likelihood of this complex forming. Furthermore, the prediction of the possibility of interaction between PGRL1A and S261 was negative, similar to the prediction of PRPS1 and S261 (Figure 25A). Upon examination of the complex, it was observed that S261 predominantly binds to PGR5, acting as a bridge between PGR5 and Fd (Figure 25B). Fd serves as a link between the FNR and the complex consistin of S261, PGR5 and Fd (Figure 25C).

To validate the predicted interactions, a BIFC assay was performed for PGR5 and S261. In the BIFC experiment, the Dsred signal was utilized as a control for the detection of positive transformed cells. The YFP signal can only be detected if the proteins interact as the N-terminus of YFP is fused to the C-terminus of PGR5 and the C-terminus of YFP is fused to the C-terminus of S261. When there is an interaction, the two halves of the YFP protein fuse together to form an active YFP that can produce a light signal when excited. An interaction was observed for the positive control (PGR5-PGRL1A) and also for PGR5 and S261, confirming the accuracy of the AlphaFold 2 prediction. Correspondingly, the negative control S261-PRPS1 showed no YFP signal (Figure 25D). In order to observe

the localisation of the expressed proteins, in addition, Chl *a* fluorescence (auto) was detected, serving as an indicator of chloroplast localization. In the merged image, a perfect overlapping of the YFP signal and the Chl *a* fluorescence was observed (Figure 25D).

In conclusion, the interaction between PGR5 and S261 has been confirmed. Interaction of S261 with the other proteins involved in PGR5-mediated CEF (Fd and FNR) has a high probability as predicted by the AlphaFold 2 tool. These results suggest an additional function of S261 beyond its role in the stability or assembly of the Cyt b_6f complex, but further work is needed to elucidate its exact function.



4.6.3 Photosynthetic activity of *pgr5-1 S261-Cas* lines

Measurements of photosynthetic performance during an IRC and under FL were performed to further investigate the *pgr5* suppressor mechanism in the *pgr5 S261* line. The IRC measurement would give a more general view of photosynthetic activity in lines without S261, while the FL measurement was performed to directly investigate possible

links between photosynthetic activity and the suppression of the *pgr5-1* lethal phenotype. For the experiment, Col-5 was used as a wild-type control and the mutant genotypes were the generated CAS lines (*pgr5-1 S261-Cas#1* and *pgr5-1 S261-Cas#2*) and *pgr5-1*.

The following PSII-related parameters were calculated from the measured Chl fluorescence and analyzed in the IRC measurements: Y(II) represents the quantum yield of PSII, while NPQ stands for non-photochemical quenching, Y(NO) indicates energy dissipation and can also be interpreted as the formation of ROS, and additionally 1-qL reflects the reduction state of the PQ pool. For PSII activity (Y(II)), the wild-type control (Col-5) and *pgr5-1* behaved similarly, while lines *pgr5-1 S261-Cas#1* and *pgr5-1 S261-Cas#2* had slightly lower PSII activity in the induction phase (Figure 26A). In the case of NPQ and Y(NO), the lines *pgr5-1*, *pgr5-1 S261-Cas#1*, and *pgr5-1 S261-Cas#2* exhibited similar induction patterns. NPQ showed minimal induction in these lines. On the other hand, Y(NO) indicated stronger energy dissipation compared to the wild-type control Col-5 in these lines (Figure 26C and E). Regarding the 1-qL data, *pgr5-1* and the generated Cas lines (*pgr5-1 S261-Cas#1* and *pgr5-1 S261-Cas#2*) were more reduced in the light phase than the wild type (Col-5). Interestingly, line *pgr5-1 S261-Cas#1* recovered its Y(II) in the recovery phase, whereas Col-5 and the other two lines (*pgr5-1* and *pgr5-1 S261-Cas#2*) were completely oxidised (Figure 26G).

The parameters representing the PSI side of photosynthetic activity (Y(I) reflecting the quantum yield of PSI, Y(ND) representing the donor side limitation of the PSI also known as photosynthetic control and Y(NA) indicating the acceptor side limitation of PSI) were measured using the IRC protocol and calculated out of the absorption at 875 nm minus 830 nm. All lines lacking PGR5 showed a lower activity of PSI (Y(I)). However, *pgr5-1* and *pgr5-1 S261-Cas#1* behaved similarly, with a slightly higher activity of PSI than the line *pgr5-1 S261-Cas#2* (Figure 26B). In the lines *pgr5-1*, *pgr5-1 S261-Cas#1*, and *pgr5-1 S261-Cas#2*, no limitation of the value representing the donor-side limitation of PSI was observed. During the induction phase, a lower supply of electrons from the donor side was observed in the wild-type line. However, this observation was not made when the steady state was reached (Figure 26D). Throughout the measurement, the detected acceptor-side limitation was higher in lines *pgr5-1*, *pgr5-1 S261-Cas#1*, and *pgr5-1 S261-Cas#2* compared to the wild-type line (Col-5) (Figure 26F).

In summary, no clear differences were observed in the IRC between the single mutant *pgr5-1* and the double mutants *pgr5-1 S261-Cas#1* and *pgr5-1 S261-Cas#2*.

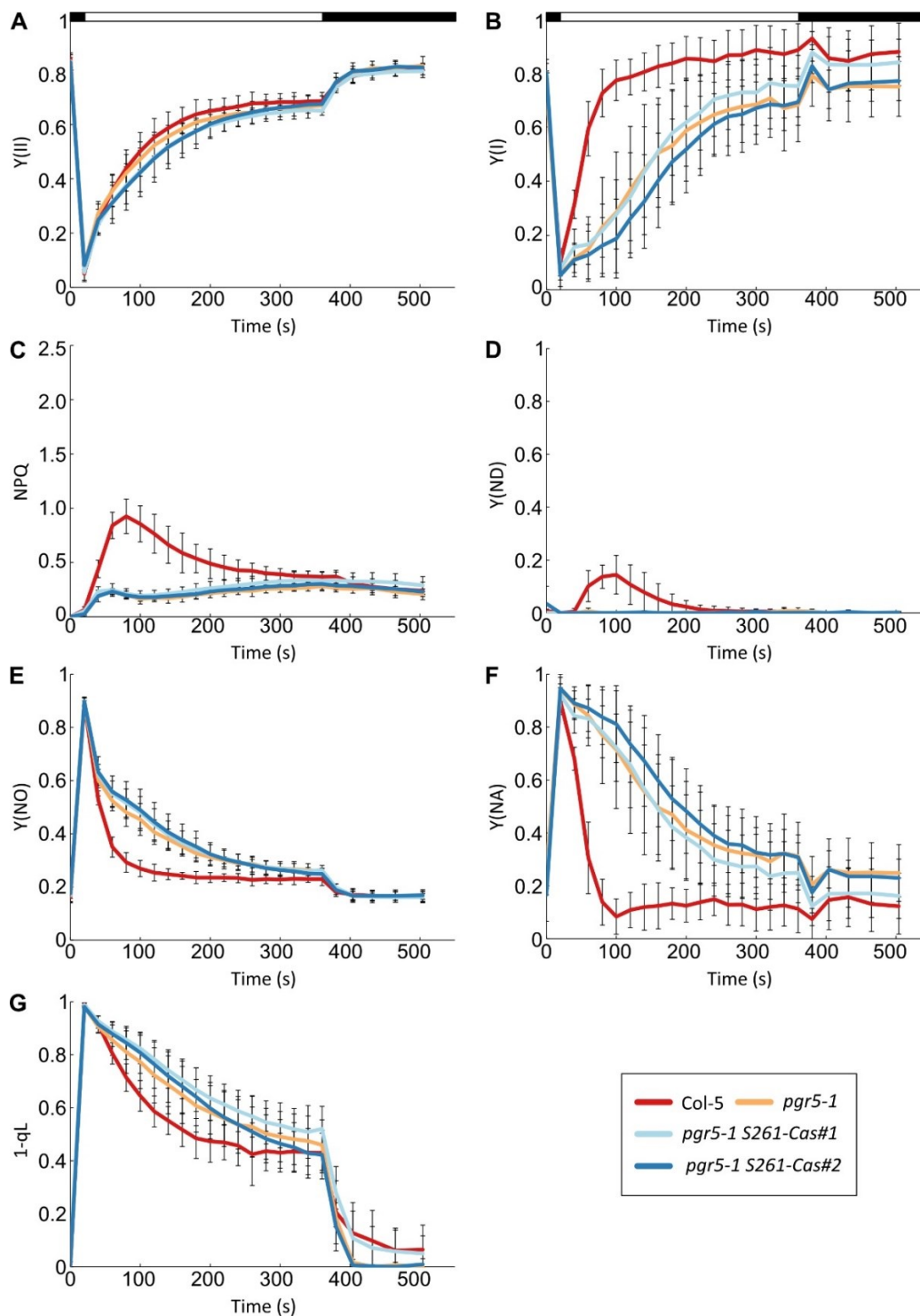


Figure 26: **IRC of *S261-Cas* suppressor lines in *pgr5-1* background.** Five-week-old plants were grown under control conditions (12 h light, $100 \mu\text{mol photons m}^{-2} \text{s}^{-1}$). The genotypes were WT (Col-5) and mutant (*pgr5-1*, *pgr5-1 S261-Cas#1* and *pgr5-1 S261-Cas#2*) plants, which were dark adapted, followed by 6 min of induction of the photosynthesis by subjecting to actinic light ($100 \mu\text{mol photons m}^{-2} \text{s}^{-1}$, white bar). After the illumination, plants were recovering for 3 min in the dark (black bar). Over the time frame of induction and recovery, the photosynthetic parameters were measured by applying saturation pulses every 20 s. For each genotype, five replicates were measured. **A**, Photosystem two quantum yield ($Y(\text{II})$) was measured by Chl fluorescence in the described plants. **B**, Quantum yield of Photosystem I ($Y(\text{I})$) was uncovered by measuring the absorption at 875 nm minus 830 nm. **C**, With the fluorescence measurement of Chl, NPQ was determined. **D**, Measurement of the donor-side limitation of PSI ($Y(\text{ND})$). **E**, Measurement of quantum-yield of non-regulated energy dissipation ($Y(\text{NO})$). **F**, Acceptor-side limitation of Photosystem I ($Y(\text{NA})$) was calculated from the measurements represented in (**B**). **G**, The qL value was measured by Chl fluorescence in the described plants and subtracted from 1 to achieve 1-qL. The Error bars represent \pm SD.

In addition, PAM measurements were conducted mimicking FL conditions providing a better insight into the mechanism of acclimation to FL in the *S261* mutant lines. For this purpose, the same protocol as in Figure 10 was used. Focusing on the parameter representing PSII activity, $Y(II)$, no differences were observed between *pgr5-1* and the *S261-Cas* lines (*pgr5-1 S261-Cas#1* and *pgr5-1 S261-Cas#2*). All three lines showed a slightly lower PSII activity compared to Col-5 in both LL and HL, which recovered in the dark phase (Figure 27A). Similar results were obtained for NPQ measurements between the mutant genotypes (*pgr5-1*, *pgr5-1 S261-Cas#1* and *pgr5-1 S261-Cas#2*). No induction of NPQ was observed in the mutant lines during the HL phases of the measurement, whereas it was induced in the Col-5 (Figure 27B). The 1-qL value correlates with the redox state of the PQ pool, i.e. if a bottleneck occurs on the Cyt b_6f side, a greater reduction of the PQ pool can be expected. However, the 1-qL values were only slightly different between the mutant lines *pgr5-1*, *pgr5-1 S261-Cas#1* and *pgr5-1 S261-Cas#2*. The lines *pgr5-1 S261-Cas#1* and *pgr5-1 S261-Cas#2* showed a slightly less reduced plastoquinone pool than *pgr5-1*. When comparing the mutant lines with Col-5, a greater reduction of the PQ pool was observed in all lines (Figure 27C).

In terms of PSI, it was observed that the mutant lines (*pgr5-1*, *pgr5-1 S261-Cas#1*, and *pgr5-1 S261-Cas#2*) behaved similarly and exhibited lower PSI activity in comparison to the wild type (Col-5) (Figure 28A). No donor side limitation was detected in the *pgr5-1* containing genotypes, and only a small donor side limitation was observed in *pgr5-1 S261-Cas#1* in the first high light peak of the measurement. In contrast, the wild type was affected by donor side limitation in the HL phases of the measurement (Figure 28B). The lines *pgr5-1*, *pgr5-1 S261-Cas#1* and *pgr5-1 S261-Cas#2* showed a higher PSI acceptor side limitation than the wild type, especially in the HL phase of the measurement (Figure 28C). Therefore, no major differences between the *pgr5* lines were observed in the measurements mimicking the FL condition.

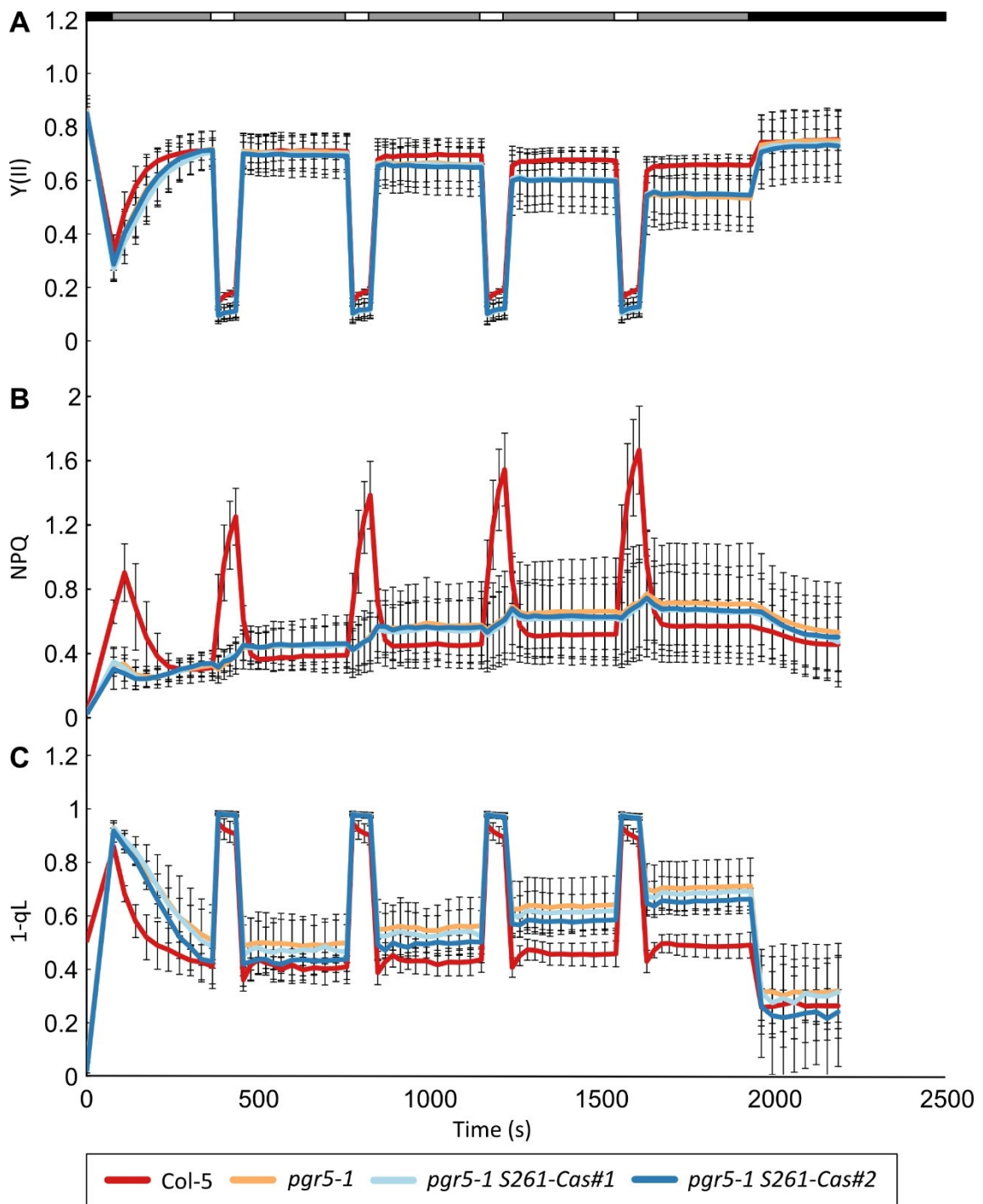


Figure 27: **Photosystem II parameters of *S261*-mutant lines under FL.** Five-week-old WT (Col-5) and mutant (*pgr5-1*, *pgr5-1 S261-Cas#1* and *pgr5-1 S261-Cas#2*) plants grown under control conditions (12 h light, $100 \mu\text{mol photons m}^{-2} \text{s}^{-1}$) were dark adapted (black bar) and followed by 5 min of illumination with actinic light ($50 \mu\text{mol photons m}^{-2} \text{s}^{-1}$, dark grey bar). After the illumination with low light, plants were subjected to high light for 1 min ($500 \mu\text{mol photons m}^{-2} \text{s}^{-1}$, white bar). Low light and high light phase repeated alternately four times, followed by a recovery phase for 5 min in the dark (black bar). Over the time frame of induction and recovery, photosynthetic parameters were measured by applying saturation pulses every 20 s in the low light phase and recovery phase and every 15 s in the high light phase. **A**, Y(II) values measured by Chl fluorescence in the described plants. **B**, Determined of values of the non-photochemical quenching (NPQ). **C**, The qL value was measured by Chl fluorescence in the described plants and subtracted from 1 to achieve $1-qL \pm \text{SD}$ were represented as error bars.

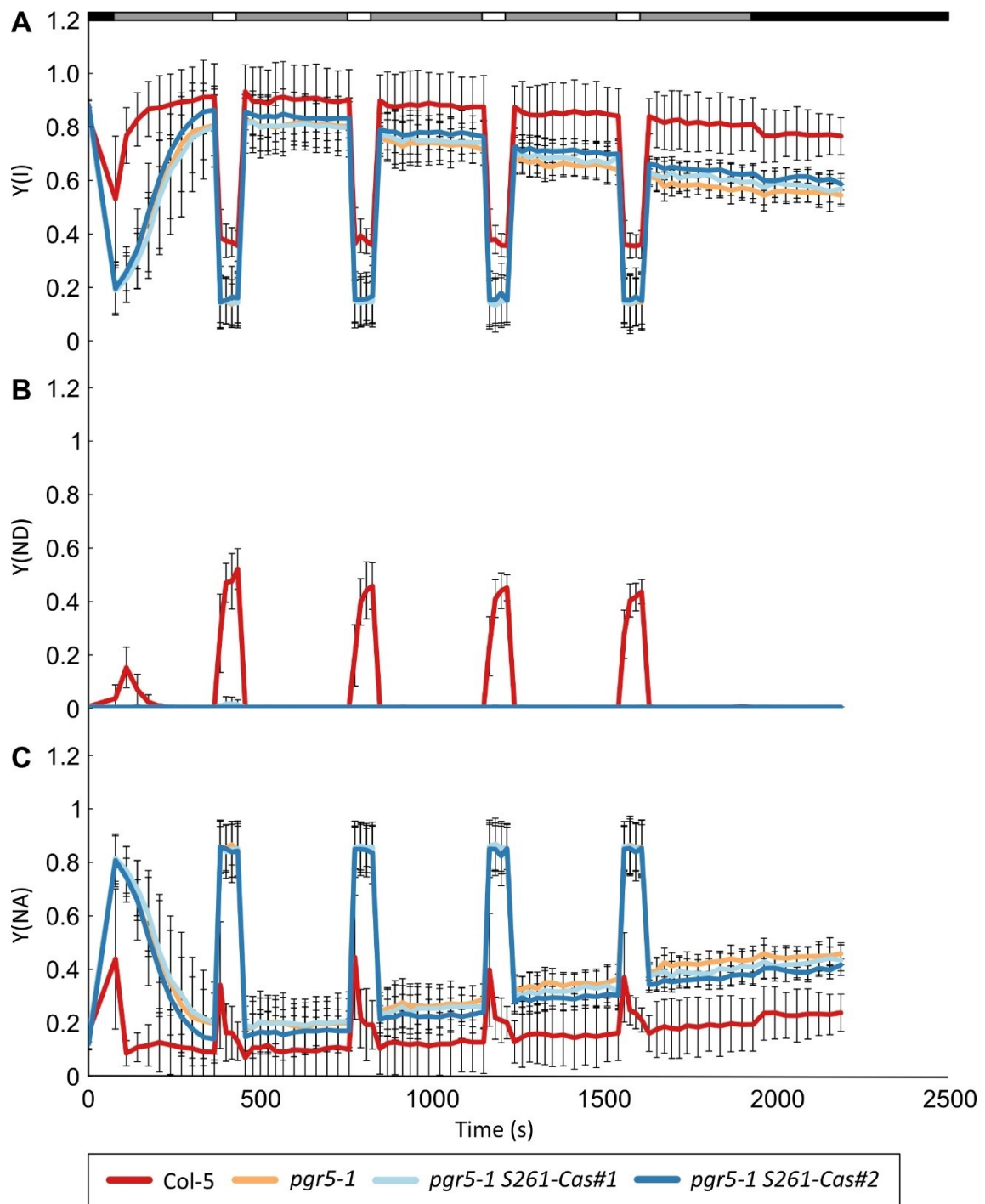


Figure 28: **Photosystem I parameters of S261-mutant lines under FL.** Plants from different genotypes were grown for 5 weeks under control conditions (12 h light, $100 \mu\text{mol photons m}^{-2} \text{s}^{-1}$). WT (Col-5) and mutant (*pgr5-1*, *pgr5-1 S261-Cas#1* and *pgr5-1 S261-Cas#2*) plants were dark adapted (black bar), followed by 5 min of illumination with actinic light ($50 \mu\text{mol photons m}^{-2} \text{s}^{-1}$, dark grey bar). After the illumination with low light, plants were subjected to high light for 1 min ($500 \mu\text{mol photons m}^{-2} \text{s}^{-1}$, white bar). Low light and high light phase repeated alternately four times followed by a recovery phase for 5 min in the dark (black bar). Over the time frame of induction and recovery, photosynthetic parameters were measured by applying saturation pulses every 20 s in the low light phase and recovery phase, and every 15 s in the high light phase. For each genotype three replicates were measured. **A**, Quantum yield of Photosystem I (Y(I)) were uncovered by measuring the absorption at 875nm minus 830nm. **B**, Donor-side limitation (Y(ND)) and **C**, Acceptor-side limitation (Y(NA)) of Photosystem I were calculated from the measurements represented in (A). The error bars represent \pm SD.

4.7 Generation of *pgr5-Cas* as a true PGR5 knock-out line

During this thesis (Figure 4, Figure 13 and Figure 24), as well as in other works (Barbato et al., 2020; Naranjo et al., 2021; Rühle et al., 2021), very small amounts of PGR5 have been repeatedly observed in the *pgr5-1* line (Munekage et al., 2002). This finding led us to generate additional true PGR5 knock-out mutant lines using the new gene-editing method CRISPR/Cas. In this section, a comparison is made between the well-studied *pgr5-1* mutant (Munekage et al., 2002; Suorsa et al., 2012), the *pgr1lab*, a knockout line of PGRL1A and PGRL1B (DalCorso et al., 2008), and the newly generated *pgr5-Cas#1* and *pgr5-Cas#2* lines. Included controls were a complementation line (*35S::PGR5 pgr5-1#1*) and an overexpression line of PGR5 (*35S::PGR5 pgr5-1#2*) in the *pgr5-1* background.

4.7.1 Complete knock-out lines of PGR5 via CRISPR/Cas resemble in growth phenotype *pgr5-1* under control and fluctuating light conditions

The new *pgr5* mutants were generated using CRISPR/Cas9 gene editing technology. A guide RNA targeting the first exon of PGR5, from nucleotides 132 to 152, was selected and introduced into the CRISPR/Cas9 vector pHEE401-E (Wang et al., 2015). Two independent lines were selected that contained an additional nucleotide between position 132 and 133 of PGR5 (Figure 29A). An additional adenine (A) was inserted in line *pgr5-Cas#1* and an additional thymine (T) was inserted in line *pgr5-Cas#2*. Both insertions resulted in a premature stop codon at position 65 of PGR5, 5 amino acids downstream of the chloroplast-transit peptide (Figure 29A). In the original *pgr5* line, *pgr5-1*, there is an amino acid exchange from glycine (G) to serine (S) at position 130 (Munekage et al., 2002). This exchange resulted in a strong reduction of PGR5_{G130S} to an amount of 4 % of wild-type PGR5. In contrast, no PGR5 was detectable in the novel *pgr5-Cas* lines or in *pgr1lab* (Figure 29B).

In addition, PGR5 overexpression lines were generated in the *pgr5-1* background to complement the *pgr5* phenotype and to observe the effects of higher levels of native PGR5 accumulated in the *pgr5-1* line. The *35S::PGR5 pgr5-1#1* line accumulated 1.5 times more PGR5 than the wild-type controls, while the second *35S::PGR5 pgr5-1#2* line accumulated up to three times more PGR5 than the wild-type (Figure 29B). In the different lines, no detectable amount of PGRL1 protein was observed in the *pgr1lab* line, and the *pgr5-1* line showed the next strongest reduction in PGRL1 accumulation at 64 % ± 9 %, while the *pgr5-Cas#1* and *pgr5-Cas#2* lines were not as strongly reduced in their PGRL1

accumulation as the other two lines. In comparison, a reduction of 22 % (*pgr5-Cas#2*) and 26 % (*pgr5-Cas#1*) was observed compared to WT. In the complementation lines *35S::PGR5 pgr5-1#1* and *35S::PGR5 pgr5-1#2*, a rescued amount of PGRL1 was observed compared to *pgr5-1*. A notable observation was a secondary band with a slightly lower molecular weight than the PGRL1 band in the lines where PGR5_{G130S} is present.

Comparison of the growth phenotype of all these lines under LD conditions showed no differences between the genotypes. Under fluctuating light, the *pgr5-Cas*, *pgr5-1* and *pgr1lab* plants died at the seedling stage (Figure 29C). This phenotype was complemented by the expression of PGR5 in the *35S::PGR5 pgr5-1#1* and *35S::PGR5 pgr5-1#2* lines. Interestingly, retarded growth under FL was observed in *35S::PGR5 pgr5-1#2* (Figure 29C), which could be attributed to the higher amount of PGR5 accumulating in this line (Okegawa et al., 2007).

Results

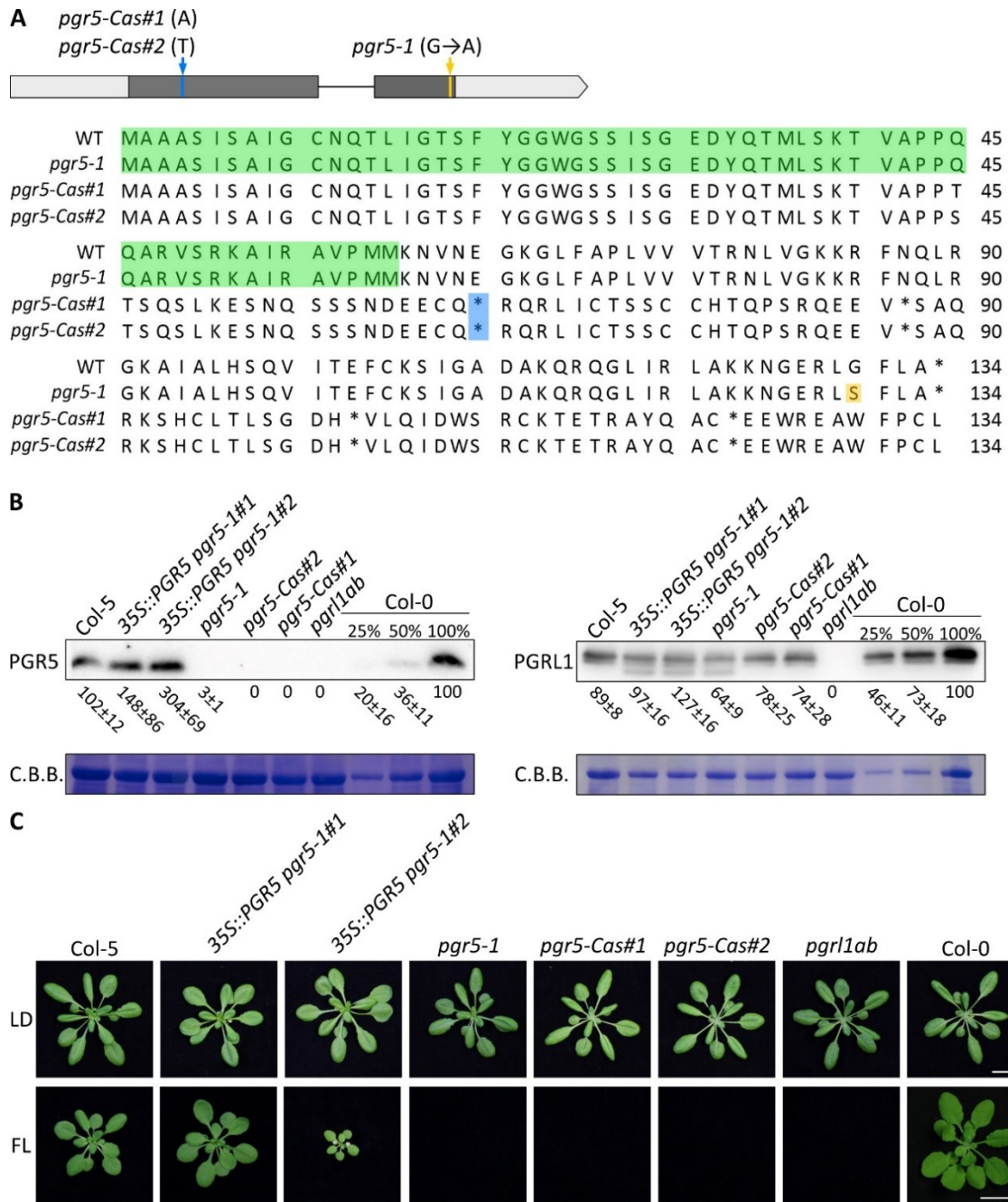


Figure 29: Growth of *PGR5* knock-out lines *pgr5-Cas* under long day and fluctuating light conditions.
A, Schematical representation of the *A. thaliana* *PGR5* CDS. Exonic sequence is marked in dark grey, the UTR regions as bright grey boxes and intronic sequence represented as black line. Insertion side of the additional nucleotide in the *pgr5-cas* lines is indicated (blue) as the position of the nucleotide exchange in *pgr5-1* (yellow). Below alignment of the of the protein sequence of Col-0/Col-5 (WT), *pgr5-1*, *pgr5-cas#1* and *pgr5-cas#2*. The intact transit peptide is marked with a green background in the sequence of *pgr5-1* and WT, with a blue background the premature stop codon of *pgr5-cas#1* and #2 is marked at position 65 and the amino acid substitution G/S in *pgr5-1* (yellow). **B**, Proteins extracted from the whole leaf from Col-5, 35S::PGR5 *pgr5-1#1*, 35S::PGR5 *pgr5-1#2*, *pgr5-1*, *pgr5-Cas#2*, *pgr5-Cas#1*, *pgr1lab* and Col-0 grown for 3 weeks under long day conditions were separated by SDS-PAGE and subjected to immunoblotting using PGR5- or PGRL1-specific antibody. Membrane were stained with Coomassie Brilliant Blue (C.B.B.) to visualize protein loading. One representative blot of three independent experiments is shown with numbers below corresponding to the average detected band intensity relative to the Col-0 100% band \pm SD. **C**, Images of WT-lines (Col-5 and Col-0) and mutant-lines (35S::PGR5 *pgr5-1#1*, 35S::PGR5 *pgr5-1#2*, *pgr1lab*, *pgr5-1*, *pgr5-Cas#1* and *pgr5-Cas#2*) grown under LD (16 h light, 100 $\mu\text{mol photons m}^{-2} \text{s}^{-1}$) for 3 weeks or fluctuating light (FL) (12 h light, cycles of low light (50 $\mu\text{mol photons m}^{-2} \text{s}^{-1}$) for 5 min and high light (500 $\mu\text{mol photons m}^{-2} \text{s}^{-1}$) for 1 min) conditions for 4 weeks. Scale bar in the images represents 2 cm.

4.7.2 The novel *pgr5-Cas* mutants are more similar in photosynthetic performance to *pgr1lab* than to *pgr5-1*

The effect of the small amount of PGR5_{G130S} on the photosynthetic performance of *pgr5-1* was of interest compared to the lines completely lacking PGR5 (*pgr5-Cas#1*, *pgr5-Cas#2*, and *pgr1lab*) and the complementation lines (*35S::PGR5 pgr5-1#1* and *35S::PGR5 pgr5-1#2*). To investigate this question, an IRC measurement was performed. Similarly, in all measured photosynthetic parameters, the mutant lines with impaired amounts of PGR5 (*pgr5-1*, *pgr1lab*, *pgr5-Cas#1*, and *pgr5-Cas#2*) exhibited similar behavior. A lower Y(II), which indicates a lower quantum yield of the PSII and a reduced electron supply to the LEF by the PSII, was demonstrated by them. The activity of the PSI was lower in *pgr5-1*, *pgr1lab*, *pgr5-Cas#1*, and *pgr5-Cas#2*. The value Y(NO), which can be regarded as ROS formation and energy dissipation, was found to be enhanced in the mutant lines (*pgr5-1*, *pgr1lab*, *pgr5-Cas#1*, and *pgr5-Cas#2*). Furthermore, a higher acceptor side limitation Y(NA) in the mutant lines compared to the WT resulted in limited activity of PSI. Additionally, a lower Y(ND), indicating a higher electron supply to PSI from the donor side, was observed in the mutant lines compared to the WT (Figure 30). Interestingly, *pgr5-1* was more affected in these parameters than *pgr1lab* and the *pgr5-Cas* knockout alleles. In the complementation lines, the expression of PGR5 in the *pgr5-1* background could restore most parameters to the level of the wild-type controls (Col-0 and Col-5), although small differences were observed. The quantum yields of the two photosystems Y(II) and Y(I) did not reach WT levels (Figure 30A and B), and Y(ND) was increased in the complementation lines (Figure 30D). Complementation was achieved in the parameters representing energy dissipation at the PSII and acceptor side limitation of PSI through the additional expression of PGR5 in the *pgr5-1* background (*35S::PGR5 pgr5-1#1* and *35S::PGR5 pgr5-1#2*) (Figure 30 C and E). At both the seedling and adult stages, the different genotypes exhibited the same photosynthetic phenotype, as indicated by an IRC (Figure 31A). The only difference observed to the measurements of adult plants compared to the seedling IRC measurements was that complete complementation of the *pgr5-1* phenotype in terms of Y(II) was attained through the expression of PGR5 (*35S::PGR5 pgr5-1#1* and *35S::PGR5 pgr5-1#2*) during the seedling stage (Figure 31).

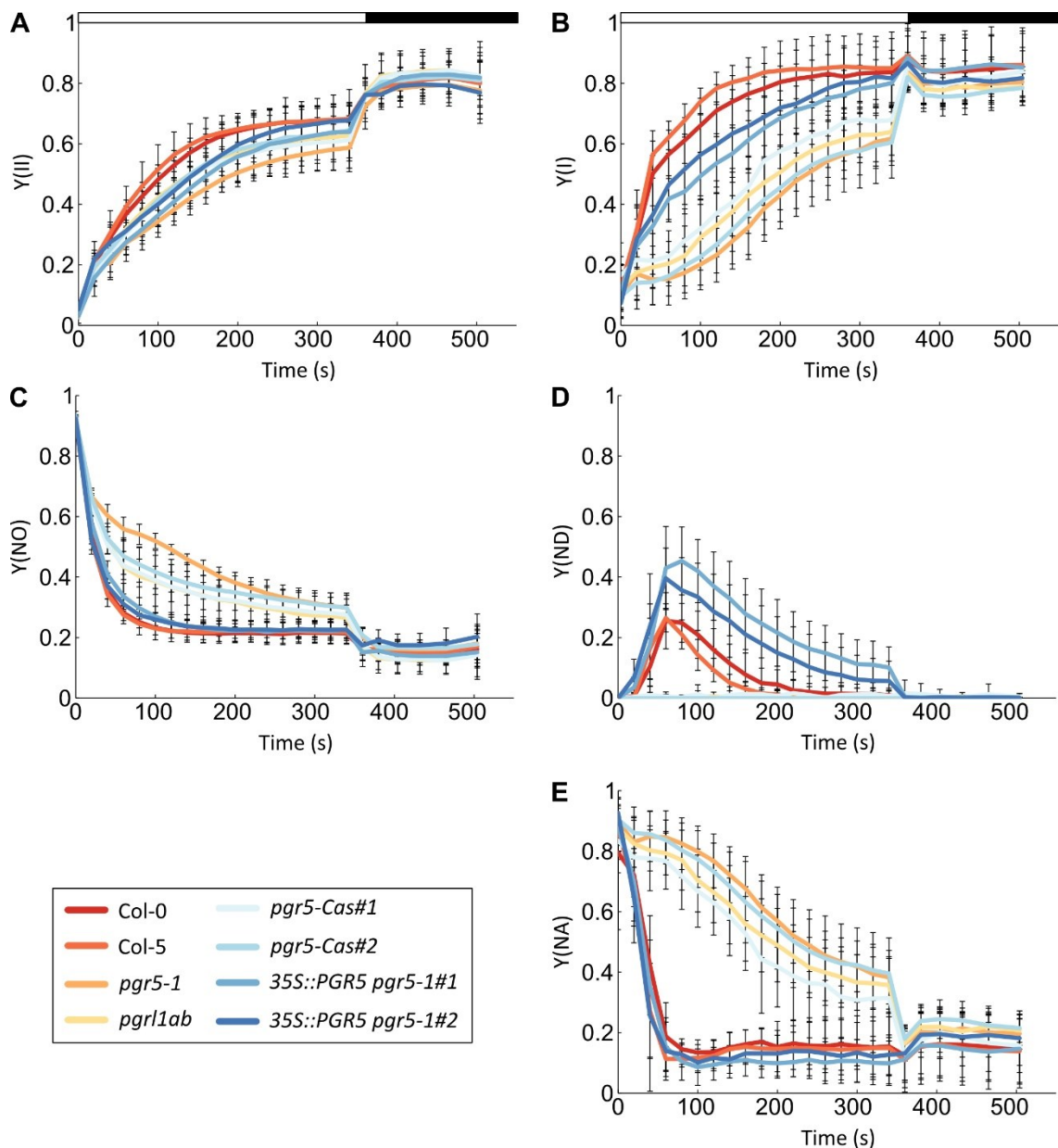


Figure 30: Photosynthetic characterization of lines with different amounts of PGR5 in induction and dark recovery. Three-week-old (16 h light, $100 \mu\text{mol photons m}^{-2} \text{s}^{-1}$) WT (Col-0 and Col-5) and mutant (*pgr5-1*, *pgr1lab*, *pgr5-Cas#1*, *pgr5-Cas#2*, *35S::PGR5 pgr5-1#1* and *35S::PGR5 pgr5-1#2*) plants were dark adapted, followed by 6 min of induction of the photosynthesis by subjecting to actinic light ($100 \mu\text{mol photons m}^{-2} \text{s}^{-1}$, white bar). After the illumination, plants were recovered for 3 min in the dark (black bar). Over the time frame of induction and recovery, the photosynthetic parameters were measured by applying saturation pulses every 20 s. For each genotype, eight replicates were measured. **A**, Photosystem two quantum yield (Y(II)) measured by Chl fluorescence in the described plants. **B**, Quantum yield of Photosystem I (Y(I)) uncovered by measuring the absorption at 875nm minus 830nm. **C**, Measurement of quantum-yield of non-regulated energy dissipation (Y(NO)). **D**, Donor-side limitation (Y(ND)) and **E**, Acceptor-side limitation (Y(NA)) of Photosystem I were calculated from the measurements represented in (**B**). The error bars represent \pm SD.

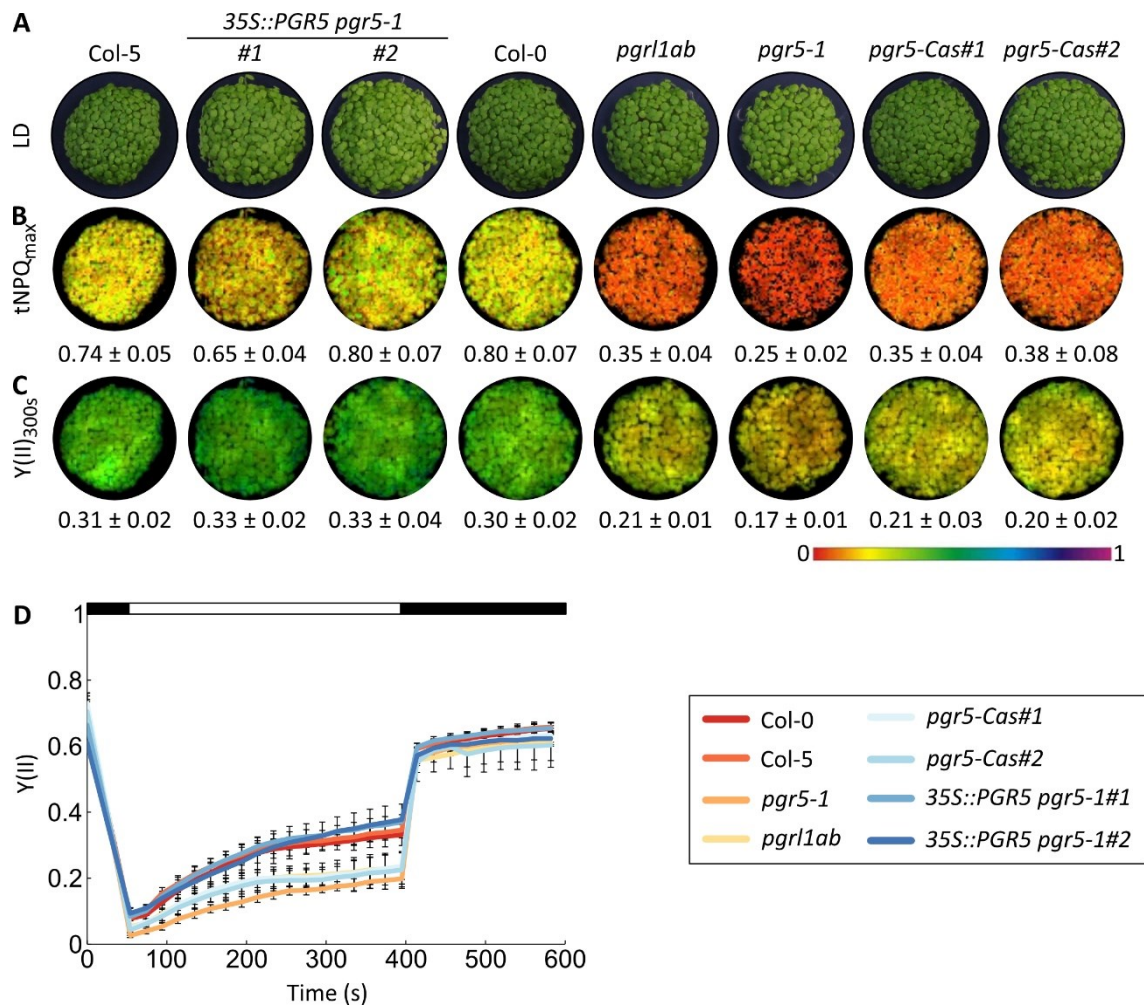


Figure 31: Growth phenotype and photosynthetic parameters of PSII in different genotypes at seedling state. **A**, Growth phenotype of 1-week-old WT (Col-0 and Col-5) and mutant (*pgr5-1*, *pgr1lab*, *pgr5-Cas#1*, *pgr5-Cas#2*, 35S::PGR5 *pgr5-1*#1 and 35S::PGR5 *pgr5-1*#2) plants grown under LD conditions (16 h light, 100 $\mu\text{mol photons m}^{-2} \text{s}^{-1}$) on $\frac{1}{2}$ MS. **B**, Same plants as in (A) were dark incubated for 30 min followed by measuring of Chl fluorescence over an induction of the photosynthesis (6 min of acting light: 110 $\mu\text{mol photons m}^{-2} \text{s}^{-1}$, white bar), followed by recovery in dark (3 min, black bar). Measurements were performed by applying a saturation pulse every 20 s. The average maximum of non-photochemical quenching in the induction phase of the measurement ($t\text{NPQ}_{\text{max}}$) was determined. **C**, Average PSII quantum yield in the stable state ($Y(\text{II})_{300\text{s}}$) in same plants as in (A) after 300 s of illumination. For the experiment, the average of six replicates was calculated \pm standard deviations. The colour coding of the measured values matches the colour bar (0 to 1). **D**, PSII quantum yield ($Y(\text{II})$) over the time frame of the measurement, determined in the same plants as in (A).

The efficiency of the cyclic electron flow (CEF) is influencing parameters such as the maximum of the transient NPQ ($t\text{NPQ}_{\text{max}}$) and the half time needed for the complete oxidation of P700 ($t_{1/2}\text{P700ox}$). To observe the effect of the different amounts and forms of PGR5 on the performance of CEF, the analysis was conducted on $t\text{NPQ}_{\text{max}}$ and $t_{1/2}\text{P700ox}$ (DalCorso et al., 2008; Munekage et al., 2002; Okegawa et al., 2008; Rühle et al., 2021; Shikanai, 2007). A lower induced NPQ was observed in the lines *pgr5-1*, *pgr1lab*, *pgr5-Cas#1*, and *pgr5-Cas#2*. Interestingly, the *pgr5-1* line was more affected than the *pgr5-Cas#1* and *pgr5-Cas#2* lines. In addition, it was noteworthy that significant differences

in $tNPQ_{max}$ were obtained between *pgr1lab* and *pgr5-1*, with the *pgr5-Cas* alleles being intermediate and more similar to *pgr1lab* (Figure 32A and B). Furthermore, the complementation lines showed a rescued NPQ with WT-like $tNPQ_{max}$ values (Figure 32A and B).

The time required to oxidize P700 (P700ox) was analyzed as an additional indicator of CEF, and the time required to oxidize 50% of P700 was compared. All mutant lines (*pgr5-1*, *pgr5-Cas#1*, *pgr5-Cas#2*, *pgr1lab*, *35S::PGR5 pgr5-1#1* and *35S::PGR5 pgr5-1#2*) showed a faster oxidation compared to WT (Col-0 and Col-5) (Figure 32D). A significant difference between *pgr1lab* and *pgr5-1* was observed in the $t_{1/2}P700$ analysis (Figure 32D). The *pgr5-Cas* mutants behaved like an intermediate between *pgr1lab* and *pgr5-1* (*pgr5-Cas#1*) or like *pgr1lab* (*pgr5-Cas#2*). The impaired P700 oxidation time of *pgr5-1* could only be partially and not significantly rescued by the *35S::PGR5 pgr5-1* complementation lines (Figure 32C and D).

In conclusion, the photosynthetic parameters and their analysis indicate that the novel *pgr5-Cas* lines and the established mutants with low or undetectable PGR5 (*pgr5-1* and *pgr1lab*) were similarly affected in photosynthesis and CEF. Interestingly, *pgr5-1* with a low level of PGR5_{G130S} was more affected than the other lines in all measured parameters. This could indicate an additive negative effect of PGR5_{G130S}, which was underlined by the incomplete complementation of P700ox in the *35S::PGR5 pgr5-1* lines.

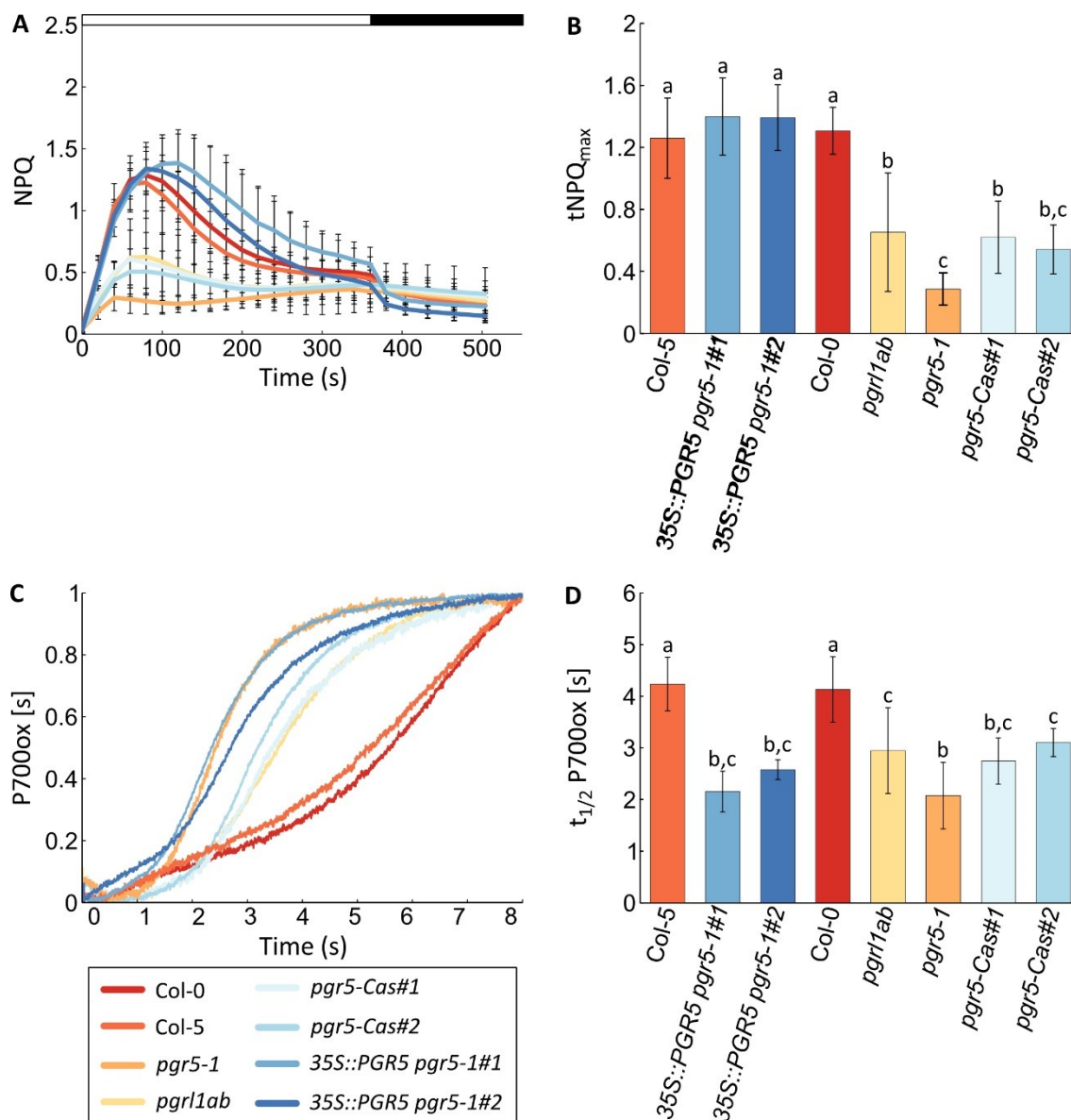


Figure 32: Assessment of parameters affected by CEF activity in different genotypes. Three-week-old (16 h light, $100 \mu\text{mol photons m}^{-2} \text{s}^{-1}$) WT (Col-0 and Col-5) and mutant (*pgr5-1*, *pgr11ab*, *pgr5-Cas#1*, *pgr5-Cas#2*, *35S::PGR5 pgr5-1#1* and *35S::PGR5 pgr5-1#2*) plants were dark adapted, followed by 6 min of induction of the photosynthesis by subjecting to actinic light ($100 \mu\text{mol photons m}^{-2} \text{s}^{-1}$, white bar). After the illumination, plants were recovering for 3 min in the dark (black bar). Over the time frame of induction and recovery the photosynthetic parameters were measured by applying saturation pulses every 20 s. For each genotype, eight replicates were measured. **A**, Non-photochemical quenching (NPQ) values based on fluorescence measurements of Chl a. **B**, Average of maximum non-photochemical quenching in the induction phase ($t\text{NPQ}_{\text{max}}$) of the measurements represented in (A). **C**, For the P700ox measurements, the same genotypes as in (A) grown under the described condition were dark adapted for 30 min followed by illumination for 5 s with actinic light ($660 \mu\text{mol photons m}^{-2} \text{s}^{-1}$), subsequently the light was switched off for 2 s. After the dark phase, the plants were subjected to far-red light (FR) and the P700 oxidation state was observed by measuring the absorption at 875nm minus the absorption at 830nm. One representative measurement of eight replicates was selected and the time needed to completely oxidise a reduced P700 displayed. **D**, Average of time needed to oxidise 50% of P700 ($t_{1/2}\text{P700ox}$). Error bars in C and D display \pm SD. Statistical differences ($p < 0.05$) were determined by Tukey's test and represented as letters above the SD.

4.7.3 The *prg5-1* mutant is strongly affected in the accumulation and stability of chloroplast proteins

Significant differences in photosynthetic parameters were observed between the original *prg5* mutant, *prg5-1*, and the novel knockout lines *prg5-Cas*. Possible variations in the chloroplast proteome between these lines that could explain the photosynthetic phenotypes were further investigated. Therefore, a proteome analysis was performed by Dr Giada Marino in extracted chloroplasts of the WT control lines Col-0 and Col-5 (Col-0 representing the WT control for *prg11ab* and *prg5-Cas* lines and Col-5 representing the WT control for *prg5-1*) and the mutant lines *prg5-1*, *prg11ab*, *prg5-Cas#1* and *prg5-Cas#2*. The differentially expressed proteins (DEPs) were grouped according to their molecular function and biological process (Figure 33).

In the *prg5-1* line, the chloroplast proteome was up-regulated (131 proteins) and down-regulated (131 proteins) compared to the wild-type background (Col-5). The large number of up- and down-regulated proteins was specific to *prg5-1*, whereas in the other lines devoid of PGR5 (*prg11ab*, *prg5-Cas#1* and *prg5-Cas#2*), PGR5 itself was down-regulated to the point of no detection, as in *prg5-1*. The newly discovered component PGRL2 of the complex around PGR5 (Rühle et al., 2021) could not be detected in the WT samples and was not analysed further. Interestingly, the reduced level of PGRL1A (Figure 33B) in the immunodetection was confirmed in the proteomic analysis of the *prg5-1* line. PGRL1B was not detected in the *prg5-1* sample and could not be analysed. The strongest reduction of PGRL1A and PGRL1B was observed in the T-DNA insertion line *prg11ab* (DalCorso et al., 2008). The *prg5-Cas* lines were not affected in PGRL1A and PGRL1B content, making the reduction of PGRL1 a unique feature of *prg5-1* (Figure 33A).

Interestingly, further analysis of the chloroplast proteome showed that only in the *prg5-1* line most of the thylakoid complexes were down- or up-regulated compared to the WT background. In the other mutant lines lacking PGR5, namely *prg11ab* and *prg5-Cas*, only minor effects were observed with no significant differences. Categorisation of the different proteins expressed in *prg5-1* according to their function in thylakoid complexes or biological processes revealed an interesting picture. Proteins associated with the CBB-cycle were up-regulated, in particular a pronounced increase in the abundance of Rubisco small chain proteins was observed compared to Col-5. In contrast, photosynthetic complexes and proteins involved in the photosynthetic electron transport chain were down-regulated (Figure 33B).

These data suggest that the different composition of the chloroplast proteome results in a greater impairment of photosynthesis in *prg5-1*.

The abundance of some affected proteins in the *35S::PGR5 pgr5-1* lines was tested to investigate whether the accumulation of PGR5_{G130S} caused the differences in the proteome between the *pgr5* mutants. In none of the complemented lines were the levels of FBPase, PsbO, PsaA or NdhB rescued (Table 5). These observations indicated that PGR5_{G130S} itself did not affect the proteome of *pgr5-1*.

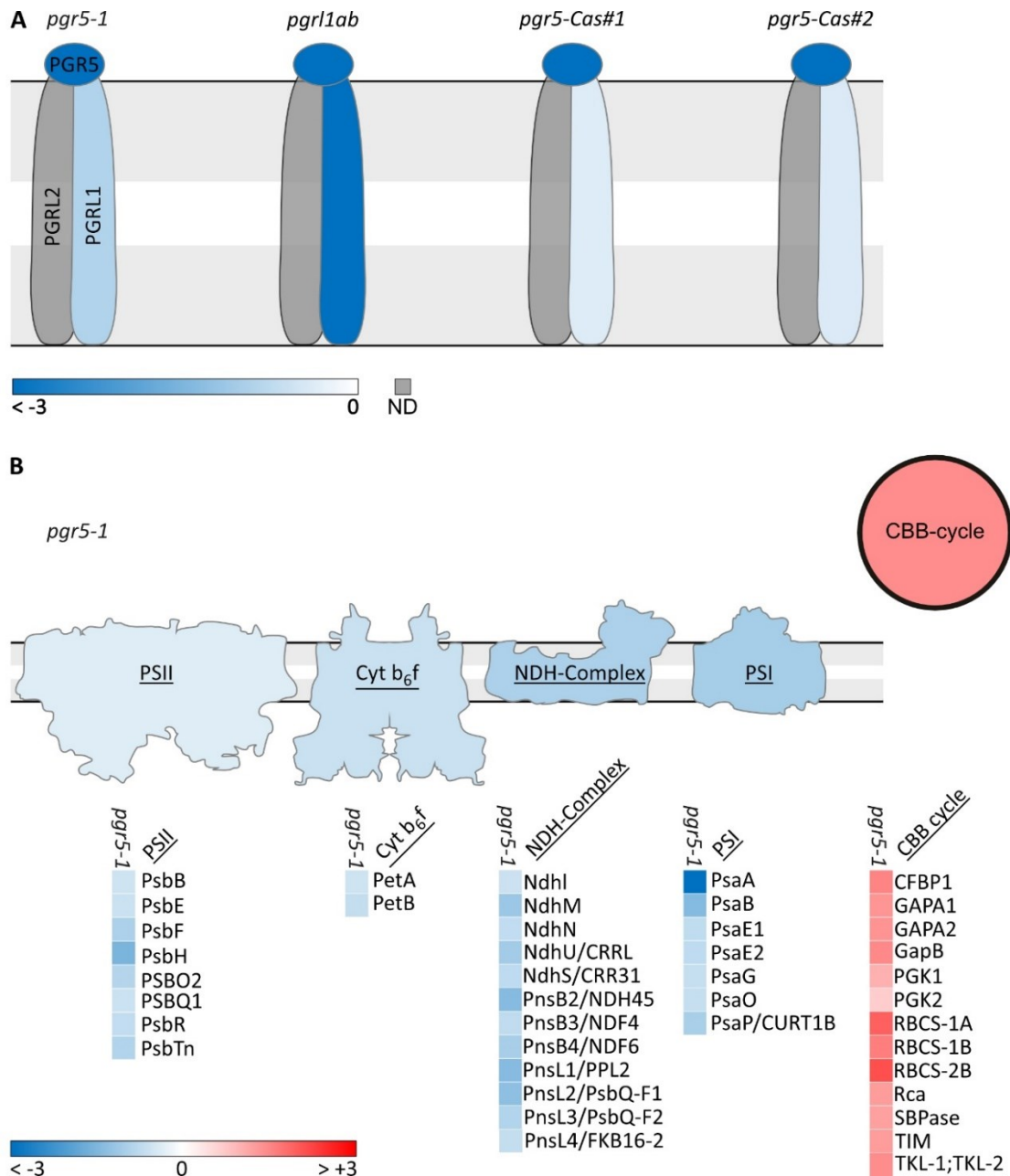


Figure 33: **Analysis of chloroplast proteome of PGR5 deficient genotypes.** **A**, Plants were grown for chloroplast extraction for 5 weeks in short day conditions (8 h light, $100 \mu\text{mol photons m}^{-2} \text{s}^{-1}$). Samples were harvested in the dark and the protein content of the extracted chloroplast was determined. For proteomic determination, the samples were loaded according to their protein content on equal levels. Statistically significant changes in the log₂ ratio of the mutant lines (*pgr5-1*, *pgr11ab*, *pgr5-Cas#1* and *pgr5-Cas#2*) compared to the WT-background (for *pgr5-1* Col-5 and for *pgr5-Cas#1*, *pgr5-Cas#2* and *pgr11ab* Col-0) are schematically presented for the different proteins involved in the PGR5-mediated CEF (PGR5, PGRL1 and PGRL2) in colour coding (dark blue ≤ -3 , white = 0 and grey = not detected). **B**, Significant changes in the ratio of proteins are categorized according to their biological function (PSII, Cyt- b_6f , NDH-Complex, PSI and CBB-cycle) of the mutant line *pgr5-1* colour coding (blue ≤ -3 , white = 0 and red $\geq +3$).

Table 5: quantification in means \pm SD of protein abundance after immunodetection in *pgr5-1*, *pgr11ab*, *pgr5-cas* and the complementation lines.

lines	FBPase	PsaA	PsbO	NdhB
Col-5	100	100	100	100
<i>35S::PGR5 pgr5-1#1</i>	147 \pm 36	91 \pm 14	85 \pm 9	60 \pm 7
<i>35S::PGR5 pgr5-1#2</i>	186 \pm 97	78 \pm 22	73 \pm 5	45 \pm 6
Col-0	100	100	100	100
<i>pgr11ab</i>	130 \pm 19	97 \pm 18	126 \pm 8	138 \pm 18
<i>pgr5-1</i>	228 \pm 45	59 \pm 8	57 \pm 4	43 \pm 4
<i>pgr5-Cas#1</i>	109 \pm 16	117 \pm 27	98 \pm 9	101 \pm 10
<i>pgr5-Cas#2</i>	120 \pm 17	118 \pm 32	95 \pm 14	104 \pm 16

4.7.4 Additional SNPs in the second chromosome can be found in *pgr5-1*

The notable differences in the plastid composition of *pgr5-1* could be resulting from the expressed PGR5_{G130S} or from additional second-side mutations undetected so far, since *pgr5-1* is a point mutation line originated in an EMS screen. To address this open question, the genome of *pgr5-1* was sequenced and compared to the genome of the original background Col-5. The comparison was performed by Dr. Tatjana Kleine. Interestingly, several SNPs, localized in all five chromosomes were detected, adding up to the total number of 48 non-synonymous mutations.

Ten other genes on the second chromosome were affected by coding mutations resulting in amino acid exchanges. All had a single nucleotide mutation, which was facilitated by EMS mutagenesis (Table 6). Of all the second-site mutations found in *pgr5-1*, five were in genes for plastid proteins. The proteins encoded by the affected genes were PsbO2, a subunit of the oxygen evolution complex (Lundin et al., 2007; Yi et al., 2005); CGL20A, a factor involved in ribosome biogenesis (Reiter et al., 2020); HCEF136, a PSII assembly factor (Meurer et al., 1998); and ABCI11, an ATPase-coupled transmembrane transporter (Voith von Voithenberg et al., 2019). Among these proteins, PsbO2, HCEF136 and PGR5 were downregulated compared to WT (Table 6). For further analysis, only those SNPs located on the same chromosome as PGR5 were selected. This was done because it is likely that the mutation leading to the specific phenotype of *pgr5-1* is located in close

proximity to the mutation in PGR5 (Munekage et al., 2002). CGL20A is a likely candidate for the differences observed between the generated *pgr5-Cas* lines and *pgr5-1*. Its localisation in the plastid and as a factor involved in ribosome biogenesis could explain the high diversity of affected proteins. CGL20A is encoded on chromosome 2 and the distance between CGL20A and PGR5 is less than 5,500 kbp, which could explain the persistence of the *pgr5-1* phenotype even in crossed lines (Figure 8C, Figure 12).

Table 6: Additional SNPs at the chromosome 2 or plastid localized in *pgr5-1*.

Gene	Name	Plastid-localised	Chromosome	SNPs analysis		Proteomics	
				nt	AA (pos)	Ratio <i>pgr5-1/Col-5</i>	adj p-val
AT2G03480	PMT5	no	2	T/C	L/F	ND	ND
AT2G05620	PGR5	yes	2	T/C	G/S	0.015	3.77E-05
AT2G07050	CAS1	no	2	T/C	T/M	ND	ND
AT2G11015	AT2G11015	no	2	T/C	T/M	ND	ND
AT2G16900	AT2G16900	no	2	T/C	G/D	ND	ND
AT2G17240	CGL20A	yes	2	T/C	P/L	ND	ND
AT2G18960	AHA1	no	2	T/C	L/F	ND	ND
AT2G21610	PME11	no	2	T/C	G/E	ND	ND
AT2G22500	PUMP5	no	2	T/C	G/E	ND	ND
AT2G22590	UGT91A1	no	2	T/C	R/W	ND	ND
AT3G50820	PsbO2	yes	3	T/G	P/Q	0.544	4.66E-03
AT5G14100	ABC11	yes	5	A/G	A/V	ND	ND
AT5G23120	HCF136	yes	5	A/G	R/K	0.696	1.27E-02

nt = nucleotide, AA = amino acid, pos = position, ND = not detected

4.7.5 PGRL1 without PGR5 is harmful under high light conditions

Other studies have shown that antimycin A-sensitive CEF is important for protecting plants from photoinhibition under different types of light stress (Barbato et al., 2020;

Rantala et al., 2020; Suorsa et al., 2016; Takahashi et al., 2009; Yamamoto & Shikanai, 2019). Due to the observed differences in photosynthesis and the chloroplast proteome, the question arose as to whether the *pgr5-Cas* lines were less sensitive to high light as a source of photoinhibition compared to *pgr5-1*.

Several parameters were analyzed in the mutant lines (*pgr5-1*, *pgr11ab*, *pgr5-Cas#1*, *pgr5-Cas#2*, *35S::PGR5 pgr5-1#1* and *35S::PGR5 pgr5-1#2*) as well as in the WT controls (Col-0 and Col-5) after two weeks of growth under HL conditions (500 $\mu\text{mol photons m}^{-2} \text{s}^{-1}$) (Figure 34A). A notable observation was that the PGR5-deficient lines (*pgr11ab* and *pgr5-Cas* lines), which behaved similarly in terms of growth and photosynthesis under normal light conditions, showed significant differences in most of the measured parameters under HL. The *pgr5-Cas* lines had lower fresh weight and anthocyanin content compared to WT. Strikingly, the *pgr5-Cas* lines showed the same values as *pgr5-1* with no significant differences (Figure 34B and D). Only the lower amount of Chl in *pgr5-1* was specific to this background (Figure 34F). The levels of Chl, anthocyanin and fresh weight were not affected in the *pgr11ab* mutants, in contrast to the other lines with lower PGR5 levels (*pgr5-1*, *pgr5-Cas#1* and *pgr5-Cas#2*) (Figure 34A, B, D and E). Rescue of the HL phenotype of *pgr5-1* by overexpression of PGR5 was only partially possible. Indeed, the anthocyanin content was complemented in the complementation lines (*35S::PGR5 pgr5-1#2*) and enriched in the overexpressor line *35S::PGR5 pgr5-1#1* (Figure 34D). Fresh weight and Chl content were only slightly increased in the overexpressor lines (*35S::PGR5 pgr5-1#1* and *35S::PGR5 pgr5-1#2*) (Figure 34B and F).

To obtain a clearer understanding of the *pgr5*-specific HL phenotype, measurements were taken for the PSII quantum yield and NPQ of these plants. Interestingly, *pgr5-1* and *pgr5-Cas* mutants were strongly altered in the Y(II) parameter, showing a strong reduction in PSII activity compared to WT, whereas in the *pgr11ab* line, Y(II) was WT-like (Figure 34C and E).

The results of the HL experiment revealed a so far unknown phenotype of CEF mutants, with reduced PGR5 content but remaining PGRL1. This may indicate a function of the PGR5/PGRL1 complex under HL, which has a deleterious effect when one of the components is missing.

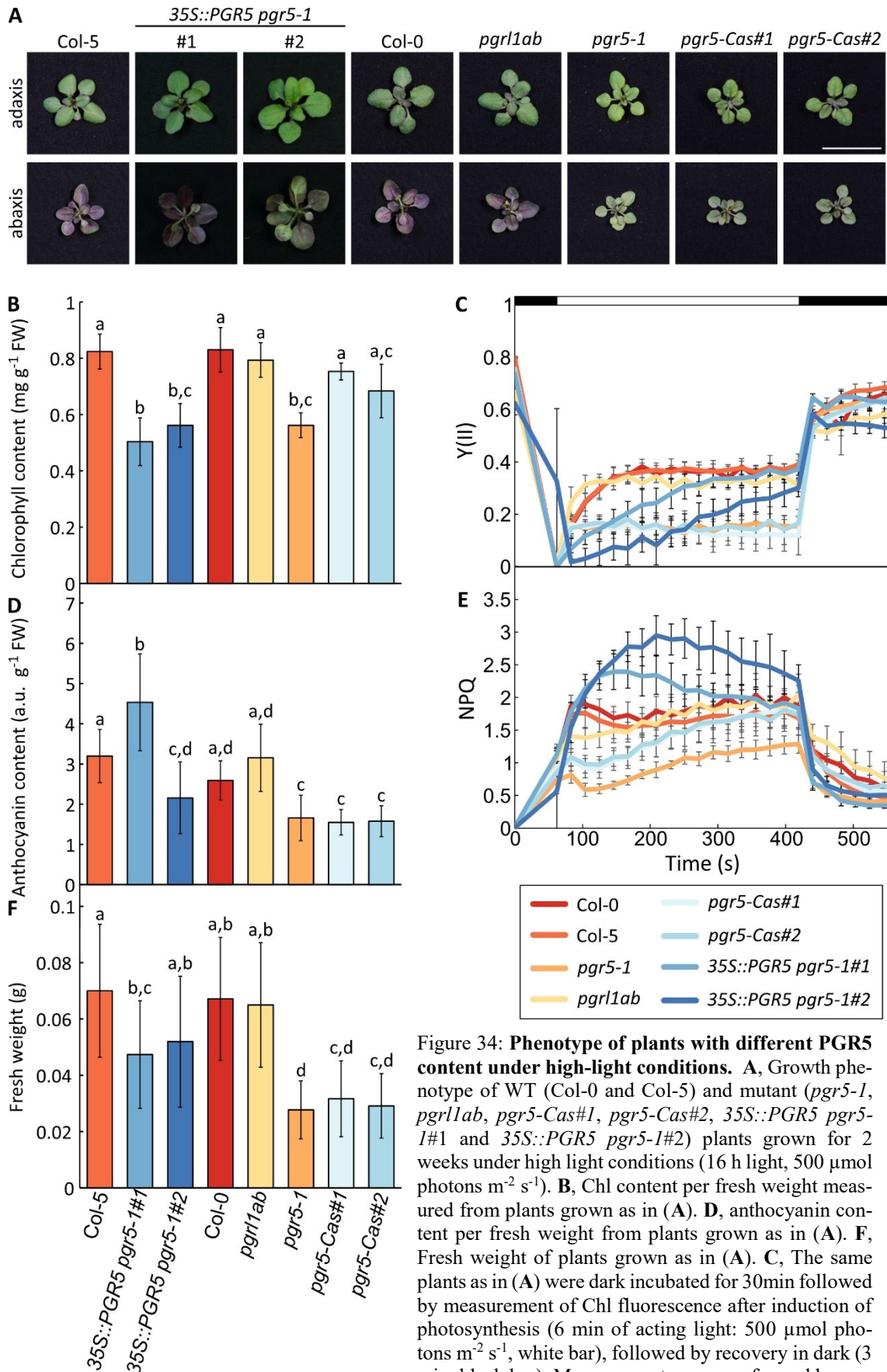


Figure 34: Phenotype of plants with different PGR5 content under high-light conditions. A, Growth phenotype of WT (Col-0 and Col-5) and mutant (*pgr5-1*, *pgr1lab*, *pgr5-Cas#1*, *pgr5-Cas#2*, 35S::PGR5 pgr5-1#1 and 35S::PGR5 pgr5-1#2) plants grown for 2 weeks under high light conditions (16 h light, 500 $\mu\text{mol photons m}^{-2} \text{s}^{-1}$). B, Chl content per fresh weight measured from plants grown as in (A). D, anthocyanin content per fresh weight from plants grown as in (A). F, Fresh weight of plants grown as in (A). C, The same plants as in (A) were dark incubated for 30min followed by measurement of Chl fluorescence after induction of photosynthesis (6 min of acting light: 500 $\mu\text{mol photons m}^{-2} \text{s}^{-1}$, white bar), followed by recovery in dark (3 min, black bar). Measurements were performed by

applying a saturation pulse every 20 s. Photosystem II quantum yields (Y(II)) were determined over the time frame of the measurement. E, NPQ determined from measurements in (C). For the Chl measurement, anthocyanin-content and fresh weight, the average of at least 6 plants is shown \pm standard deviation. Letters above error bars indicates significant groups ($p < 0.05$) calculated by Tukey's test. For the photosynthetic parameters the average of at least 6 replicates is represented.

5. Discussion

The here described *pgr5* suppressor screen under FL conditions allowed to identify both previously described and novel ways to suppress *pgr5* lethality under FL. With this new knowledge, it was possible to gain a clearer picture of the interactions and links between different pathways to acclimate the plant to FL. These will be discussed in the following part.

5.1 PSII functionality has a major impact on FL acclimation

In the screen, the majority of suppressors were mutated in genes that affect the stability or assembly of PSII (Table 4 and Figure 7). This could be due to down-regulation of the LEF through a decrease in PSII activity, which protects PSI from over-excitation by reducing the number of electrons entering the system. Indeed, it has already been shown by Suorsa et al. 2016 that mutations in PSII can suppress the lethality of *pgr5-1* under FL (Figure 36 and A). In their work, a *pgr5-1* line containing PsbQ, PsbQ2, PsbR, PsbO1 and PsbP2 was generated and named $\Delta 5$ *pgr5* (Suorsa et al., 2016). A similar effect was seen in the mutants *pgr5-1 lpa66* and *pgr5-1 pam68* (Figure 8 and Figure 12). Interestingly, these lines were able to induce NPQ even in the absence of PGR5 after the transition from the LL to the HL phase of FL. However, no NPQ was observed in the $\Delta 5$ *pgr5* mutant (Suorsa et al., 2016), which could be due to either a difference in measurements (LL measurement $53 \mu\text{mol photons m}^{-2}\text{s}^{-1}$), or different effects of the mutations. The lack of induced NPQ in the $\Delta 5$ *pgr5* line, but its induction in the $\Delta 5$ and $\Delta 5$ *crr4-3* lines (lines with PGR5-mediated CEF), was explained by Suorsa et al. in their 2016 study. They proposed that this difference was due to a compensatory process where the PGR5-mediated CEF compensates for the absence of LEF (Suorsa et al., 2016). If the up-regulated NPQ in *pgr5-1 lpa66* and *pgr5-1 pam68* derives from NDH-dependent CEF, this could be further investigated, for example by generating the appropriate mutants, such as the double *pam68 ndh5* or *pam68 crr2-2*.

Another interesting observation was a higher accumulation of PGR5 in the *pgr5-1 pam68* line compared to *pgr5-1* (Figure 13B), but not in *pgr5-1 lpa66* (Figure 9B). This result could be an interesting starting point for investigating PGR5 degradation, which has been described as essential for the regulation of PGR5-CEF, although the mechanism is still unclear (Rühle et al., 2021). It is known that PGRL1 is required for PGR5 stability

(DalCorso et al., 2008), while PGRL2 is involved in PGR5 degradation (Rühle et al., 2021), but the exact mechanism and the protease(s) involved remain elusive. Interestingly, illumination is required for the degradation of PGR5 (Rühle et al., 2021). Thus, LEF may play a role in PGR5 degradation. An interesting observation that questions the importance of LEF in this process is that no higher accumulation of PGR5 was observed in the *pgr5-1 lpa66* line (Figure 9B). This result suggests that PAM68, which has a stronger effect on LEF, leads to a higher accumulation of PGR5_{G130S}. To investigate this in more detail, further experiments would be needed to pinpoint the exact point of degradation. This can be done by producing specific double mutant lines or inhibiting complexes by chemicals.

Consistent with a reduced LEF acting as a mechanism that suppress effects of the *pgr5* mutation under FL, three of the identified *pgr5-1* suppressors were mutated in PAA1. This gene encodes a copper transporter protein that belongs to the family of metal-transporting P-type ATPases (Shikanai et al., 2003) and is localised in the chloroplast outer membrane (Abdel-Ghany et al., 2005). In the single mutant *paal-1*, a lower accumulation of holoplastocyanin was found, resulting in a strong reduction of the PC level (Shikanai et al., 2003). Thus, a lower PC level down-regulates the LEF (Pesaresi et al., 2009), which could cause the suppression of the lethal phenotype of *pgr5-1* under FL (Figure 36 and C). However, it remains to be proven whether lowering PC levels alone suppresses the lethal phenotype of *pgr5-1*. In fact, generating double mutant lines between *pgr5-1* and knockout lines of one or both isoforms encoding PC (*pete1* or *pete2*) and testing these lines for photosynthetic activity and viability under FL could answer this question.

5.2 Altered PSI accumulation does not improve FL acclimation

To investigate whether the lethal phenotype of *pgr5-1* under FL could be suppressed by altering PSI accumulation, the *psad1* line was crossed with *pgr5-1*. The *psad1* mutant was selected because it has enhanced CEF activity (DalCorso et al., 2008) and the double mutant between *pgr1lab* and *psad1-1* showed an additive phenotype with reduced growth under CL (DalCorso et al., 2008). Furthermore, this upregulation in CEF was suppressed by introducing the *pgr1lab* mutation in the *psad1* background (DalCorso et al., 2008; Ilnatowicz et al., 2004). The same effect was observed in the double mutant line *pgr5-1 psad1-1* that was generated (Figure 15A), which can be explained by the absence of PGR5 and the lack of PGR5-mediated CEF as in the *pgr1lab psad1-1* line (DalCorso et al., 2008; Hertle et al., 2013; Rühle et al., 2021). Furthermore, the absence of PGR5-mediated CEF

and altered PSI composition does not result in survival under FL. In addition to the lethal phenotype of *pgr5 psad1* under FL (Figure 12), no candidate PSI was found in the suppressor screen. Indeed, it has been shown that PSI protection against overexcitation is one of the critical points for plant acclimation and survival to FL under these conditions (Chen et al., 2022; Suorsa et al., 2012), which also explains why further mutated PSI, as present in the *psad1-1* line, is not beneficial for survival under FL.

5.3 Cyt b₆f mutants are unlocking FL survival in pgr5-1 background

Additionally, Cyt b₆f-related mutants were found in the *pgr5* screen, which is consistent with the identification of PSII and PC mutants as suppressors of *pgr5*. These mutants reduce LEF and, as a result, PSI is protected from photoinhibition (Figure 36 and B). Interestingly, a *pgr5* suppressor was discovered with a mutation in *Ccda* (*pgr5-S281*) (Table 4), which is involved in the assembly of the Cyt b₆f complex (Page et al., 2004), as well as a suppressor mutated in a gene encoding an unknown protein, *S261*, which has recently been described to be also involved in Cyt b₆f assembly (Li et al., 2022; Sandoval-Ibanez et al., 2022). As shown by Yamamoto and Shikanai, the Cyt b₆f complex is an efficient point of photosynthetic control, and defects in this complex, such as in the *pgr1* mutant, suppress the photosynthetic phenotype of *pgr5-1*, resulting in the *pgr1 pgr5-1* double mutant that performs photosynthesis similarly to WT plants (Yamamoto & Shikanai, 2019). However, the work of Yamamoto and Shikanai did not show whether this double mutant could also survive under FL conditions, and the suppression of the growth phenotype was only hypothetical (Yamamoto & Shikanai, 2019). Indeed, in our hands, this double mutant *pgr1 pgr5-1* did not survive under FL (Figure 12), which could be due to the very low reduction of Cyt b₆f in the *pgr1* mutant, which is affected in the Rieske protein (Yamamoto & Shikanai, 2019). In contrast, *pgr5 S281* and *pgr5 S261* survived under FL (Figure 22A). Therefore, further studies are needed to establish the relationship between Cyt b₆f accumulation and FL survival, as well as the possible role of PGR5 in the stability of this complex (see below). Photosynthetic control at the Cyt b₆f complex is a highly effective way of regulating the balance between PSI and PSII activity more rapidly than other protective mechanisms such as NPQ (Johnson & Berry, 2021).

Therefore, by regulating Cyt b₆f accumulation, it is possible to suppress the lethal phenotype of *pgr5-1* under FL (Figure 36 and B).

5.4 S261 is involved in the accumulation of the Cyt b₆f complex, together with PGR5

It has recently been shown that a mutation in the Col-0 background that reduces the accumulation of S261 to 30 % of the wild type results in a decrease in the Cyt b₆f complex to the point where it is undetectable by WB and BN (Sandoval-Ibanez et al., 2022). This reduced accumulation of the Cyt b₆f complex ultimately leads to plant death under CL intensity (Sandoval-Ibanez et al., 2022). Indeed, these data correlate with our difficulties in generating a knock-out line in the Col-5 background (*S261-Cas#1*). The *S261-Cas#1* line could not develop true leaves and its growth was arrested at the cotyledon stage under normal light conditions. However, the results in the *pgr5-1* background suggested a different function for S261. The function of S261 proposed in previous publications was as an assembly factor (Sandoval-Ibanez et al., 2022). In a plant lacking S261, if it is involved solely in the assembly of the Cyt b₆f complex, one would not expect to observe wild-type levels of Cyt b₆f accumulation. This is an effect observed mainly in proteins involved in degradation, such as the double mutant between *fugaeril* (*fug1*) and *var2*, a mutant lacking FtsH2 (Kato et al., 2009). On the other hand, if S261 is involved in the degradation of the Cyt b₆f complex, either as part of a degradation complex or in a signalling pathway that induces the degradation of the Cyt b₆f complex, an accumulation of Cyt b₆f could be expected in *pgr5* mutants, since PGR5 is presumed to be required for the degradation together with S261. In this context, it was observed that the Cyt b₆f complex accumulated to levels close to that of the WT in the various *pgr5 S261* lines (Figure 24), which contradicts the publication of (Sandoval-Ibanez et al., 2022) and suggests that PGR5 is an essential part of the reduced accumulation of Cyt b₆f in the *S261* knock-out mutant. The formation of a complex between S261 and PGR5, and perhaps also Fd (Figure 25A and B), would explain why degradation of Cyt b₆f occurs in the *S261* single mutant but is inhibited in the *pgr5-1* background (Figure 24A). In addition, the inhibited degradation of the Cyt b₆f complex in the absence of PGR5 has a positive effect on growth. Under both FL and CL conditions, the double mutant lines *pgr5-1 S261-Cas* are able to grow and survive, especially under CL where they are indistinguishable from WT in terms of growth. The improved growth and survival under CL of the double mutants (*pgr5-1 S261-Cas#1* and *pgr5-1 S261-Cas#2*) compared to the *S261-Cas#1* line can be explained by an

intact Cyt b₆f complex, which is essential for plant survival under light conditions higher than LL (Page et al., 2004; Sandoval-Ibanez et al., 2022). Therefore, inhibiting the degradation of Cyt b₆f allows the plant to survive. It has recently been published that the Cyt b₆f complex, along with PSI, is the structure that is most stressed in terms of its structural integrity under FL (Chen et al., 2022). This could mean that protecting Cyt b₆f from degradation rescues the plant, as seen in the comparison of the single *S261* mutant and the double line. However, to investigate the mechanism behind the reduced degradation of the Cyt b₆f complex by *S261* in the absence of *PGR5*, further experiments are needed, comparing with mutants that have lower levels of certain Cyt b₆f subunits, such as *ccda* (Page et al., 2004), *petG*, *petN* (Schwenkert et al., 2007) or *petm* (Lan et al., 2021).

A higher accumulation of *PGR5*_{G130S} was observed in the suppressor lines *pgr5-S261*, *pgr5-1 S261-Cas#1* and *pgr5-1 S261-Cas#2* than in the *pgr5-1* line itself (Figure 24). These results may indicate that a functional and correctly assembled Cyt b₆f complex is required for efficient degradation of *PGR5*.

5.5 NDH-mediated CEF compensates the lack of *PGR5* under certain conditions

It was observed that lines with the *pgr5-1* background and carrying a mutation in the FBPase (*pgr5 S111* and *pgr5-1 hcefl*) were able to survive under FL conditions in our experiments (Figure 16). The measurements carried out to study CEF activity in these lines (Figure 18) showed that in the *pgr5-1 hcefl* mutant, CEF was restored to WT levels, explaining the suppression of the *pgr5* lethal phenotype under FL (Figure 36 and D). It has been published that there is an overaccumulation of the NDH complex in the FBPase knockout line (*hcefl*), resulting in a higher CEF mediated by the NDH complex (Livingston et al., 2010). This overaccumulation and higher activity of the NDH complex, results in the *pgr5-1 hcefl* line to survive under FL, whereas in the *pgr5-1* background without the *hcefl* mutation the low amount of NDH complex cannot compensate for the lack of *PGR5*-mediated CEF. It could be concluded from this work that the NDH complex is mainly responsible for acclimation to the low light phase, mainly by oxidising PSI from the acceptor side. In the double mutants *pgr5-1 hcefl*, a higher accumulation of the NDH complex could also oxidise the PSI in the HL phases (Figure 20A), indicating that although the NDH-mediated CEF is active under different light conditions, it cannot replace the *PGR5*-mediated CEF in the *pgr5* single mutant due to its lower activity.

5.6 The FBPase functions as a security valve for PSI

Additionally, it was found that the *pgr5-1* lines containing a premature stop codon in ACHT2 (*pgr5-1 S336* and *pgr5-1 acht2-Cas*) were capable of surviving under FL conditions (Figure 17C). This protein has recently been described to oxidise and consequently inactivate the FBPase (Yokochi et al., 2021). Indeed, the *pgr5-1 S336* mutants showed a similar or lower CEF compared to *pgr5-1* (Figure 18B and C); this is expected due to the presumably more active FBPase in *pgr5-1 S336*. Conversely, the *pgr5-1 hcefl* mutant suppresses *pgr5-1* lethality under FL and is the result of a different mechanism rather than restoration of CEF. The reason for the suppression of *pgr5* could be that in the absence of ACHT2, the FBPase is lesser oxidized and by this more active during LL, producing a higher demand in NADPH and reduce the deficiency of PSI electron acceptors in *pgr5* (Figure 36 and E). Indeed, a slight reduction of Y(NA) during the LL phases of the FL program could be detected, although it was not as strong as expected (Figure 20B). A lower acceptor side limitation leads to a lower an over-reduction of PSI, thus avoiding ROS formation in the active centre of PSI and photoinhibition. A comparable example of this phenomenon was shown by suppressing the photosynthetic phenotype of *pgr5-1* with reduced Y(NA) by introducing flavodiiron proteins into *pgr5-1* and establishing a pseudo-CEF (Yamamoto et al., 2016). Furthermore, previous literature has shown that when NTRC is overexpressed in the *pgr5-1* background, there is less acceptor-side restriction in the LL phase of FL compared to *pgr5-1* (Nikkanen et al., 2018). NTRC is another redox regulator that mainly reduces 2-Cys peroxiredoxin (2-Cys PRX); plants lacking this protein show a strongly induced NPQ and a retarded growth phenotype (Naranjo et al., 2016; Perez-Ruiz et al., 2017). This is noteworthy for our work because overexpression of NTRC results in a stronger reduction of FBPase (Nikkanen et al., 2016), which could be comparable to that of the *acht2* mutant.

This suggests that the role of FBPase in the acclimation of plants to FL is more significant than previously thought. It was demonstrated that in the absence of FBPase, CEF occurs even in the background of *pgr5-1* (Figure 18B and C), considering that the CEF measured in this background is mediated by the NDH complex as previously described (Livingston et al., 2010). Furthermore, it was demonstrated that knocking out the thioredoxin-like ACHT2 partially rescues the high PSI electron acceptor deficit in *pgr5*, likely attributed to a higher activity of the CBB-cycle (Figure 21). In support of this result, Yokochi et al. generated an ACHT2-overexpressing line that showed a more strongly induced NPQ and a retarded growth phenotype; the phenotype observed in the ACHT2-overexpressing line

has strong similarities with the *ntrc* mutant (Yokochi et al., 2021). It has previously been shown that the strongly induced NPQ and growth phenotype in the *ntrc* line result from an overactive PGR5-mediated CEF. However, a direct link between NTRC and the regulation of PGR5 could not be found (Naranjo et al., 2021). The missing link between the two proteins may be provided by ACHT2 and its role in oxidising FBPase. In the work of Yokochi and colleagues, the ACHT1 and ACHT2 knockout line (*acht*) suppresses the growth phenotype and photosynthetic parameters of *ntrc* (Yokochi et al., 2021). Until now, this has only been observed by knocking out PGR5 (Naranjo et al., 2021) or 2-Cys PRX (Perez-Ruiz et al., 2017). A possible interaction of ACHT1 and ACHT4 with 2-Cys PRX was shown by work on the ACHT family (Eliyahu et al., 2015). Furthermore, ACHT2, the protein found in the screen, can reduce 2-Cys PRX during the transition from light to dark (Yokochi et al., 2021). The last missing piece of the puzzle is the redox regulator and interactor of PGR5-mediated CEF and FBPase. Which is that the PGR5-mediated CEF and the CBB-cycle compete for electron flow and are finely balanced. This balance between the two pathways can be tipped in favour of either pathway, but it appears that the PGR5-mediated CEF is favoured (Okegawa et al., 2022). In addition, the chloroplast thioredoxin m4 (Trx m4) reduces FBPase at the dark-to-light transition, thereby activating the CBB-cycle at the onset of photosynthesis (Okegawa & Motohashi, 2020; Okegawa et al., 2022). Trx m4 inhibits PGRL1 by forming a complex and down-regulating the activity of PGR5-mediated CEF (Okegawa & Motohashi, 2020). It is interesting to note that by connecting the different interactions and regulations of NTRC, ACHT2, and Trx m4 known, a model can be drawn (Figure 35). In the dark to light transition, NTRC regulates 2-Cys PRX (Perez-Ruiz et al., 2017). 2-Cys PRX is regulated by ACHT2 during the transition from light to dark (Yokochi et al., 2021). In addition, ACHT2 oxidises FBPase and inactivates it during the light-dark phase (Yokochi et al., 2021). Trx m4 can inactivate PGR5-CEF (Okegawa & Motohashi, 2020) and oxidise FBPase (Telman et al., 2020). If the inactivator of FBPase, ACHT2, is missing, then the increased FBPase activity results in a higher electron sink, which is the case in the *acht2* knockout line (Figure 21, (Yokochi et al., 2021)). Therefore, the hypothesis is that if FBPase is strongly downregulated by ACHT2, Trx m4 will mainly reduce FBPase and therefore bind less PGRL1, resulting in higher PGR5-mediated CEF, as observed by the strong NPQ in *oeACHT2* or *ntrc*. In the absence of FBPase, the NDH complex overac-

cumulates and NPQ is strongly induced (Figure 35, Livingston et al., 2010), so that additional Trx m4 no longer inactivates FBPase and instead binds more PGR1, strongly down-regulating PGR5-mediated CEF.

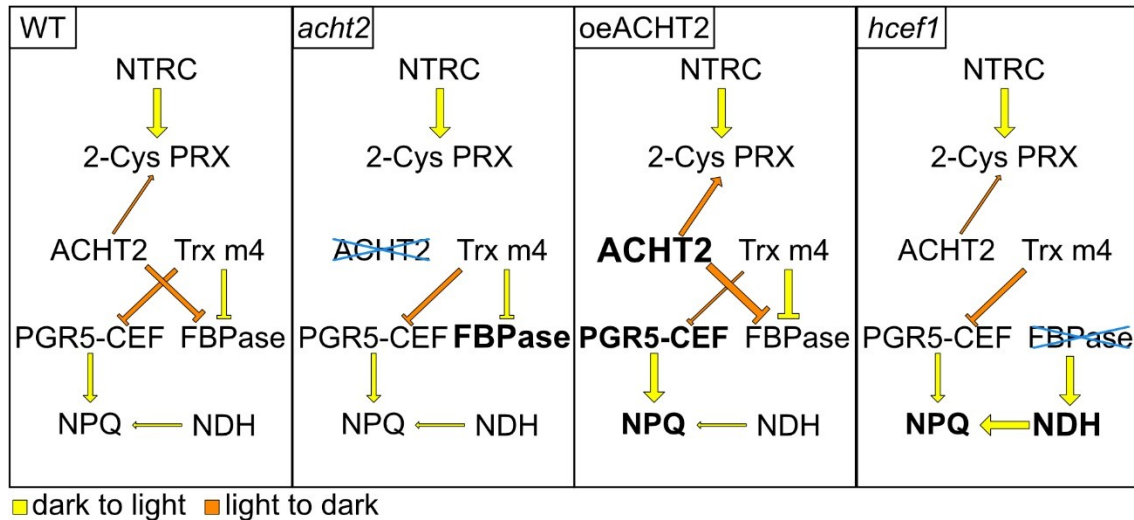


Figure 35: **Model of the activation network of CEF around FBPase and the interacting redox regulators.** Schematic representation of the activation (arrow) and inactivation (blunt arrow) network of 2-Cys PRX and FBPase in wild type (WT), ACHT2 knockout line (*acht2*), ACHT2 overexpression line (*oeAcht2*) and FBPase knockout (*hcef1*). Knocked out proteins are marked with a blue cross. Activation and inactivation of 2-Cys PRX, FBPase, PGR5-mediated CEF (PGR5-CEF), NPQ and NDH are dependent on the shift from dark to light (yellow) and from light to dark (orange).

5.7 Regulation of LEF by the qE component of NPQ is not sufficient to ensure survival under FL

Since NPQ is one of the mechanisms protecting PSII from overexcitation and consequent photoinhibition by ROS formation, its overinduction could have a positive effect on plant survival under FL. In the VDE-PSBS-ZEP (VPZ) lines generated in *Nicotiana tabacum*, *soybean* and *Arabidopsis*, faster qE induction under HL and relaxation under LL were observed (De Souza et al., 2022; Garcia-Molina & Leister, 2020; Kromdijk et al., 2016). In the *Nicotiana tabacum* lines, a 15% increase in dry matter was observed under field conditions (Kromdijk et al., 2016), but not in *Arabidopsis* (Garcia-Molina & Leister, 2020). In our experiments, mutants with a strong and stable induction of NPQ to generate a down-regulation of LEF through lower PSII activity, as observed in both lines *cg1160* (Rühle et al., 2014) and *ntrc* (Naranjo et al., 2016) were selected. However, none of these mutations in the *pgr5-1* background suppressed lethality under FL (Figure 12). Indeed, *pgr5-1 cg1160* still induced a strong NPQ, while the NPQ in *pgr5-1 ntrc* was abolished in

the absence of PGR5 (Naranjo et al., 2021). Interestingly, neither of the double mutants exhibited a higher donor-side restriction, suggesting that the NPQ induces a lower LEF activity (Figure 15B, Naranjo et al., 2016). Furthermore, no *pgr5* suppressors with high NPQ were found in the screen (Table 4).

However, an unusual finding in the screen was a group of proteins that were thought to be PSII-associated, but on closer analysis were actually involved in state transitions. These proteins were Lhcb4 (*pgr5-S81*) and PPL1 (*pgr5-S120*, *pgr5-S271*, *pgr5-S327*, *pgr5-S386* and *pgr5-S393*) (Table 4). Both a knockout line of all Lhcb4 isoforms (*kolhcb4*) and a knockout line of PPL1 (*ppl1*) show a faster transition from state I to state II (Che et al., 2020; de Bianchi et al., 2011). State transitions, a component of NPQ, describe the transfer of LHCII from PSII to PSI and vice versa by phosphorylation or dephosphorylation. Thus, these two processes moderate the balance between the two photosystems when a change in light conditions excites only one of the photosystems. In addition, Zhou and colleagues recently observed impaired activation of the state transition in *pgr5-1* CEF mutant lines due to a reduction in the PQ pool (Zhou et al., 2022). Furthermore, a link between PGR5-mediated CEF and state transition was observed by Rühle and colleagues, where a higher phosphorylation of LHCII was shown in *pgr5-1* compared to WT, indicating that the balance of states was shifted towards state II (Rühle et al., 2021). A more recent link between PGR5 and proteins involved in state transition was found in *Cucumis sativus L.*, where an interaction among PGR5 and Lhcb3 was observed (Wu et al., 2021). This is of interest because the Lhcb3 knockout line (*kolhcb3*) showed a faster transition from state I to state II (Damkjaer et al., 2009) than *ppl1* and *kolhcb4*. Therefore, a faster induction of the state transition could suppress the lethal phenotype of *pgr5-1* under FL, but further investigations are needed with mutants where the state transition is mainly affected and not the PSII activity or with a lower LEF rate, for example *pgr5-1* lines with altered levels of STN7, a kinase responsible for the phosphorylation of LHCII and thus the switch from state I to state II (Bonardi et al., 2005).

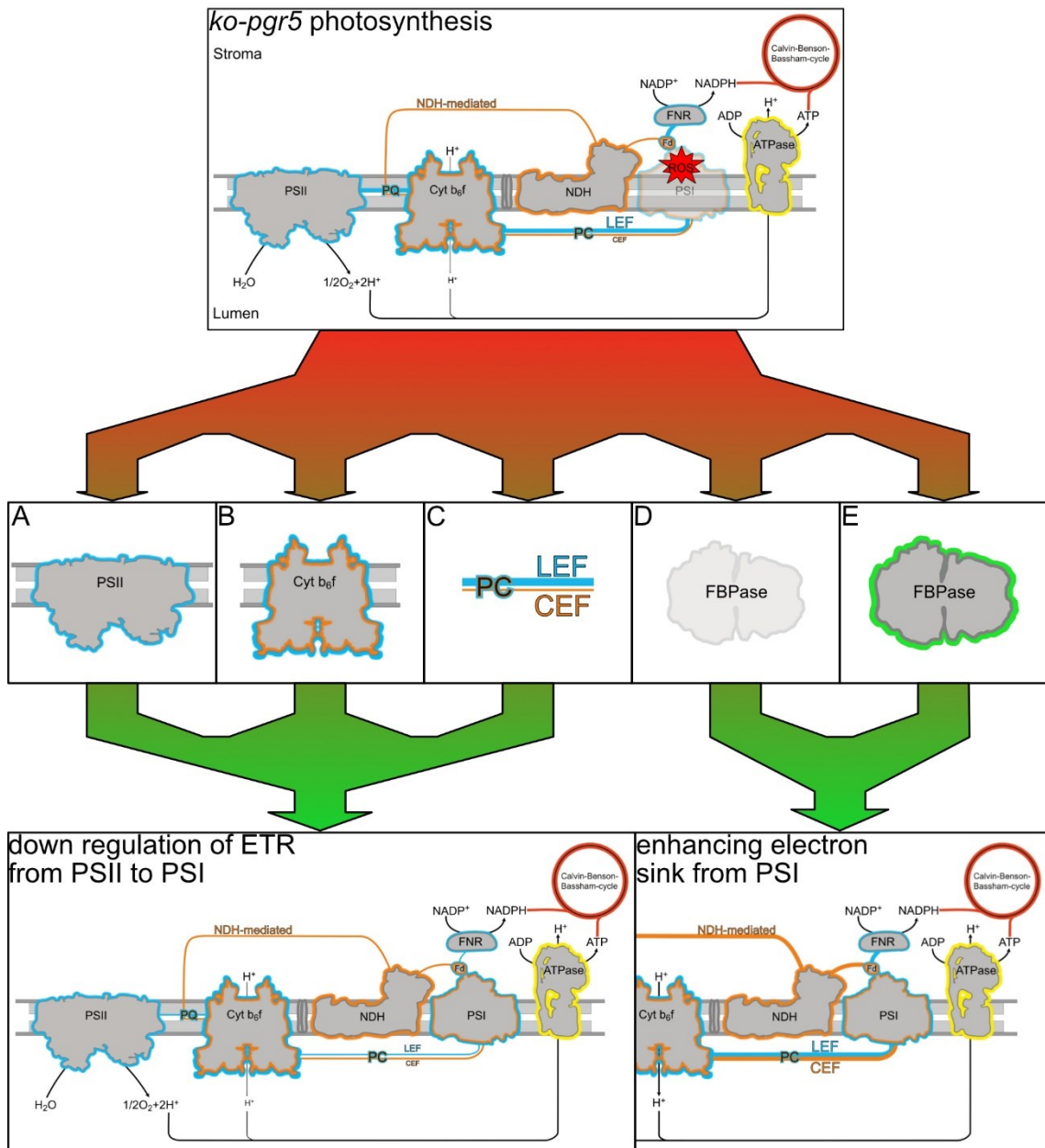


Figure 36: **Model of possible suppression of *pgr5* lethality under FL found in this work.** In a mutant line lacking the PGR5-mediated CEF, PSI lacks an electron acceptor, resulting in damage by ROS formation and stroma over-reduction. In our screen, we confirmed two different strategies that suppress the lethality of *pgr5-1* under FL. This suppression was achieved by five different set points. First, a down-regulation of the ETR from PSII to PSI through lower PSII accumulation (**A**), lower Cyt b_6/f activity (**B**) or lower PC content (**C**). A novel way is to increase the electron sink from PSI by knocking out FBPase (**D**), resulting in higher NDH activity, or to upregulate FBPase activity (**E**).

5.8 The *pgr5-Cas* mutant a PGR5 knock-out

Differences in protein accumulation and photosynthetic performance were observed in experiments involving novel *pgr5-cas* lines when compared to the original *pgr5* mutant, *pgr5-1*. The *pgr5-1* line showed a more impaired induction of photosynthesis and steady-

state photosynthetic performance, as well as CEF, than the *pgr5-cas* lines (Figure 30 and Figure 32). Furthermore, a reduction in thylakoid complexes was observed in the *pgr5-1* line, while an up-regulation was observed in others (Figure 33). Thus, the differences between the lines and the pleiotropic phenotype observed only in the *pgr5-1* line could be due to unnoticed second site mutations generated by the EMS treatment used to generate the line (Shikanai et al., 1999) or to the still detectable low level of PGR5_{G130S} in *pgr5-1* (Figure 4B, Figure 9B, Figure 13B, Figure 24B, Figure 24C and Figure 29B). During the analysis of the *pgr5-1* genome compared to the Col-5 background line, SNPs were discovered in the genes encoding the following plastid-localized proteins: PGR5, CGL20A, PsbO2, ABCI11 and HCF136 (Table 6). Among these affected proteins, only PGR5, PsbO2 and HCF136 were detectable by a proteomic approach, while others were too low in abundance to be detected by mass spectrometry (Table 6). However, the most interesting SNP was the one localised in *CGL20A*, which encodes a protein involved in the biogenesis of the plastid ribosome (Reiter et al., 2020). A notable feature of *CGL20A* is its high proline content, which makes the detected SNP particularly interesting since it causes an amino acid switch from proline to leucine (Table 6). Furthermore, in a recently published paper on an additional PGR5 knockout line called *pgr5^{hope1}*, the same mutation of *CGL20A* was detected in the *pgr5-1* line (Wada et al., 2021). The newly generated line (*pgr5^{hope1}*) had the same amino acid exchange in the PGR5 protein (G130S) as the *pgr5-1* line, but not the *CGL20A* mutation (Wada et al., 2021). In the work of Wada et al. higher Fv/Fm and lower accumulation of PsaA and NDH complex were observed in the *pgr5^{hope1}* line compared to the *pgr5-1* line (Wada et al., 2021). This suggests that the *CGL20A* mutation causes the pleiotropic phenotype of *pgr5-1*. To investigate the potential impact of PGR5_{G130S} protein accumulation on *pgr5-1*, complementation lines were examined by introducing the native PGR5 gene into the *pgr5-1* background. This was done in order to rule out the possibility of any effects resulting solely from the presence of the PGR5_{G130S} protein.

5.8.1 The PGR5_{G130S} protein affects photosynthesis

Upon complementing the *pgr5-1* line with the native PGR5 protein, a significant rescue of the majority of photosynthetic parameters was observed (Figure 30, Figure 31B, Figure 30C and Figure 30D), suggesting a negative effect of PGR5_{G130S}. Interestingly, only the induced NPQ and not the P700 oxidation was rescued by expressing the PGR5 protein in the *pgr5-1* background (Figure 32). This result suggests that P700 oxidation is still

strongly affected by the mutation in *CGL20A*, considering the lower amount and activity of PSI resulting from the inhibited translation in the chloroplast caused by the absence of *CGL20A* (Reiter et al., 2020). This would imply that the induction of NPQ more closely relates to the activity of the PGR5-driven CEF than the P700 oxidation rate. Additionally, a reduction in NDH complex proteins was detected in the *pgr5-1* line, which can be partially attributed to the partial complementation of P700 oxidation. In the complementation lines of *pgr5-1* with native PGR5, a rescue of protein content was observed compared to *pgr5-1*, indicating that the altered protein amount is not due to the additional SNPs found in the *pgr5-1* line, but to PGR5_{G130S}. However, a lower accumulation of the PGRL1 protein and the formation of a degraded form were observed in the *pgr5-1* line and the complementation lines. Therefore, this effect on PGRL1 accumulation seems to be specifically caused by the PGR5_{G130S} protein (Figure 29B). The degraded product of PGRL1 has been observed in previous work by other groups (Suorsa et al., 2012; Suorsa et al., 2016). It should be noted that the lower band observed in the PGRL1 immunoblot is a result of the N-terminus of the protein, which was used for antibody production (DalCorso et al., 2008). Furthermore, the interaction between PGRL1 and PGR5 is thought to take place at the N-terminus of the PGRL1 protein. This strengthens the assumption that PGR5_{G130S} is responsible for the protein modification that produces the additional lower band of PGRL1 in the immunodetection.

5.8.2 PGR5 and PGRL1 have different functions under HL acclimation

A severe growth-restricted phenotype was observed in the different *pgr5* lines, including *pgr5-1*, *pgr5-Cas#1*, and *pgr5-Cas#2*, when exposed to HL conditions. These lines exhibited lower levels of anthocyanin and experienced retarded growth (Figure 34A and Figure 34D). This phenotype was specific for the lines that had a lower accumulation of PGR5 but almost WT levels of PGRL1 (*pgr5-1*, *pgr5-Cas#1* and *pgr5-Cas#2*). Interestingly, the *pgrllab* line had a phenotype similar to WT under HL, in contrast to other experiments where the *pgrllab* mutant is more similar to *pgr5-1*. From this result it can be concluded that the inability of PGRL1 to interact with PGR5 has a negative effect on the plant, resulting in a retarded growth phenotype under HL conditions. This finding is rather surprising, as recent literature on the function of PGRL1 clearly shows that this protein plays an important role in the regulation of PGR5 as a stabiliser (Rühle et al., 2021), but our results suggest a novel function that requires further investigation.

6. Conclusions

1. *pgr5* suppressor screen under FL is a successful tool to identify known and novel pathways of light acclimation in plants.
2. Mutants in PSII, Cyt b₆f, PC, state transition and FBPase were identified as suppressors of *pgr5-1* lethality under FL.
3. The most effective way to suppress the *pgr5* phenotype under FL is to down-regulate PSII activity through complex stability or assembly, as demonstrated with the PET lines together with the suppressors identified in the screen. This goes along with increasing the donor side limitation to PSI, decreasing the deficit of PSI electron acceptors in the *pgr5* mutant and restoring the growth of the mutant under FL.
4. A higher electron sink on the acceptor side of PSI can rescue *pgr5* under FL, either by substitution of the PGR5 CEF by NDH (*pgr5 hcef1*) or by a higher activity of the CBB-cycle (*pgr5 acht2*).
5. The screen identified two unknown proteins (S42 and S261) as suppressors of *pgr5* under FL.
6. S261 may interact with PGR5 and its role in maintaining Cyt b₆f stability depends on PGR5: the *pgr5 S261* double mutant accumulates Cyt b₆f and grows as WT under control conditions, in contrast to the lethal phenotype of the single *S261* mutant.
7. New *pgr5* lines (*pgr5-Cas#1* and *pgr5-Cas#2*) were generated in a “clean” background using CRISPR/Cas: *pgr5-1* showed a pleiotropic phenotype caused by additional SNPs and traces of PGR5_{G130S}.
8. A *pgr5*-specific phenotype was found under HL, where the absence of PGR5 makes PGRL1 harmful to the plant.

7. Bibliography

- Abdel-Ghany S E, Muller-Moule P, Niyogi K K, Pilon M, Shikanai T (2005) Two P-type ATPases are required for copper delivery in *Arabidopsis thaliana* chloroplasts. *Plant Cell* 17: 1233-1251.
- Allen J F (1992) Protein phosphorylation in regulation of photosynthesis. *Biochim Biophys Acta* 1098: 275-335.
- Armbruster U, Zühlke J, Rengstl B, Kreller R, Makarenko E, Rühle T, Schüenemann D, Jahns P, Weisshaar B, Nickelsen J (2010) The *Arabidopsis* thylakoid protein PAM68 is required for efficient D1 biogenesis and photosystem II assembly. *Plant Cell* 22: 3439-3460.
- Arnon D I, ALLEN M B, Whatley F R (1954) Photosynthesis by isolated chloroplasts. *Nature* 174: 394-396.
- Barbato R, Tadini L, Cannata R, Peracchio C, Jeran N, Alboresi A, Morosinotto T, Bajwa A A, Paakkari V, Suorsa M (2020) Higher order photoprotection mutants reveal the importance of Δ pH-dependent photosynthesis-control in preventing light induced damage to both photosystem II and photosystem I. *Sci Rep* 10: 6770.
- Bonardi V, Pesaresi P, Becker T, Schleiff E, Wagner R, Pfannschmidt T, Jahns P, Leister D (2005) Photosystem II core phosphorylation and photosynthetic acclimation require two different protein kinases. *Nature* 437: 1179-1182
- Cai W, Ji D, Peng L, Guo J, Ma J, Zou M, Lu C, Zhang L (2009) LPA66 is required for editing psbF chloroplast transcripts in *Arabidopsis*. *Plant Physiol* 150: 1260-1271.
- Cejudo F J, Ojeda V, Delgado-Requerrey V, Gonzalez M, Perez-Ruiz J M (2019) Chloroplast Redox Regulatory Mechanisms in Plant Adaptation to Light and Darkness. *Front Plant Sci* 10: 380.
- Che Y, Kusama S, Matsui S, Suorsa M, Nakano T, Aro E M, Ifuku K (2020) *Arabidopsis* PsbP-Like Protein 1 Facilitates the Assembly of the Photosystem II Supercomplexes and Optimizes Plant Fitness under Fluctuating Light. *Plant Cell Physiol* 61: 1168-1180.

- Chen Q, Xiao Y, Ming Y, Peng R, Hu J, Wang H B, Jin H L (2022) Quantitative proteomics reveals redox-based functional regulation of photosynthesis under fluctuating light in plants. *J Integr Plant Biol* 64: 2168-2186.
- Cingolani G, Duncan T M (2011) Structure of the ATP synthase catalytic complex (F(1)) from *Escherichia coli* in an autoinhibited conformation. *Nat Struct Mol Biol* 18: 701-707.
- DalCorso G, Pesaresi P, Masiero S, Aseeva E, Schünemann D, Finazzi G, Joliot P, Barbato R, Leister D (2008) A complex containing PGRL1 and PGR5 is involved in the switch between linear and cyclic electron flow in *Arabidopsis*. *Cell* 132: 273-285.
- Damkjaer J T, Kereiche S, Johnson M P, Kovacs L, Kiss A Z, Boekema E J, Ruban A V, Horton P, Jansson S (2009) The photosystem II light-harvesting protein Lhcb3 affects the macrostructure of photosystem II and the rate of state transitions in *Arabidopsis*. *Plant Cell* 21: 3245-3256.
- Dann M, Leister D (2019) Evidence that cyanobacterial Sll1217 functions analogously to PGRL1 in enhancing PGR5-dependent cyclic electron flow. *Nat Commun* 10: 5299.
- de Bianchi S, Betterle N, Kouril R, Cazzaniga S, Boekema E, Bassi R, Dall'Osto L (2011) *Arabidopsis* mutants deleted in the light-harvesting protein Lhcb4 have a disrupted photosystem II macrostructure and are defective in photo-protection. *Plant Cell* 23: 2659-2679.
- De Souza A P, Burgess S J, Doran L, Hansen J, Manukyan L, Maryn N, Gotarkar D, Leonelli L, Niyogi K K, Long S P (2022) Soybean photosynthesis and crop yield are improved by accelerating recovery from photoprotection. *Science* 377: 851-854.
- Eliyahu E, Rog I, Inbal D, Danon A (2015) ACHT4-driven oxidation of APS1 attenuates starch synthesis under low light intensity in *Arabidopsis* plants. *Proc Natl Acad Sci U S A* 112: 12876-12881.
- Garcia-Molina A, Leister D (2020) Accelerated relaxation of photoprotection impairs biomass accumulation in *Arabidopsis*. *Nat Plants* 6: 9-12.
- Grefen C, Blatt M R (2012) A 2in1 cloning system enables ratiometric bimolecular fluorescence complementation (rBiFC). *Biotechniques* 53: 311-314.

- Hashimoto M, Endo T, Peltier G, Tasaka M, Shikanai T (2003) A nucleus-encoded factor, CRR2, is essential for the expression of chloroplast *ndhB* in *Arabidopsis*. *Plant J* 36: 541-549.
- Hertle A P, Blunder T, Wunder T, Pesaresi P, Pribil M, Armbruster U, Leister D (2013) PGRL1 is the elusive ferredoxin-plastoquinone reductase in photosynthetic cyclic electron flow. *Mol Cell* 49: 511-523.
- Ihnatowicz A, Pesaresi P, Varotto C, Richly E, Schneider A, Jahns P, Salamini F, Leister D (2004) Mutants for photosystem I subunit D of *Arabidopsis thaliana*: effects on photosynthesis, photosystem I stability and expression of nuclear genes for chloroplast functions. *Plant J* 37: 839-852.
- Iwai M, Takizawa K, Tokutsu R, Okamuro A, Takahashi Y, Minagawa J (2010) Isolation of the elusive supercomplex that drives cyclic electron flow in photosynthesis. *Nature* 464: 1210-1213.
- Jarvi S, Suorsa M, Aro E M (2015) Photosystem II repair in plant chloroplasts--Regulation, assisting proteins and shared components with photosystem II biogenesis. *Biochim Biophys Acta* 1847: 900-909.
- Johnson J, Berry J (2021) The role of cytochrome b6f in the control of steady-state photosynthesis: a conceptual and quantitative model. *Photosynth Res* 148: 101-136.
- Kato Y, Miura E, Ido K, Ifuku K, Sakamoto W (2009) The variegated mutants lacking chloroplastic FtsHs are defective in D1 degradation and accumulate reactive oxygen species. *Plant Physiol* 151: 1790-1801.
- Kleine T, Maier U G, Leister D (2009) DNA transfer from organelles to the nucleus: the idiosyncratic genetics of endosymbiosis. *Annu Rev Plant Biol* 60: 115-138.
- Klepikova A V, Kasianov A S, Gerasimov E S, Logacheva M D, Penin A A (2016) A high resolution map of the *Arabidopsis thaliana* developmental transcriptome based on RNA-seq profiling. *Plant J* 88: 1058-1070.
- Klughammer C, Schreiber U (2008) Complementary PS II quantum yields calculated from simple fluorescence parameters measured by PAM fluorometry and the Saturation Pulse method. *PAM application notes* 1: 201-247.

- Klughammer C, Schreiber U (2016) Deconvolution of ferredoxin, plastocyanin, and P700 transmittance changes in intact leaves with a new type of kinetic LED array spectrophotometer. *Photosynth Res* 128: 195-214.
- Kromdijk J, Głowacka K, Leonelli L, Gabilly S T, Iwai M, Niyogi K K, Long S P (2016) Improving photosynthesis and crop productivity by accelerating recovery from photoprotection. *Science* 354: 857-861.
- Kudoh H, Sonoike K (2002) Irreversible damage to photosystem I by chilling in the light: cause of the degradation of chlorophyll after returning to normal growth temperature. *Planta* 215: 541-548.
- Lan Y, Chen Q, Kong M, Liu Y, Lyu M A, Perveen S, Mi H (2021) PetM Is Essential for the Stabilization and Function of the Cytochrome b6f Complex in Arabidopsis. *Plant Cell Physiol* 62: 1603-1614.
- Lehretz G G, Schneider A, Leister D, Sonnewald U (2022) High non-photochemical quenching of VPZ transgenic potato plants limits CO₂ assimilation under high light conditions and reduces tuber yield under fluctuating light. *J Integr Plant Biol* 64: 1821-1832.
- Leister D, Marino G, Minagawa J, Dann M (2022) An ancient function of PGR5 in iron delivery? *Trends Plant Sci* 27: 971-980.
- Li N, Wong W S, Feng L, Wang C, Wong K S, Zhang N, Yang W, Jiang Y, Jiang L, He J-X (2022) The Thylakoid Membrane Protein NTA1 Is An Assembly Factor of Cytochrome b6f Complex Essential for Chloroplast Development in Arabidopsis. *Plant Commun* 100509.
- Lichtenthaler H K, Wellburn A R (1983) Determination of total carotenoids and chlorophylls *a* and *b* in leaf extracts in different solvents. *Biochem Soc Trans* 11: 2.
- Livingston A K, Cruz J A, Kohzuma K, Dhingra A, Kramer D M (2010) An Arabidopsis mutant with high cyclic electron flow around photosystem I (hcef) involving the NADPH dehydrogenase complex. *Plant Cell* 22: 221-233.
- Löffelhardt W (2006) *Evolution der Chloroplasten: Endosymbiose führt zu photoautotrophen Eukaryonten.*

- Lundin B, Hansson M, Schoefs B, Vener A V, Spetea C (2007) The Arabidopsis PsbO2 protein regulates dephosphorylation and turnover of the photosystem II reaction centre D1 protein. *Plant J* 49: 528-539.
- Malone L A, Proctor M S, Hitchcock A, Hunter C N, Johnson M P (2021) Cytochrome b(6)f - Orchestrator of photosynthetic electron transfer. *Biochim Biophys Acta Bioenerg* 1862: 148380.
- Maple J, Møller S G (2007) Mutagenesis in arabidopsis. *Circadian Rhythms: Meth Prot* 197-206.
- Meurer J, Plücker H, Kowallik K V, Westhoff P (1998) A nuclear-encoded protein of prokaryotic origin is essential for the stability of photosystem II in *Arabidopsis thaliana*. *EMBO j* 17: 5286-5297.
- Michelet L, Zaffagnini M, Morisse S, Sparla F, Perez-Perez M E, Francia F, Dannon A, Marchand C H, Fermani S, Trost P, Lemaire S D (2013) Redox regulation of the Calvin-Benson cycle: something old, something new. *Front Plant Sci* 4: 470.
- Munekage Y, Hojo M, Meurer J, Endo T, Tasaka M, Shikanai T (2002) PGR5 is involved in cyclic electron flow around photosystem I and is essential for photoprotection in *Arabidopsis*. *Cell* 110: 361-371.
- Munekage Y, Takeda S, Endo T, Jahns P, Hashimoto T, Shikanai T (2001) Cytochrome b(6)f mutation specifically affects thermal dissipation of absorbed light energy in *Arabidopsis*. *Plant J* 28: 351-359.
- Nandha B, Finazzi G, Joliot P, Hald S, Johnson G N (2007) The role of PGR5 in the redox poisoning of photosynthetic electron transport. *Biochim Biophys Acta* 1767: 1252-1259.
- Naranjo B, Migné C, Krieger-Liszkay A, Hornero-Méndez D, Gallardo-Guerrero L, Cejudo F J, Lindahl M (2016) The chloroplast NADPH thioredoxin reductase C, NTRC, controls non-photochemical quenching of light energy and photosynthetic electron transport in *Arabidopsis*. *Plant Cell Environ* 39: 804-822.
- Naranjo B, Penzler J-F, Rühle T, Leister D (2021) NTRC effects on non-photochemical quenching depends on PGR5. *Antioxidants* 10: 900.

- Nickelsen J, Rengstl B (2013) Photosystem II assembly: from cyanobacteria to plants. *Annu Rev Plant Biol* 64: 609-635.
- Nikkanen L, Toivola J, Rintamäki E (2016) Crosstalk between chloroplast thioredoxin systems in regulation of photosynthesis. *Plant Cell Environ* 39: 1691-1705.
- Nikkanen L, Toivola J, Trotta A, Diaz M G, Tikkanen M, Aro E M, Rintamäki E (2018) Regulation of cyclic electron flow by chloroplast NADPH-dependent thioredoxin system. *Plant Direct* 2: e00093.
- Niyogi K K, Li X P, Rosenberg V, Jung H S (2005) Is PsbS the site of non-photochemical quenching in photosynthesis? *J Exp Bot* 56: 375-382.
- Okegawa Y, Kagawa Y, Kobayashi Y, Shikanai T (2008) Characterization of factors affecting the activity of photosystem I cyclic electron transport in chloroplasts. *Plant Cell Physiol* 49: 825-834.
- Okegawa Y, Long T A, Iwano M, Takayama S, Kobayashi Y, Covert S F, Shikanai T (2007) A balanced PGR5 level is required for chloroplast development and optimum operation of cyclic electron transport around photosystem I. *Plant Cell Physiol* 48: 1462-1471.
- Okegawa Y, Motohashi K (2020) M-type thioredoxins regulate the PGR5/PGRL1-dependent pathway by forming a disulfide-linked complex with PGRL1. *Plant Cell* 32: 3866-3883.
- Okegawa Y, Tsuda N, Sakamoto W, Motohashi K (2022) Maintaining the chloroplast redox balance through the PGR5-dependent pathway and the Trx system is required for light-dependent activation of photosynthetic reactions. *Plant Cell Physiol* 63: 92-103.
- Page M L, Hamel P P, Gabilly S T, Zegzouti H, Perea J V, Alonso J M, Ecker J R, Theg S M, Christensen S K, Merchant S (2004) A homolog of prokaryotic thiol disulfide transporter CcdA is required for the assembly of the cytochrome b6/f complex in Arabidopsis chloroplasts. *J Biol Chem* 279: 32474-32482.
- Penzler J F, Marino G, Reiter B, Kleine T, Naranjo B, Leister D (2022) Commonalities and specialties in photosynthetic functions of PROTON GRADIENT REGULATION5 variants in Arabidopsis. *Plant Physiol* 190: 1866-1882.

- Perez-Ruiz J M, Naranjo B, Ojeda V, Guinea M, Cejudo F J (2017) NTRC-dependent redox balance of 2-Cys peroxiredoxins is needed for optimal function of the photosynthetic apparatus. *Proc Natl Acad Sci U S A* 114: 12069-12074.
- Perez-Ruiz J M, Spinola M C, Kirchsteiger K, Moreno J, Sahrawy M, Cejudo F J (2006) Rice NTRC is a high-efficiency redox system for chloroplast protection against oxidative damage. *Plant Cell* 18: 2356-2368.
- Pesaresi P, Scharfenberg M, Weigel M, Granlund I, Schroder W P, Finazzi G, Rappaport F, Masiero S, Furini A, Jahns P, Leister D (2009) Mutants, overexpressors, and interactors of Arabidopsis plastocyanin isoforms: revised roles of plastocyanin in photosynthetic electron flow and thylakoid redox state. *Mol Plant* 2: 236-248.
- Pfundel E E, Dilley R A (1993) The pH dependence of violaxanthin deepoxidation in isolated pea chloroplasts. *Plant Physiol* 101: 65-71.
- Pribil M, Pesaresi P, Hertle A, Barbato R, Leister D (2010) Role of plastid protein phosphatase TAP38 in LHCII dephosphorylation and thylakoid electron flow. *PLoS Biol* 8: e1000288.
- Qin X, Suga M, Kuang T, Shen J-R (2015) Structural basis for energy transfer pathways in the plant PSI-LHCI supercomplex. *Science* 348: 989-995.
- Rantala S, Lempiäinen T, Gerotto C, Tiwari A, Aro E-M, Tikkanen M (2020) PGR5 and NDH-1 systems do not function as protective electron acceptors but mitigate the consequences of PSI inhibition. *Biochimica Biophysica Acta Bioenerg* 1861: 148154.
- Reiter B, Rosenhammer L, Marino G, Geimer S, Leister D, Rühle T (2023) CGL160-mediated recruitment of the coupling factor CF1 is required for efficient thylakoid ATP synthase assembly, photosynthesis, and chloroplast development in Arabidopsis. *Plant Cell* 35: 488-509.
- Reiter B, Vamvaka E, Marino G, Kleine T, Jahns P, Bolle C, Leister D, Rühle T (2020) The Arabidopsis protein CGL20 is required for plastid 50S ribosome biogenesis. *Plant Physiol* 182: 1222-1238.
- Richter S, Lamppa G K (2002) Determinants for removal and degradation of transit peptides of chloroplast precursor proteins. *J Biol Chem* 277: 43888-43894.

- Rojas-González J A, Soto-Suárez M, García-Díaz Á, Romero-Puertas M C, Sandalio L M, Mérida Á, Thormählen I, Geigenberger P, Serrato A J, Sahrawy M (2015) Disruption of both chloroplastic and cytosolic FBPase genes results in a dwarf phenotype and important starch and metabolite changes in *Arabidopsis thaliana*. *J Exp Bot* 66: 2673-2689.
- Rühle T, Dann M, Reiter B, Schunemann D, Naranjo B, Penzler J F, Kleine T, Leister D (2021) PGRL2 triggers degradation of PGR5 in the absence of PGRL1. *Nat Commun* 12: 3941.
- Rühle T, Razeghi J A, Vamvaka E, Viola S, Gandini C, Kleine T, Schünemann D, Barbato R, Jahns P, Leister D (2014) The Arabidopsis protein CONSERVED ONLY IN THE GREEN LINEAGE160 promotes the assembly of the membranous part of the chloroplast ATP synthase. *Plant Physiol* 165: 207-226.
- Sandoval-Ibanez O, Rolo D, Ghandour R, Hertle A P, Armarego-Marriott T, Sampathkumar A, Zoschke R, Bock R (2022) De-etiolation-induced protein 1 (DEIP1) mediates assembly of the cytochrome b(6)f complex in Arabidopsis. *Nat Commun* 13: 4045.
- Schagger H (2006) Tricine-SDS-PAGE. *Nat Protoc* 1: 16-22.
- Schagger H, Cramer W, Vonjagow G (1994) Analysis of molecular masses and oligomeric states of protein complexes by blue native electrophoresis and isolation of membrane protein complexes by two-dimensional native electrophoresis. *Anal Biochem* 217: 220-230.
- Schreiber U, Klughammer C (2008) Non-photochemical fluorescence quenching and quantum yields in PS I and PS II: analysis of heat-induced limitations using Maxi-Imaging-PAM and Dual-PAM-100. *PAM application notes* 1: 15-18.
- Schuller J M, Birrell J A, Tanaka H, Konuma T, Wulfhorst H, Cox N, Schuller S K, Thiemann J, Lubitz W, Sétif P (2019) Structural adaptations of photosynthetic complex I enable ferredoxin-dependent electron transfer. *Science* 363: 257-260.
- Schwenkert S, Legen J, Takami T, Shikanai T, Herrmann R G, Meurer J (2007) Role of the low-molecular-weight subunits PetL, PetG, and PetN in assembly,

- stability, and dimerization of the cytochrome b6f complex in tobacco. *Plant Physiol* 144: 1924-1935.
- Shikanai T (2007) Cyclic electron transport around photosystem I: genetic approaches. *Annu Rev Plant Biol* 58: 199-217.
- Shikanai T (2016) Chloroplast NDH: A different enzyme with a structure similar to that of respiratory NADH dehydrogenase. *Biochim Biophys Acta* 1857: 1015-1022.
- Shikanai T, Muller-Moule P, Munekage Y, Niyogi K K, Pilon M (2003) PAA1, a P-type ATPase of Arabidopsis, functions in copper transport in chloroplasts. *Plant Cell* 15: 1333-1346.
- Shikanai T, Munekage Y, Shimizu K, Endo T, Hashimoto T (1999) Identification and characterization of Arabidopsis mutants with reduced quenching of chlorophyll fluorescence. *Plant Cell Physiol* 40: 1134-1142.
- Stadermann K B, Holtgrawe D, Weisshaar B (2016) Chloroplast Genome Sequence of Arabidopsis thaliana Accession Landsberg erecta, Assembled from Single-Molecule, Real-Time Sequencing Data. *Genome Announc* 4.
- Steinbeck J, Ross I L, Rothnagel R, Gabelein P, Schulze S, Giles N, Ali R, Drysdale R, Sierrecki E, Gambin Y, Stahlberg H, Takahashi Y, Hippler M, Hankamer B (2018) Structure of a PSI-LHCI-cyt b(6)f supercomplex in Chlamydomonas reinhardtii promoting cyclic electron flow under anaerobic conditions. *Proc Natl Acad Sci U S A* 115: 10517-10522.
- Strand D D, Kramer D M (2014) Control of non-photochemical exciton quenching by the proton circuit of photosynthesis. *Non-photochemical quenching and energy dissipation in plants, algae and cyanobacteria* 387-408.
- Strand D D, Livingston A K, Satoh-Cruz M, Froehlich J E, Maurino V G, Kramer D M (2015) Activation of cyclic electron flow by hydrogen peroxide in vivo. *Proc Natl Acad Sci U S A* 112: 5539-5544.
- Sugimoto K, Okegawa Y, Tohri A, Long T A, Covert S F, Hisabori T, Shikanai T (2013) A single amino acid alteration in PGR5 confers resistance to antimycin A in cyclic electron transport around PSI. *Plant Cell Physiol* 54: 1525-1534.

- Suorsa M, Jarvi S, Grieco M, Nurmi M, Pietrzykowska M, Rantala M, Kangasjarvi S, Paakkanen V, Tikkanen M, Jansson S, Aro E M (2012) PROTON GRADIENT REGULATION5 is essential for proper acclimation of Arabidopsis photosystem I to naturally and artificially fluctuating light conditions. *Plant Cell* 24: 2934-2948.
- Suorsa M, Rossi F, Tadini L, Labs M, Colombo M, Jahns P, Kater M M, Leister D, Finazzi G, Aro E M, Barbato R, Pesaresi P (2016) PGR5-PGRL1-Dependent Cyclic Electron Transport Modulates Linear Electron Transport Rate in Arabidopsis thaliana. *Mol Plant* 9: 271-288.
- Takahashi S, Milward S E, Fan D-Y, Chow W S, Badger M R (2009) How does cyclic electron flow alleviate photoinhibition in Arabidopsis? *Plant Physiol* 149: 1560-1567.
- Tan S L, Huang X, Li W Q, Zhang S B, Huang W (2021) Elevated CO₂ Concentration Alters Photosynthetic Performances under Fluctuating Light in Arabidopsis thaliana. *Cells* 10.
- Telman W, Liebthal M, Dietz K-J (2020) Redox regulation by peroxiredoxins is linked to their thioredoxin-dependent oxidase function. *Photosynth Res* 145: 31-41.
- Tikkanen M, Grieco M, Kangasjarvi S, Aro E M (2010) Thylakoid protein phosphorylation in higher plant chloroplasts optimizes electron transfer under fluctuating light. *Plant Physiol* 152: 723-735.
- Vener A V, Van Kan P J, Rich P R, Ohad I, Andersson B (1997) Plastoquinol at the quinol oxidation site of reduced cytochrome b_f mediates signal transduction between light and protein phosphorylation: thylakoid protein kinase deactivation by a single-turnover flash. *Proc Natl Acad Sci U S A* 94: 1585-1590.
- Voith von Voithenberg L, Park J, Stübe R, Lux C, Lee Y, Philippar K (2019) A novel prokaryote-type ECF/ABC transporter module in chloroplast metal homeostasis. *Front Plant Sci* 10: 1264.
- Wada S, Amako K, Miyake C (2021) Identification of a novel mutation exacerbated the PSI photoinhibition in pgr5/pgrl1 mutants; caution for overestimation of the phenotypes in Arabidopsis pgr5-1 mutant. *Cells* 10: 2884.

- Wang Z-P, Xing H-L, Dong L, Zhang H-Y, Han C-Y, Wang X-C, Chen Q-J (2015) Egg cell-specific promoter-controlled CRISPR/Cas9 efficiently generates homozygous mutants for multiple target genes in Arabidopsis in a single generation. *Genome Bio* 16: 1-12.
- Wu X, Wu J, Wang Y, He M, He M, Liu W, Shu S, Sun J, Guo S (2021) The key cyclic electron flow protein PGR5 associates with cytochrome b(6)f, and its function is partially influenced by the LHCII state transition. *Hortic Res* 8: 55.
- Yamamoto H, Shikanai T (2019) PGR5-Dependent Cyclic Electron Flow Protects Photosystem I under Fluctuating Light at Donor and Acceptor Sides. *Plant Physiol* 179: 588-600.
- Yamamoto H, Takahashi S, Badger M R, Shikanai T (2016) Artificial remodelling of alternative electron flow by flavodiiron proteins in Arabidopsis. *Nat Plant* 2: 16012.
- Yamori W, Shikanai T (2016) Physiological Functions of Cyclic Electron Transport Around Photosystem I in Sustaining Photosynthesis and Plant Growth. *Annu Rev Plant Biol* 67: 81-106.
- Yi X, McChargue M, Laborde S, Frankel L K, Bricker T M (2005) The manganese-stabilizing protein is required for photosystem II assembly/stability and photoautotrophy in higher plants. *J Biol Chem* 280: 16170-16174.
- Yokochi Y, Fukushi Y, Wakabayashi K I, Yoshida K, Hisabori T (2021) Oxidative regulation of chloroplast enzymes by thioredoxin and thioredoxin-like proteins in Arabidopsis thaliana. *Proc Natl Acad Sci U S A* 118.
- Yu C-A, Xia J-Z, Kachurin A M, Yu L, Xia D, Kim H, Deisenhofer J (1996) Crystallization and preliminary structure of beef heart mitochondrial cytochrome-bc1 complex. *Biochim Biophys Acta* 1275: 47-53.
- Zhou, Q., Yamamoto, H., & Shikanai, T. (2022). Distinct contribution of two cyclic electron transport pathways to P700 oxidation. *Plant Physiol* 192: 326-341.

8. Danksagung

An dieser Stelle möchte ich meinen besonderen Dank nachstehenden Personen entgegenbringen, die mich während meiner Bearbeitung der Doktorarbeit unterstützt haben.

Mein Dank gilt zunächst Prof. Dr. Dario Leister für die Möglichkeit, dass ich meine Doktorarbeit mit einem höchst interessanten Thema in seiner Arbeitsgruppe durchführen konnte. In meiner Doktorarbeit gab es mehrere Rückschläge, sei es durch konkurrierende Publikationen oder dass meinen Labbetreuerin bedauerlicherweise das Labor wechselte, in diesen Momenten motivierte und unterstützte mich Prof. Leister besonders, so dass ich meine Arbeit erfolgreich weiterführte. Auch für das mir entgegengebrachte Vertrauen, dass ich das Projekt gerecht vertreten kann, sei es durch Präsentation der Projekte bei Kongressen oder die Einarbeitung und Betreuung von Studenten, bin ich Prof. Leister zutiefst dankbar. Hierdurch wurde mein Interesse an einer akademischen Laufbahn vertieft.

Ich danke Belén für die Betreuung meiner Arbeiten im Labor in den ersten Jahren. Die Zeit, in der wir die Projekte bearbeitet haben, war immer sehr lehrreich und hat mir viel Freude bereitet. Es freut mich sehr, dass meine ehemaligen Betreuerin, die jetzt erfolgreich in Sevilla arbeitet, eine Bezugsperson für mich geworden ist, an die ich mich in allen Situationen wenden kann und die mich arbeitsbedingt und auch anderweitig immer unterstützt und mit gutem Rat zur Seite steht. Auch ihre kritischen, fairen und motivierenden Kommentare und Korrekturen meiner Doktorarbeit haben zu einer erfolgreichen Vollendung der Arbeit beigetragen.

Milena, Maysoon, Catharina, Weien, Theo, Feng und Alex danke ich für den Unterstützung und die Ratschläge. Die Mittagspausen mit euch und die gemeinsamen Wandertouren in den Alpen sind mir immer ein großes Vergnügen. Ich konnte fast jeden Samstag meinen kulinarischen Horizont mit euch erweitern.

Sabrina danke ich für die kleinen und großen Ablenkungen von meiner Arbeit und der Doktorarbeit, welche meine Gedanken nicht nur um die Wissenschaft kreisen ließen.

Catharina, Chris und Thilo danke ich für die Korrektur und das kritische Lesen der Doktorarbeit. Durch eure Unterstützung konnte ich die Qualität der Arbeit steigern.

Bei Hannah bedanke ich mich für die Hilfe im Labor. Besonders auf der Zielgeraden der Doktorarbeit hat deine Unterstützung mir sehr geholfen.

Für Tipps zu „how to start write your thesis“ und Unterstützung im Labor so wie in mehreren Projekten danke ich Giada.

Tatjana danken ich für die Mitarbeit an dem *pgr5*-screen, in dem Sie die Resequenzierungsdaten für uns analysiert hat.

Der gesamten AG Leister danke ich für die viele Unterstützung, Hilfsbereitschaft, das Interesse an meiner Arbeit und einer positiven und freundlichen Arbeitsatmosphäre.

Zweimal die Woche konnte ich beim Bouldern in der Früh mit Victoria und Moritz Motivation sammeln und Stress abbauen. Dafür bedanke ich mich, da alleine die Motivation manchmal gefehlt hätte.

Den Gärtnern der AG Leister danke ich für die Pflege der vielen Pflanzen, die ich in der Zeit meines PhDs herangezogen habe. Insbesondere bedanke ich mich bei Ariel. Er hatte immer ein offenes Ohr, falls mal eine Kammer Probleme bereitete, oder anderweitig etwas anfiel.

Mein besonderer Dank gilt meiner Familie, die mich durch Zuspruch, Kraft und Beistand unterstützte und mir in der Endphase der Doktorarbeit viel Verständnis entgegengebracht hat.

Publikationsliste

1. Marino G*, Naranjo B*, Wang J*, Penzler J-F, Kleine T & Leister D (2019). Relationship of GUN 1 to FUG 1 in chloroplast protein homeostasis. *The Plant Journal*, 99(3), 521-535. [doi: 10.1111/tpj.14342](https://doi.org/10.1111/tpj.14342).
2. Naranjo B*, Penzler J-F*, Rühle T & Leister D (2021). NTRC effects on non-photochemical quenching depends on PGR5. *Antioxidants*, 10(6), 900. [doi: 10.3390/antiox10060900](https://doi.org/10.3390/antiox10060900)
3. Rühle T, Dann M, Reiter B, Schünemann D, Naranjo B, Penzler J-F, Kleine T & Leister D (2021). PGRL2 triggers degradation of PGR5 in the absence of PGRL1. *Nature communications*, 12(1), 3941. [doi: 10.1038/s41467-021-24107-7](https://doi.org/10.1038/s41467-021-24107-7)
4. #Penzler J-F*, Marino G*, Reiter B, Kleine T, Naranjo B, & Leister D (2022). Commonalities and specialties in photosynthetic functions of PROTON GRADIENT REGULATION5 variants in Arabidopsis. *Plant Physiology*, 190(3), 1866-1882. [doi: 10.1093/plphys/kiac362](https://doi.org/10.1093/plphys/kiac362)
5. Penzler J-F, Kleine T, Leister D (2023) COG1 - A master transcription factor regulating photosynthesis. *Mol Plant* 16: 1890–1892. [doi: 10.1016/j.molp.2023.11.006](https://doi.org/10.1016/j.molp.2023.11.006)

(* These authors contributed equally)

(# publication related to this dissertation)